

ผลของสารตัวเติมต่อสมบัติของพอลิพรอพิลีนสำหรับเทคนิคการพิมพ์สามมิติแบบฟิวส์ดีโพลีชัน
โมเดลลิ่ง



บทคัดย่อและแฟ้มข้อมูลฉบับเต็มของวิทยานิพนธ์ตั้งแต่ปีการศึกษา 2554 ที่ให้บริการในคลังปัญญาจุฬาฯ (CUIR)
เป็นแฟ้มข้อมูลของนิสิตเจ้าของวิทยานิพนธ์ ที่ส่งผ่านทางบัณฑิตวิทยาลัย

The abstract and full text of theses from the academic year 2011 in Chulalongkorn University Intellectual Repository (CUIR)
are the thesis authors' files submitted through the University Graduate School.

วิทยานิพนธ์นี้เป็นส่วนหนึ่งของการศึกษาตามหลักสูตรปริญญาวิศวกรรมศาสตรมหาบัณฑิต
สาขาวิชาวิศวกรรมเคมี ภาควิชาวิศวกรรมเคมี
คณะวิศวกรรมศาสตร์ จุฬาลงกรณ์มหาวิทยาลัย
ปีการศึกษา 2560
ลิขสิทธิ์ของจุฬาลงกรณ์มหาวิทยาลัย

EFFECTS OF FILLERS ON THE PROPERTIES OF POLYPROPYLENE FOR FUSED
DEPOSITION MODELING-BASED 3D PRINTING TECHNIQUE

Miss Chomphoonut Buaprommee



A Thesis Submitted in Partial Fulfillment of the Requirements
for the Degree of Master of Engineering Program in Chemical Engineering

Department of Chemical Engineering

Faculty of Engineering

Chulalongkorn University

Academic Year 2017

Copyright of Chulalongkorn University

Thesis Title EFFECTS OF FILLERS ON THE PROPERTIES OF
POLYPROPYLENE FOR FUSED DEPOSITION
MODELING-BASED 3D PRINTING TECHNIQUE
By Miss Chomphoonut Buaprommee
Field of Study Chemical Engineering
Thesis Advisor Associate Professor Anongnat Somwangthanaroj,
Ph.D.

Accepted by the Faculty of Engineering, Chulalongkorn University in Partial
Fulfillment of the Requirements for the Master's Degree

..... Dean of the Faculty of Engineering
(Associate Professor Supot Teachavorasinskun, D.Eng.)

THESIS COMMITTEE

..... Chairman
(Professor Siriporn Damrongsakkul, Ph.D.)

..... Thesis Advisor
(Associate Professor Anongnat Somwangthanaroj, Ph.D.)

..... Examiner
(Palang Bumroongsakulsawat, Ph.D.)

..... External Examiner
(Wasana Jamsak, D.Eng.)

ชมพูนุท บัวพรมมี : ผลของสารตัวเติมต่อสมบัติของพอลิพรอพิลีนสำหรับเทคนิคการพิมพ์สามมิติแบบฟิวส์ดีโพลีชันโมเดลลิ่ง (EFFECTS OF FILLERS ON THE PROPERTIES OF POLYPROPYLENE FOR FUSED DEPOSITION MODELING-BASED 3D PRINTING TECHNIQUE) อ.ที่ปรึกษาวิทยานิพนธ์หลัก: รศ. ดร.อนงค์นาฏ สมหวังธนโรจน์, 116 หน้า.

งานวิจัยนี้มีวัตถุประสงค์เพื่อศึกษาผลของปริมาณสารตัวเติมและชนิดของสารตัวเติมที่มีต่อสมบัติทางกลและพฤติกรรมการหดตัวของพอลิพรอพิลีนคอมโพสิต เพื่อพัฒนาสมบัติของพอลิพรอพิลีนให้สามารถเป็นวัสดุสำหรับเทคนิคการพิมพ์สามมิติแบบฟิวส์ดีโพลีชันโมเดลลิ่ง ซึ่งพอลิพรอพิลีนถูกคอมปาวด์กับสารเติมแต่ง 3 ชนิด ได้แก่ ทัลคัม ไยแก้วบดที่มีอัตราส่วนลักษณะ 5.4 และ 15.4 ในอัตราส่วนร้อยละ 10, 20 และ 30 โดยน้ำหนัก จากนั้นชิ้นงานทดสอบจะถูกขึ้นรูปด้วยเทคนิคการพิมพ์สามมิติแบบฟิวส์ดีโพลีชันโมเดลลิ่ง และการฉีดขึ้นรูปเพื่อทดสอบแรงดึงและการหดตัว

จากการทดสอบพบว่าเมื่อเพิ่มปริมาณสารตัวเติมลงในพอลิพรอพิลีน ส่งผลให้ค่ามอดูลัสมีแนวโน้มสูงขึ้น และความทนแรงดึงมีแนวโน้มลดลงในทั้งสองกระบวนการขึ้นรูป ยกเว้นความทนแรงดึงของทัลคอมโพสิตที่ขึ้นรูปโดยการฉีดที่มีค่าไม่เปลี่ยนแปลง ในกระบวนการขึ้นรูปแบบฉีดพบว่าใยแก้วบดที่มีอัตราส่วนลักษณะ 15.4 และทัลคอมโพสิตแสดงค่ามอดูลัสและค่าความแข็งแรงต่อแรงดึงสูงที่สุดตามลำดับ นอกจากนี้ยังพบว่าชนิดของสารตัวเติมไม่ได้ส่งผลอย่างมีนัยสำคัญต่อค่ามอดูลัสและความทนแรงดึงในเทคนิคการขึ้นรูปแบบฟิวส์ดีโพลีชันโมเดลลิ่ง สำหรับค่าการหดตัวพบว่าทั้งสองเทคนิคการขึ้นรูปให้แนวโน้มแบบเดียวกันคือ เมื่อปริมาณสารตัวเติมเพิ่มมากขึ้นส่งผลให้อัตราการหดตัวลดลง และคอมโพสิตที่เติมทัลคัมมีค่าการหดตัวน้อยที่สุดในขณะที่คอมโพสิตที่เติมใยแก้วบดที่มีอัตราส่วนลักษณะ 5.4 มีค่าการหดตัวมากที่สุด ทั้งหมดนี้กล่าวได้ว่าพอลิพรอพิลีนสามารถที่จะเป็นวัสดุสำหรับเทคนิคการพิมพ์สามมิติแบบฟิวส์ดีโพลีชันโมเดลลิ่งในการขึ้นรูปชิ้นส่วนเล็กๆ หรือแบบจำลองต่างๆ ได้

ภาควิชา วิศวกรรมเคมี ลายมือชื่อนิสิต

สาขาวิชา วิศวกรรมเคมี ลายมือชื่อ อ.ที่ปรึกษาหลัก

ปีการศึกษา 2560

5770989221 : MAJOR CHEMICAL ENGINEERING

KEYWORDS: FUSED DEPOSITION MODELING / POLYPROPYLENE / SHRINKAGE /
MILLED GLASS FIBER / TALCUM / TENSILE PROPERTIES

CHOMPHOONUT BUAPROMMEE: EFFECTS OF FILLERS ON THE PROPERTIES
OF POLYPROPYLENE FOR FUSED DEPOSITION MODELING-BASED 3D
PRINTING TECHNIQUE. ADVISOR: ASSOC. PROF. ANONGNAT
SOMWANGTHANAROJ, Ph.D., 116 pp.

The objective of this research was to study the influence of filler contents and filler types on the tensile properties and shrinkage behavior of polypropylene composites to develop the properties of polypropylene (PP) to be a raw material for fused deposition modeling (FDM) technique. PP was compounded with three fillers, i.e., talc and milled glass fiber with aspect ratio 5.4 and 15.4, at various contents of 10, 20 and 30 wt%. The test specimens were fabricated by FDM and injection molding techniques for tensile and shrinkage tests.

The findings showed that the increase of filler contents into PP matrix tended to increase the tensile modulus and decrease the tensile strength in both techniques except the strength of talc-filled PP molded by injection molding remained unchanged. In injection molding, milled glass fiber (AR 15.4) and talc composites exhibited the highest tensile modulus and tensile strength, respectively. In addition, the filler types did not significantly affect the tensile modulus and strength for FDM process. For shrinkage behavior, it was found that the increase of filler content declined in shrinkage rate and talc-filled PP composites tended to the lowest shrinkage meanwhile milled glass fiber with aspect ratio 5.4 exhibited the highest shrinkage in both injection molding and FDM techniques. Finally, PP composites may be an alternative feedstock material for FDM technique to produce small parts or mockups.

Department: Chemical Engineering Student's Signature

Field of Study: Chemical Engineering Advisor's Signature

Academic Year: 2017

ACKNOWLEDGEMENTS

I would like to express my sincere appreciation to my thesis advisor, Associate Professor Dr. Anongnat Somwangthanaroj for her invaluable suggestions, assistance and continuous encouragement throughout the completion of this research.

I would also like to extend my gratitude to the Chairman, Professor Dr. Siriporn Damrongsakkul, and thesis committee members, Dr. Palang Bumroongsakulsawat and Dr. Wasana Jamsak, for their helpful comments, guidance and suggestions which have been very useful for this research.

In addition, I am most grateful to my friends in Chemical Engineering at Chulalongkorn University, my colleagues at PTT Global Chemical Public Company Limited and everyone for their kind help and valuable recommendations. Also, I would like to thank Mektec Manufacturing Corporation and Center of Excellence on Catalysis and Catalytic Reaction Engineering for their assistance in thermal conductivity test. Moreover, I would like to thank Mr. Oliver Berset for kindly proofreading my work.

Finally, I would like to gratefully thank my family for all their generous support, motivation and encouragement.

CONTENTS

	Page
THAI ABSTRACT	iv
ENGLISH ABSTRACT	v
ACKNOWLEDGEMENTS.....	vi
CONTENTS.....	vii
LIST OF TABLES.....	1
LIST OF FIGURES	2
LIST OF ABBREVIATIONS	6
CHAPTER I INTRODUCTION.....	1
1.1 General background	1
1.2 Objective.....	3
1.3 Scopes of Study	3
CHAPTER II THEORY AND LITERATURE REVIEW.....	4
2.1 Theory	4
2.1.1 Fused Deposition Modeling (FDM)	4
2.1.1.1 FDM technique.....	4
2.1.1.2 Basic properties of the materials	5
2.1.2 Polypropylene.....	6
2.1.2.1 Structures and Properties of Polypropylene.....	6
2.1.2.2 Applications of Polypropylene	9
2.1.2.3 Main Problems of Polypropylene	10
2.1.3 Fillers for Property Modification of Polypropylene	11
2.1.3.1 Talcum.....	13

	Page
2.1.3.2 Calcium carbonate.....	14
2.1.3.3 Glass fiber.....	15
2.1.4 Shrinkage behavior of polymers.....	16
2.1.4.1 Fundamental concepts of part shrinkage.....	16
2.1.4.2 Effect of fillers on shrinkage.....	19
2.2 Literature Reviews.....	20
2.2.1 Effect of fillers on the mechanical properties of the printed samples by FDM technique.....	20
2.2.2 Effect of fillers on the shrinkage behavior of polypropylene.....	22
2.2.3 Effect of fillers on the filament bonding of the printed samples by FDM technique.....	25
2.2.4 Effect of printing conditions on the mechanical properties.....	26
CHAPTER III EXPERIMENT.....	28
3.1 Materials.....	28
3.2 Material Screening.....	30
3.2.1 Melt Flow Index Measurement.....	30
3.2.2 Shear Viscosity Measurement.....	30
3.3 Sample Preparation.....	31
3.3.1 Polypropylene Compounding.....	31
3.3.2 Ash content.....	32
3.3.3 Filament Preparation.....	33
3.3.4 Test Specimen Preparation.....	34
3.3.4.1 3D Printing.....	34

	Page
3.3.4.2 Injection.....	36
3.4 Characterization Methods.....	36
3.4.1 Differential Scanning Calorimetry (DSC).....	36
3.4.2 Tensile Property Measurement	37
3.4.3 Scanning Electron Microscope (SEM)	38
3.4.4 Die swell	39
3.4.5 Thermal conductivity	39
3.4.6 Shrinkage Measurement	40
3.4.7 Fiber length measurement	41
3.4.8 Particle size analysis	42
3.4.9 Porosity calculation	43
CHAPTER IV RESULTS AND DISCUSSION.....	44
4.1 Rheological properties of PLA, ABS and neat PP	44
4.2 Ash content measurement of PP composites.....	46
4.3 Effect of filler content and filler type on void formation	47
4.3.1 Filler content	47
4.3.2 Filler type	50
4.4 Effect of filler content and filler type on tensile properties	58
4.4.1 Filler content	58
4.4.2 Filler type	61
4.5 Effect of filler content and filler type on shrinkage behavior	64
4.5.1 Filler content	64

	Page
4.5.2 Filler type	68
CHAPTER V CONCLUSIONS AND RECOMMENDATIONS	72
5.1 Conclusions.....	72
5.2 Recommendations	74
REFERENCES.....	75
Appendix A Data of raw material properties.....	81
Appendix B Data of mechanical properties.....	84
Appendix C Data of shrinkage behavior.....	94
Appendix D Data of thermal properties.....	98
Appendix E Data of thermal conductivity	102
Appendix F Data of die swell	106
Appendix G Data of porosity.....	111
VITA	116

LIST OF TABLES

Table 2.1 Typical properties of polypropylene	8
Table 2.2 Typical applications of PP in each market sector	9
Table 2.3 Comparison of unfilled PP with other thermoplastics	11
Table 2.4 Fillers for modification of polypropylene property	12
Table 2.5 Effect of 30% talc on shrinkage compared with pure ABS	14
Table 2.6 Shrinkage phenomenon of polymers	17
Table 3.1 Polypropylene homopolymer in order of melt flow rate (MFR).....	28
Table 3.2 The recipes of composites used in this study.....	32
Table 4.1 The measured melt flow rate (MFR) of PLA and ABS	44
Table 4.2 PP in order of melt flow rate (MFR at 230°C/2.16kg load)	45
Table 4.3 Ash content of PP composites at various filler contents	47
Table 4.4 Comparison of crystallinity of PP composites at the same loading	64
Table 4.5 Comparison of crystallinity of PP composites at various contents	68

LIST OF FIGURES

Figure 2.1 Illustration of the FDM process based on RepRap [16].....	5
Figure 2.2 Polymerization of propylene to polypropylene	7
Figure 2.3 PP configurations in a) isotactic, b) syndiotactic and c) atactic forms.....	7
Figure 2.4 The problem of printed PP sample by 3D printing technique	11
Figure 2.5 Schematic images of talc (a) chemical structure, and (b) SEM	13
Figure 2.6 Effect of talc on stiffness. □ High crystalline PP; △ Homopolymer PP; ◇ Copolymer PP	14
Figure 2.7 Crystal forms of calcium carbonate (a) trigonal-rhombohedral calcite; (b) trigonal-scalenohedral calcite	15
Figure 2.8 PVT diagram for polypropylene (semicrystalline resin). ■ P=0.1Mpa; △ P=20MPa; ◇ P=40MPa; x P=60MPa; ● P=100MPa; □ P=160MPa	18
Figure 2.9 PVT diagram for polycarbonate (amorphous resin). ■ P=0Mpa; △ P=30MPa; □ P=60MPa; ◇ P=90MPa; x P=120MPa	18
Figure 2.10 Tensile properties of polypropylene (PP) and glass reinforced polypropylene (GRPP) by FDM technique: (a) modulus; (b) strength	20
Figure 2.11 Tensile strength of short glass fiber reinforced ABS by FDM	21
Figure 2.12 Effect of fiber loading and produced technique on (a) tensile strength, and (b) tensile modulus, of ABS/CF composites	22
Figure 2.13 Shrinkage of various talc contents in flow direction	23
Figure 2.14 Shrinkage of PP at various amounts of glass fiber	24
Figure 2.15 Shrinkage behavior of CaCO ₃ filled-PP composites	24
Figure 2.16 Effect of filler type on shrinkage behavior of polypropylene	25

Figure 2.17 SEM micrographs of fracture surface of (e) Neat ABS, (f) 10%CF, (g) 20%CF, and (h) 30%CF	26
Figure 2.18 Tensile modulus and tensile strength of the printed parts by FDM	27
Figure 3.1 Flowchart of experimental work.....	29
Figure 3.2 Melt flow indexer (Goettfert, Model MI-4).....	30
Figure 3.3 Capillary rheometer (Malvern, Model RH7).....	31
Figure 3.4 Twin screw extruder (LabTech, Model LTE26-40).....	32
Figure 3.5 Muffle Furnace (CABOLITE, model GPC12/131).....	33
Figure 3.6 Single screw extruder (LabTech, LE25-30)	34
Figure 3.7 Filament spool of 1.75 mm diameter.....	34
Figure 3.8 FDM 3D printer (Siamreap, Model Delta X pro)	35
Figure 3.9 (a) Orientation of crossed 45° ($\pm 45^\circ$); (b) Orientation of 0-90°	35
Figure 3.10 Electric injection machine (Toshiba, model EC100NII-2A).....	36
Figure 3.11 Differential Scanning Calorimeter (Netzsch, Model DSC 204 F1)	37
Figure 3.12 Universal testing machine (Zwick/Roell, Model Z050).....	38
Figure 3.13 Scanning Electron Microscope (JEOL, Model JSM-6510LV)	39
Figure 3.14 3D scanner (INFINITE 2.0, CimCore).....	41
Figure 3.15 Measuring microscope (StarLite, Model 250).....	41
Figure 3.16 Microscope (Olympus model BX51 and DP72)	42
Figure 3.17 Particle Size Analyzer (Malvern model Mastersizer 2000)	43
Figure 4.1 Shear viscosity vs shear rate flow curves of PLA, ABS and PP.....	46
Figure 4.2 SEM micrographs of cross-sectional fractured surface of talc-filled PP	48
Figure 4.3 Porosity inside the printed samples of talc-filled PP.....	49

Figure 4.4 Thermal conductivity of talc-filled PP	49
Figure 4.5 Die swell ratio of talc-filled PP	50
Figure 4.6 SEM micrographs of fractured surface of FDM samples at 10wt% filler loading.....	51
Figure 4.7 Porosity inside the printed samples at 10wt% filler loading	51
Figure 4.8 Thermal conductivity at 10 wt% filler loading.....	52
Figure 4.9 Die-swell at 10 wt% filler loading.....	52
Figure 4.10 SEM micrographs of fractured surface of FDM samples at 20wt% filler loading.....	53
Figure 4.11 Porosity inside the printed samples at 20wt% filler loading	53
Figure 4.12 Thermal conductivity at 20wt% filler loading	54
Figure 4.13 Die-swell at 20wt% filler loading.....	54
Figure 4.14 Dynamic DSC first cooling thermograms of 20wt% filler loading	55
Figure 4.15 SEM micrographs of fractured surface of FDM samples at 30wt% filler loading.....	56
Figure 4.16 Porosity inside the printed samples at 30wt% filler loading	56
Figure 4.17 Thermal conductivity at 30wt% filler loading	57
Figure 4.18 Die-swell at 30wt% filler loading.....	57
Figure 4.19 Dynamic DSC first cooling thermograms of 30wt% filler loading	58
Figure 4.20 Tensile strength of talc-filled PP at various contents	59
Figure 4.21 Tensile strength of milled glass fiber (AR 5.4)-filled PP at various contents	60
Figure 4.22 Tensile strength of milled glass fiber (AR 15.4)-filled PP at various contents	60

Figure 4.23 SEM micrographs of PP composites indicating interfacial adhesion between filler and PP matrix.....	61
Figure 4.24 Effect of filler type on tensile strength at 10wt% filler loading	62
Figure 4.25 Effect of filler type on tensile strength at 20wt% filler loading	63
Figure 4.26 Effect of filler type on tensile strength at 30wt% filler loading	63
Figure 4.27 Mold shrinkage of talc-filled PP at various contents	65
Figure 4.28 Mold shrinkage of milled glass fiber with aspect ratio 5.4-filled PP at various contents	65
Figure 4.29 Mold shrinkage of milled glass fiber with aspect ratio 15.4-filled PP at various contents	66
Figure 4.30 3D shrinkage contour plot at various contents in FDM process.....	67
Figure 4.31 Effect of filler type on mold shrinkage at 10wt% filler loading	69
Figure 4.32 Effect of filler type on mold shrinkage at 20wt% filler loading	70
Figure 4.33 Effect of filler type on mold shrinkage at 30wt% filler loading	70
Figure 4.34 3D shrinkage contour plot in FDM process	71

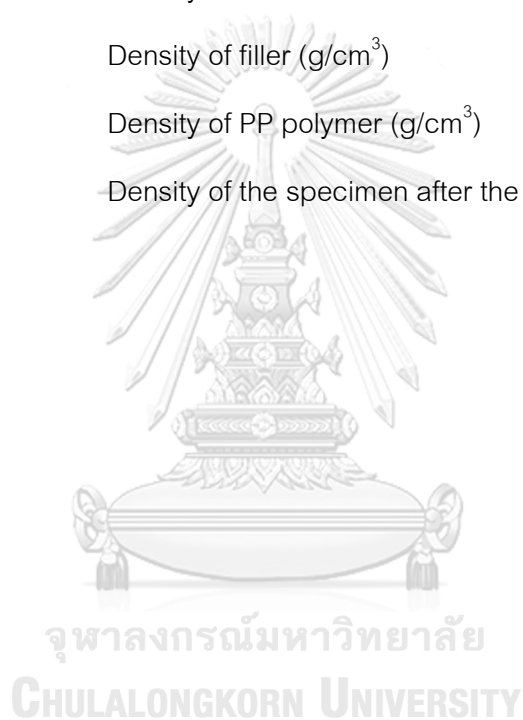
LIST OF ABBREVIATIONS

%Crys	Percentage of crystallinity (%)
ΔH_m°	specific melting heat of 100% crystalline isotactic PP (J/g)
ΔH_m	specific heat of melting (J/g)
μm	Micrometer or micron
3DP	Three dimensional printing
A	Weight of the specimen in air (g)
ABS	Acrylonitrile butadiene styrene
AM	Additive manufacturing
AR	Aspect ratio
ASTM	American Society for Testing and Materials
B	Weight of the specimen in distilled water (g)
C	Carbon
CaCO_3	Calcium carbonate
CAD	Computer aided design
CAM	Computer aided manufacture
CF	Carbon fiber
CM	Compression molding
C_p	Specific heat capacity [J/(g·K)]
CTE	Coefficient of thermal expansion
DSC	Differential scanning calorimeter
EDS	Energy dispersive spectroscopy
FDM	Fused deposition modeling
GF	Glass fiber
GFABS	Short glass fiber reinforced ABS

GRPP	Glass fiber reinforced polypropylene
H	Hydrogen
HDT	Heat distortion temperature or heat deflection temperature
HIPS	High impact polystyrene
iPP	Isotactic polypropylene
kN	Kilonewton
kV	Kilovolt
l	Thickness of the sample (mm)
L/D	Aspect ratio of length to diameter
l_i	Length of fiber (μm)
LLDPE	Linear low density polyethylene
L_m	Mold length in longitudinal to flow (mm)
L_n	Average fiber length (μm)
LOM	Laminated object manufacturing
L_s	Specimen length in longitudinal to flow (mm)
MD	Machine direction
MF	Milled glass fiber
MFI	Melt flow index
MFR	Melt flow rate
ml	Milliliter
mm	Millimeter
N	Newton
n_i	Number of fibers
P	Porosity (%)
PA	Polyamide

PC	Polycarbonate
PLA	Polylactic acid
PP	Polypropylene
PPSF	Polyphenylsulfone
PVT	Pressure-specific volume-temperature
RP	Rapid prototyping
rpm	Rounds per minute
SEBS	Styrene ethylene butadiene styrene
SEM	Scanning electron microscope
S_L	Shrinkage in longitudinal to flow (%)
SLA	Stereolithography apparatus
SLS	Selective laser sintering
S_T	Shrinkage in transverse to flow (%)
STL	Stereolithography
$t_{1/2}$	Time to reach half of the maximum temperature increase (s)
Talc	Talcum
T_c	Crystallization temperature ($^{\circ}\text{C}$)
TD	Transverse direction
TLCP	Thermotropic liquid crystalline polymer
T_m	Melting temperature ($^{\circ}\text{C}$)
UHMWPE	Ultra-high molecular weight polyethylene
w_1	Mass of crucible (g)
w_2	Mass of crucible plus mass of sample (g)
w_3	Mass of crucible plus mass of ash (g)
W_m	Mold length in transverse to flow (mm)

W_s	Specimen length in transverse to flow (mm)
wt%	Percentage by weight
X	Weight fraction of PP in the composites
α	Thermal diffusivity (mm^2/s)
λ	Thermal conductivity [$\text{W}/(\text{m}\cdot\text{K})$]
ρ	Density of the specimen (g/cm^3)
ρ_0	Density of the distilled water at testing temperature (g/cm^3)
ρ_{Filler}	Density of filler (g/cm^3)
ρ_{PP}	Density of PP polymer (g/cm^3)
ρ_t	Density of the specimen after the FDM process



CHAPTER I

INTRODUCTION

1.1 General background

Rapid prototyping (RP), Additive Manufacturing (AM) technology or 3D printing (3DP) have gained enormous amounts of interest over the past years. 3D printing is a technique that produces three-dimensional objects by addition of layers after layers of material from a digital file [1]. Computer aided design (CAD) or computer aided manufacture (CAM) software is used to design a desired concept in stereolithography (STL) file and then a designed object is sliced into horizontal thin layers. The thickness of each layer depends on the desire of customers. The first 3D printer was invented by Chuck Hull in 1984 (about 30 years ago), which was a stereolithography apparatus (SLA) using lasers to cure photopolymer [2, 3].

Over recent years, the industry of 3D printing has been growing continuously. The worldwide 3D printing industry has grown to \$3.07 billion in revenue in 2013. The worldwide revenue is expected to grow to \$12.8 billion by 2018 and exceed \$21 billion by 2020. As it expands and prices drop, 3D printing technology is aimed to change almost every major industry and make differences in the way we live, work and play from now on [4]. 3D printing is extensively used in aerospace, aeronautics, automotive, medical, architecture, education, fashion, and other fields [5-11]. The advantages of this technology compared with conventional processing techniques are the capability to build complex geometries, lower material waste, reduced production costs, higher prototype fabrication speed, and shortened commercialization time for a new product [2, 12-15].

The representative techniques of 3D printing technology are stereolithography apparatus (SLA), selective laser sintering (SLS), laminated object manufacturing (LOM),

fused deposition modeling (FDM), etc. Among the different additive manufacturing techniques, FDM process is currently the most popular technique for building parts of thermoplastic materials [2]. The strong points of FDM are using affordable machines and low-cost materials, a large variety of material available, minimal wastage, allowing the use of different colors or materials in one object, enabling operation in office and ease of use [5, 16, 17]. However, the weak point of parts processed from FDM technique is that they tend to have anisotropic material properties in the build direction [18].

At the present time, commercial thermoplastic filaments used for FDM technique as feedstocks are acrylonitrile butadiene styrene (ABS), polylactic acid (PLA), polycarbonate (PC), polyamide (PA), high impact polystyrene (HIPS), polyphenylsulfone (PPSF or PPSU) and investment casting wax [5, 19-22]. In this research, polypropylene (PP) was selected as the material because it has a low cost compared to existing materials and it is widely used in many applications such as automotive, medical devices, packaging, home appliances and stationery [16]. If polypropylene can be used as a material for FDM process, its value will become higher and will open new opportunity in 3D printing application. Currently, the pure thermoplastics are only used to fabricate mockups and conceptual prototypes because they lack strength thus not being able to be fully functional and resistant to high loads and also lack of dimensional stability due to material structure [23-25]. This dimensional instability is a serious problem that leads to failure of the printed part. Therefore, there is a need to enhance the mechanical properties and dimensional stability to get rid of the limitations and to drive this technique for final consumer products and end-use parts [26]. One of the easy and effective approaches to improve the mechanical properties and dimensional stability of polymer is an incorporation of filler, in order to reduce the volume fraction of shrinkable polymer part. The crystalline structure is stronger than the amorphous structure but has greater thermal

shrinkage when polymers cool down from the molten state. However, different type and loading of filler also provide different degree of crystallinity and volume fraction. Therefore, the effect of fillers on tensile properties and dimensional stability of polypropylene composites after FDM method will be studied in this research.

1.2 Objective

To study the effects of filler content and filler type on the properties of polypropylene for fused deposition modeling-based 3D printing technique

1.3 Scopes of Study

- 1.3.1 The polypropylene grade is selected using melt flow rate (MFR) and shear viscosity to be compared to the existing materials (PLA and ABS).
- 1.3.2 The effects of filler content (0, 10, 20 and 30 wt%) and filler type (talc, milled glass fiber with aspect ratio 5.4 and 15.4) on the properties of polypropylene are investigated.
- 1.3.3 The properties including tensile properties, shrinkage behavior and void formation in the printed specimens are studied.

CHAPTER II

THEORY AND LITERATURE REVIEW

2.1 Theory

2.1.1 Fused Deposition Modeling (FDM)

2.1.1.1 FDM technique

The fused deposition modeling, as illustrated in Figure 2.1 [16], is an extrusion solid-based additive manufacturing technology, originally invented by Stratasys Inc. Objects are fabricated from molten polymeric materials such as ABS and PLA, which are two of the most popular materials used in FDM process. FDM begins with a STL file format, created by CAD or CAM software, and then this file is transformed into several horizontal thin layers. Printing conditions, such as nozzle temperature, printing speed, orientation and infill degree, are set in software in order to define parameter values. In the physical printing process, a thermoplastic filament is moved from a filament spool by rolling to an extrusion nozzle at a constant rate. The filament is heated above the melting temperature and extruded through the nozzle as a molten filament onto a heated bed platform. Since the filament is driven in a semi-liquid state, each filament or layer is adjoined to the previous one. After one layer is built in X-Y plane, the extrusion nozzle moves up one step in Z direction in order to deposit the next layer. Finally, the nozzle head moves around until the object is finished as designed [2, 3, 11, 27].

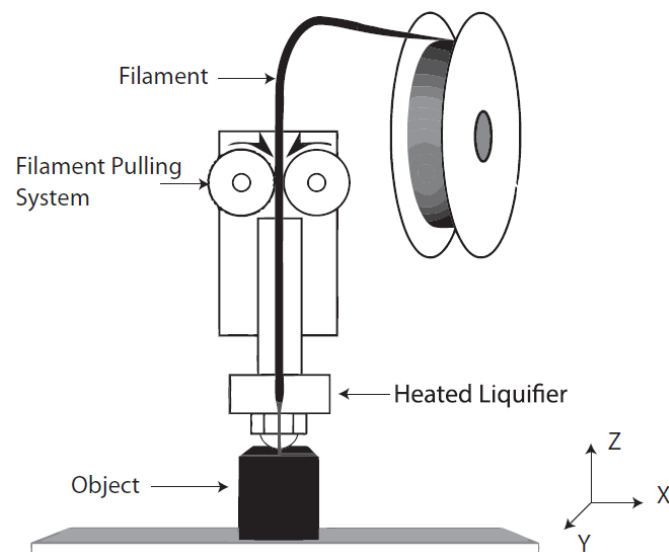


Figure 2.1 Illustration of the FDM process based on RepRap [16]

2.1.1.2 Basic properties of the materials

The materials for FDM process should have reasonable thermal, physical and mechanical properties to fulfill the design and application requirements of printed parts, and moreover they should have proper rheological properties for processing by the FDM technique. Key thermal and physical properties consist of 1) a suitable range of melting and solidification temperatures, 2) high heat distortion temperature, 3) low thermal expansion coefficient, 4) low shrinkage, 5) few volatile organic compounds in molten state, 6) no solid-state phase transformation, and 7) good bonding between filaments. In order to avoid high processing temperature, the melting temperature of materials must not be too high. Nevertheless, the melting temperature must not be too low in order to withstand heat deflection. The dimensional accuracy of printed parts is necessary to have a lower thermal expansion coefficient [25]. The fabricated parts in the FDM process should have linear shrinkage of less than 1.2% [11].

The requirements of the materials for mechanical properties are strength, stiffness, ductility and flexibility. In the FDM printing process, the filament as the feedstock

material is melted inside the nozzle and is pushed through the orifice die by the upstream parts of solid filament. Consequently, the material must have sufficient strength, ductility and flexibility to do as a plunger to push the semi-molten out of the nozzle die. In addition, the materials need adequate stiffness to resist deformation when applied force and require enough hardness to protect the surface from abrasion. Finally, suitable rheological properties are required for printing process. The materials with lower viscosity, or higher melt flow rate, will flow easier and faster solidification will fabricate an object in shorter time. However, the solidification period should not be too fast because it will create poor bonding of the filaments and high internal stress [25].

2.1.2 Polypropylene

2.1.2.1 Structures and Properties of Polypropylene

Polypropylene, a thermoplastic polymer, is synthesized by polymerization of propylene monomers using a catalyst which is Ziegler-Natta or metallocene catalyst, as shown in Figure 2.2. The chemical structures of PP are composed only of carbon (C) and hydrogen (H) atoms. The macromolecule of PP consists of 10,000 to 20,000 repeating units. The difference of stereochemical arrangement of methyl groups affects the properties of PP. Polypropylene has three types of chemical structure which are isotactic, syndiotactic and atactic. The methyl groups are arranged along the same side of the polymer chain, the structure is known as isotactic PP (semicrystalline). A structure which the methyl groups have a regular alternation of opposite configurations along the polymer backbone is referred to as syndiotactic PP (semicrystalline). The pendant methyl groups are added with a random orientation on the polymer chains, it is called atactic PP (amorphous). Figure 2.3 shows illustration of isotactic, syndiotactic and atactic PP chains [28]. Among polypropylene chemical structures, isotactic polypropylene (iPP) is the most commercial form and stable structure. iPP can crystallize into several crystal structures

such as monoclinic (α -form), being the most common form, hexagonal (β -form) and triclinic (γ -form).

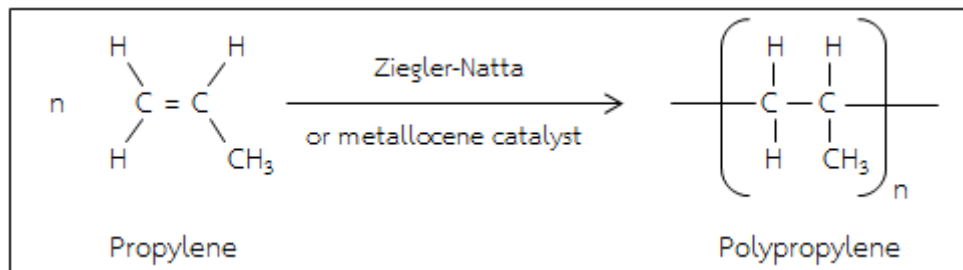
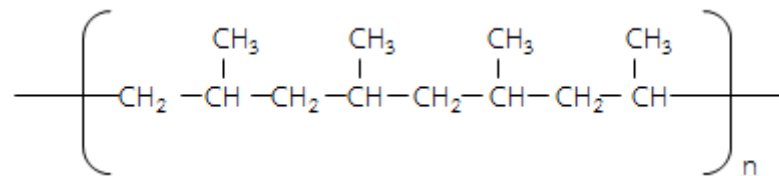
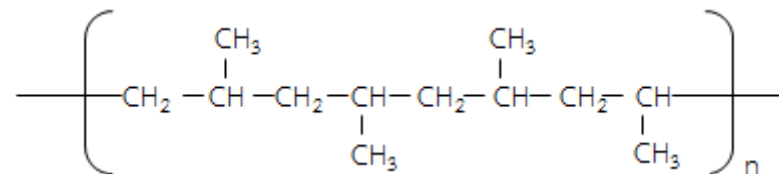


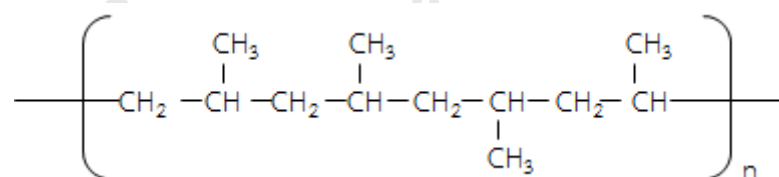
Figure 2.2 Polymerization of propylene to polypropylene



a) Isotactic polypropylene



b) Syndiotactic polypropylene



c) Atactic polypropylene

Figure 2.3 PP configurations in a) isotactic, b) syndiotactic and c) atactic forms

Polypropylene has good balance properties with excellent physical, mechanical and thermal properties at room temperature. General properties of polypropylene include low density, high stiffness, good heat and chemical resistance, and

recyclability. These properties are related to intrinsic polymer structure such as tacticity, polymer chain lengths and comonomers. Depending on the desired properties, polypropylene is produced commercially in many types. Polypropylene having only propylene monomer in the polymer chains is known as homopolymer PP, and it is meant to be the isotactic polypropylene. Random and block copolymers contain about 1-8% by weight of ethylene or higher alkenes as a comonomer. Impact copolymers have a rubber phase content of 5-25% such as ethylene-propylene rubber (EPR) and ethylene-propylene-diene monomer (EPDM) rubber.

Homopolymer polypropylene is the most commonly utilized material. Homopolymers exhibit more stiffness, toughness, high heat resistance, chemical resistance and surface hardness than copolymers but their impact strength at low temperature is poor. Copolymers have a slightly higher impact resistance and flexibility, better clarity and lower melting point than homopolymers. By increasing the ethylene comonomer content, the melting point is decreased. Impact copolymers have enhanced impact properties at both room and low temperatures at the expense of the stiffness [28-32]. Table 2.1 shows typical properties of polypropylene.

Table 2.1 Typical properties of polypropylene [28-32]

Properties	Units	PP
Physical		
Density	g/cm ³	0.90–0.91
Hardness (Shore)	D scale	D76
Water absorption, 24 h	%	<0.01
Shrinkage	%	1.0-2.0

Table 2.1 Typical properties of polypropylene [28-32] (cont'd)

Properties	Units	PP
Mechanical		
Tensile modulus	GPa	1.4–1.8
Tensile strength	MPa	22–35
Elongation at break	%	10–60
Flexural modulus	GPa	1.0–1.39
Notched Izod	kJ/m	0.03–0.13
Thermal		
HDT at 1.81 MPa	°C	60–65
HDT at 0.45 MPa	°C	75–107
Thermal		
Vicat softening temperature	°C	130–148
CTE	$10^{-5}/^{\circ}\text{C}$	9.0

2.1.2.2 Applications of Polypropylene

Polypropylene is one of the most multipurpose thermoplastic materials and very popular as a high volume plastic commodity. Its low cost makes it useful in various applications. Polypropylene can be made for a wide range of applications by compounding with fillers, pigments, elastomers, etc. Table 2.2 shows the main applications of PP in different market sectors [28, 31].

Table 2.2 Typical applications of PP in each market sector [28, 31]

Market sector	Typical applications
Household	Buckets, toys, luggages, food processors, bowls, bottles, bottle caps, containers, laundry baskets, etc.

Table 2.2 Typical applications of PP in each market sect [28, 31] (cont'd)

Market sector	Typical applications
Automotive	Bumpers, steering, wheel covers, spoilers, tool boxes, battery cases, mudguards, consoles, wheel arch liners, side protective strips, radiator grilles, etc.
Fibers	Woven carpet backings, monofilament for ropes and cordages, geotextiles, outdoor apparels, disposable diapers, woven filters, packaging sacks, etc.
Domestic appliances	Microwave oven cabinets, hand mixers, iron and coffee maker body parts, refrigerator parts, washing machine parts, juice centrifuges, etc.
Packaging	Films, margarine and ice-cream tubs, meal trays, blister packaging, dessert cups, strapping tapes, etc.
Pipes and fittings	Waste water pipes, pressure pipes, heat exchangers, corrugated pipes, drinking straws, etc.
Furniture	Stackable chairs, garden tables, etc.
Medical devices	Centrifuge tubes, connectors, syringes, needle shields, drug containers, surgical trays, etc.

2.1.2.3 Main Problems of Polypropylene

The major disadvantages of unfilled polypropylene compared with other thermoplastic materials are significantly higher shrinkage, higher thermal expansion, lower impact strength (especially at low temperatures), and higher warpage than ABS and HIPS. Table 2.3 shows the properties of PP compared with other thermoplastics [31]. Polypropylene shows a high shrinkage coefficient during cooling owing to its

semicrystalline nature which negatively affects the dimensional stability and leads to distortion and warpage. In addition, it has a low adhesion to the typical surfaces as a bed platform of 3D printer (see Figure 2.4) [16, 28].

Table 2.3 Comparison of unfilled PP with other thermoplastics [31]

Property	PP	ABS	HIPS
Shrinkage (%)	1.9	0.6	0.5
Thermal expansion ($\times 10^{-5}/^{\circ}\text{C}$)	9.0	8.0	7.0
Notched Izod impact strength at 23 °C (kJ/m)	0.07	0.2	0.1



Figure 2.4 The problem of printed PP sample by 3D printing technique [16]

2.1.3 Fillers for Property Modification of Polypropylene

Fillers for PP have been used in large quantities in many fields of applications for many years. Generally, fillers are classified into inorganic and organic fillers. The examples of inorganic and organic fillers can be used for property modification of PP as shown in Table 2.4 [33]. Fillers are mixed with PP to reduce costs or improve properties [34]. Typically, inert fillers or extenders are inexpensive materials that are added mainly

to increase bulk, and make the filled polymer composites cheaper. However, fillers, such as calcium carbonate (CaCO_3), talcum, clay and barium sulfate, can enhance stiffness and heat resistance. Reinforcing fillers improve mechanical and thermal properties such as tensile strength, tensile modulus and heat distortion temperature due to decreasing chain mobility and increasing orientation of polymers. Reinforcing fillers include glass fiber, mica, wollastonite, etc. The effect of fillers on the composite properties intensively depends on particle size, particle size distribution, purity, shape, aspect ratio (L/D), surface treatment, and degree of dispersion of filler in polymer [31, 35].

Table 2.4 Fillers for modification of polypropylene property [33]

Type	Subtype	Example
Inorganic filler	Oxide	Silica, Titanium oxide, Magnesium oxide, Antimony oxide
	Hydroxide	Aluminum hydroxide, Magnesium hydroxide, Calcium hydroxide
	Carbonate	Calcium carbonate, Dolomite
	Sulfate	Basic magnesium sulfate, Barite
	Silicate	Talcum, Glass fiber, Clay, Mica, Glass balloon, Glass beads, Calcium silicate, Montmorillonite, Bentonite, Wollastonite
	Carbon	Carbon black, Graphite, Carbon fiber
Organic filler		Wood powder, Jute, Kenaf fiber, Hemp fiber, Nylon Fiber, Aromatic polyamide fiber

Among the variety of fillers used in PP formulations, talcum, calcium carbonate (CaCO_3) and glass fiber are applied in the largest quantities [31, 35, 36]. The important information about them will be discussed in the following paragraphs.

2.1.3.1 Talcum

Talc is a hydrated magnesium silicate mineral with the chemical composition of $\text{Mg}_3\text{Si}_4\text{O}_{10}(\text{OH})_2$. The mineral talc consists of thin layers of magnesium hydroxide in octahedral coordination sandwiched between layers of silica in tetrahedron coordination (Figure 2.5) [37]. The sandwiched sheets are weakly bonded by van der Waals forces resulting in them being very easily breakable. Talc is the softest mineral (Mohs hardness of 1.0), very crumbly and slippery. The commercial form of talc is plate-like with an aspect ratio of 15-20. Talc has particle size from 2 μm to larger than 45 μm and specific gravity from 2.7 to 2.8. It is used as an extender due to its inexpensive price.

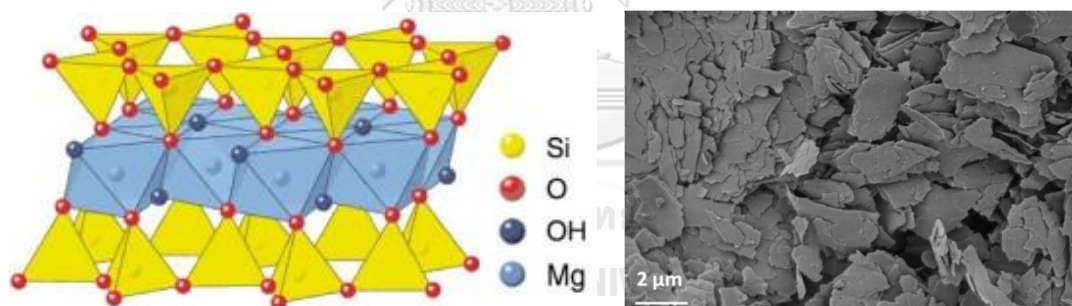


Figure 2.5 Schematic images of talc (a) chemical structure, and (b) SEM [37]

(Source: <http://vaaidehiminerals.com/mineralogy-geology/>)

Talc is typically used in polypropylene at loading of 10-40% by weight. Talc-filled PP grades exhibit increased stiffness (Figure 2.6), flexural modulus, heat deflection temperature, surface aesthetics, improved scratch and mar resistance, low coefficient of thermal expansion, low shrinkage (Table 2.5), low tensile strength, and low impact strength. The color of talc-filled resins ranges from white to brown depending on the original source of talc [29, 31, 35, 38, 39].

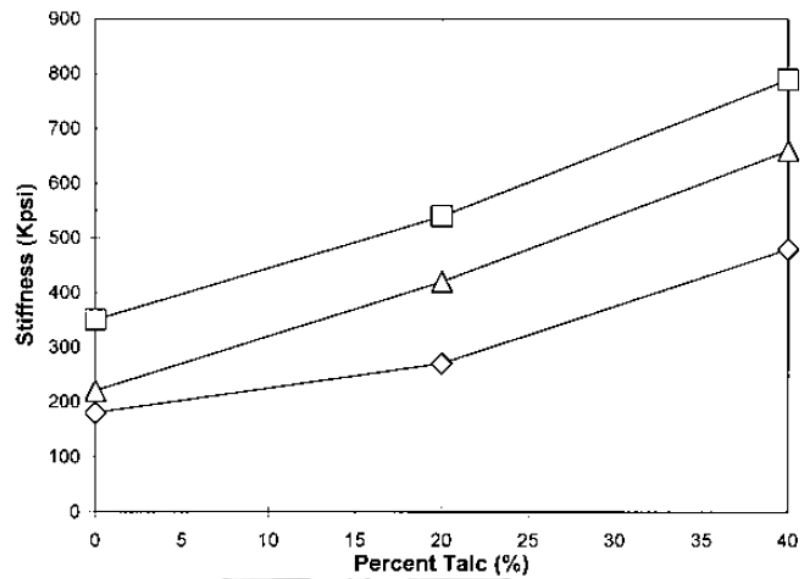


Figure 2.6 Effect of talc on stiffness. □ High crystalline PP; △ Homopolymer PP; ◇ Copolymer PP [29]

Table 2.5 Effect of 30% talc on shrinkage compared with pure ABS [29]

Polymer	Talc (wt%)	Shrinkage (in./in.)	%Change
Homopolymer PP	0	0.018	39
	30	0.011	
Copolymer PP	0	0.021	59
	30	0.009	
ABS (comparison)	0	0.005	-

2.1.3.2 Calcium carbonate

Calcium carbonate (CaCO_3) has three types of crystalline forms, which are calcite (Trigonal), aragonite (Orthorhombic) and vaterite (Hexagonal). Calcite is the most stable crystal structure as shown in Figure 2.7 [40]. CaCO_3 is produced from chalk, limestone or marble. Commercial grades typically comprise 95-98% CaCO_3 , with the

remainder being of metal oxides. It has a specific gravity of 2.7, Mohs hardness of 3, and particle sizes range from 1 to 100 microns [39].

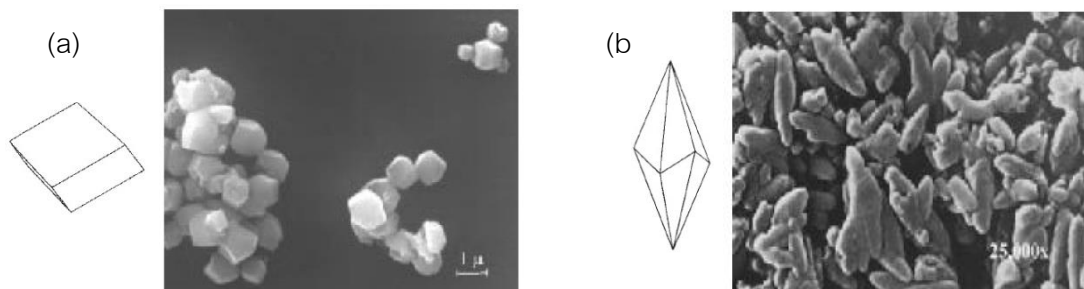


Figure 2.7 Crystal forms of calcium carbonate (a) trigonal-rhombohedral calcite; (b) trigonal-scalenohedral calcite [40]

Calcium carbonate is one of the most used fillers for plastics, and is commonly used in PP at the same loading as talc (10-40% by weight). It is inexpensive and generally used as a bulk extender. It tends to enhance dimensional stability and surface finish compared to unfilled grades [28, 31, 41].

2.1.3.3 Glass fiber

Glass fiber is an inorganic material containing more than 50% silica (SiO_2) and having arbitrary structures. The fibers are manufactured by blending quarry products (sand, kaolin, limestone and colemanite). The properties of fibers depend on the composition of the raw materials. It has specific gravity of about 2.4 to 2.6 g/cm^3 and tensile strength of about 3445 to 4890 MPa. Glass fibers are produced in several types with different chemical compositions to use in different applications.

A-glass (for alkali) is the original glass fiber type used in windows, bottles, etc. It is not popular in plastic composites due to its moisture absorption.

C-glass (for chemical) has especially good chemical resistance and is used in corrosive acid environments.

D-glass (for dielectric) is a glass type with low dielectric constant used mainly in electronics industry.

E-glass (for electrical) is a general purpose borosilicate glass with poor acid resistance, good moisture resistance and excellent electrical resistivity. It is the most commonly used for reinforcement purposes.

S-glass (for stiff) has an extra high strength, modulus and stability in extreme environments for advance composites in military, aerospace and defense applications.

Glass fibers are used to enhance strength and rigidity. The composites exhibit high tensile modulus, tensile strength, heat deflection temperature, and compressive strength compared to the unmodified resins. Shrinkage is highly reduced in the flow direction due to the orientation of glass fibers during processing. Unfortunately, the addition of glass fibers decreases the ductility and impact strength of these composites [29, 31, 32, 38, 41].

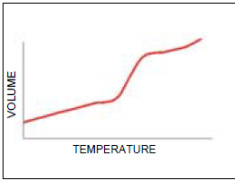
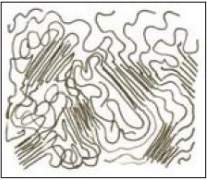
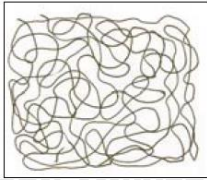
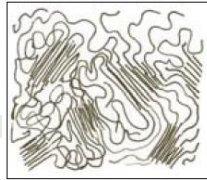
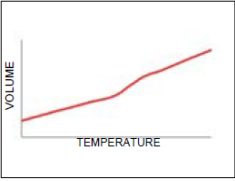
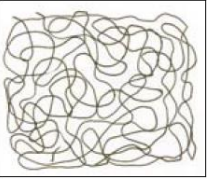
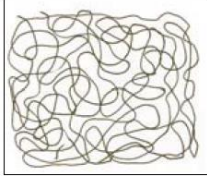
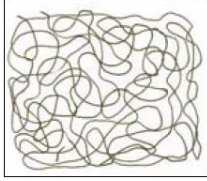
2.1.4 Shrinkage behavior of polymers

2.1.4.1 Fundamental concepts of part shrinkage

In injection molding process, pressure is given to the molten polymer to produce parts and is cooled to room temperature. The cooled polymer shrinks due to changes in temperature and pressure. It is necessary to consider three parameters in order to control and predict the shrinkage: 1) Material (Degree of crystallinity, thermal properties, PVT (pressure-specific volume-temperature) diagram plots, and melt rheology), 2) Process conditions (Processing temperature, pressure, and cooling cycle time), and 3) Part geometry (Dimensions of length, width and thickness) [29]. So, it is needed to determine the effect of crystalline and amorphous structure on specific volume as a function of pressure, temperature, and cooling rate. Figure 2.8-2.9 show PVT

relationship for polypropylene (semicrystalline) and polycarbonate (amorphous). Moreover, the percent of shrinkage depends on the arrangement of polymer chains during polymerization process. Semicrystalline plastics include dense crystalline regions surrounded by amorphous regions. In melting state, both regions of molecule merge into one phase of disentangled and expanded chains. In cooling state, the molecules of polymer tend to arrange themselves back to their natural structure. There is no rearrangement of molecules for the amorphous plastic in cooling state. Therefore, semicrystalline plastics have a higher shrinkage than amorphous plastics [29, 31, 42]. Table 2.6 shows shrinkage phenomenon of polymers [43].

Table 2.6 Shrinkage phenomenon of polymers [43]

Polymer	Before transformation (Structure)	Heating effect (Volume increase)	Cooling effect	Shrinkage
Semi-crystalline 				Volumetric shrinkage due to cooling + Molecular organization <i>High shrinkage</i>
Amorphous 				Only volumetric shrinkage due to cooling <i>Low shrinkage</i>

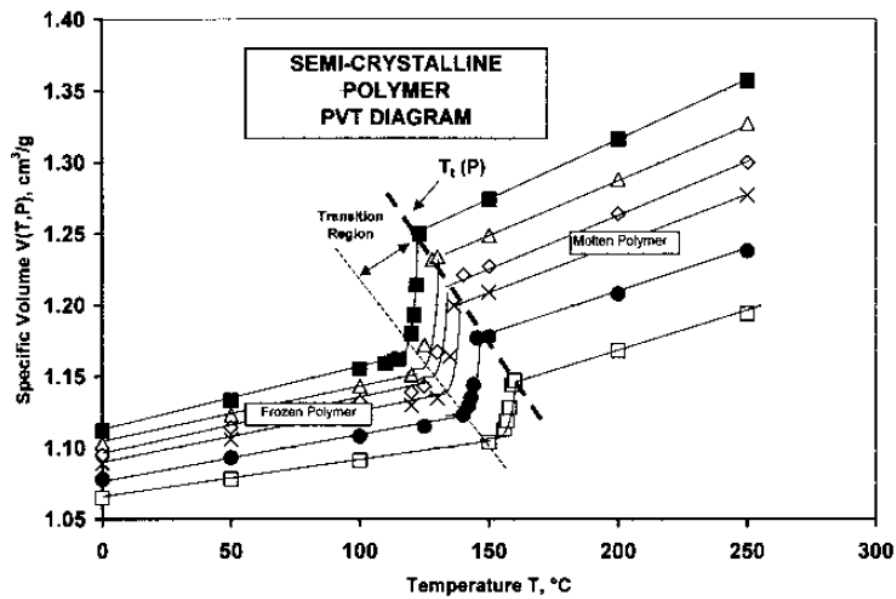


Figure 2.8 PVT diagram for polypropylene (semicrystalline resin). ■ $P=0.1\text{MPa}$; Δ $P=20\text{MPa}$; \diamond $P=40\text{MPa}$; \times $P=60\text{MPa}$; \bullet $P=100\text{MPa}$; \square $P=160\text{MPa}$ [29]

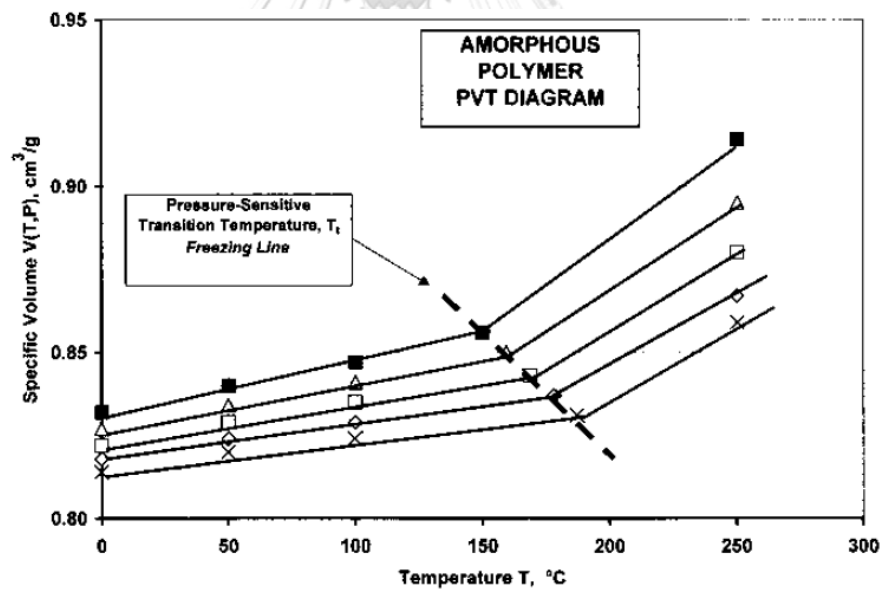


Figure 2.9 PVT diagram for polycarbonate (amorphous resin). ■ $P=0\text{MPa}$; Δ $P=30\text{MPa}$; \square $P=60\text{MPa}$; \diamond $P=90\text{MPa}$; \times $P=120\text{MPa}$ [29]

Generally, the linear shrinkage of amorphous and crystalline polymers is 0.1-0.8% and 1.0-2.0%, respectively. It is about 1.7% for polypropylene [35]. Shrinkage affects the dimensional stability of products. The linear shrinkage along the longitudinal

(parallel) flow direction is referred to as S_L and the transverse (perpendicular) flow direction is S_T . The shrinkage was calculated by the following equation [44]:

$$S_L = \left(\frac{L_m - L_s}{L_m} \right) \times 100 \quad (1)$$

where: S_L = shrinkage in longitudinal to flow, %
 L_m = mold length in longitudinal to flow, mm
 L_s = specimen length in longitudinal to flow, mm

$$S_T = \left(\frac{W_m - W_s}{W_m} \right) \times 100 \quad (2)$$

where: S_T = shrinkage in transverse to flow, %
 W_m = mold length in transverse to flow, mm
 W_s = specimen length in transverse to flow, mm

2.1.4.2 Effect of fillers on shrinkage

The magnitude of shrinkage for polymers depends on resin density or specific volume to change in pressure and temperature. The presence of fillers in the polymer matrix can reduce the shrinkage behavior of unfilled polymers. Moreover, filler type and filler content directly affect the shrinkage reduction. As fillers have a higher solid density than the polymer resins, the addition of filler to the polymer decreases the sensitivity of the density of composites to variations in pressure and temperature [31, 45]. Particulate fillers, such as talc, CaCO_3 and carbon black, have a low aspect ratio resulting in the balance of shrinkage of polymer composites which means isotropic shrinkage behavior because it shrinks equally in the longitudinal flow and transverse flow directions. On the other hand, reinforcing fillers, such as glass fiber, carbon fiber and wollastonite, have a high aspect ratio and rigid structure. The polymer composites exhibit differential shrinkage or anisotropic behavior because transverse flow direction has greater shrinkage than longitudinal flow direction [29, 36].

2.2 Literature Reviews

2.2.1 Effect of fillers on the mechanical properties of the printed samples by FDM technique

Carneiro et al. [16] used two commercial polypropylene homopolymer extrusion grades, a PP reinforced with 30 wt% glass fiber (GRPP) and a neat PP in this study in order to evaluate the performance of the fabricated parts by the FDM technique. The results indicated that the tensile modulus and ultimate tensile strength of GRPP-printed samples increased by around 30% and 40%, respectively, compared with unfilled PP specimens (see Figure 2.10). The presence of glass fibers in polypropylene matrix improved the performance of materials due to the reinforcement effect and showed the potential of glass fiber reinforced material for the FDM technique.

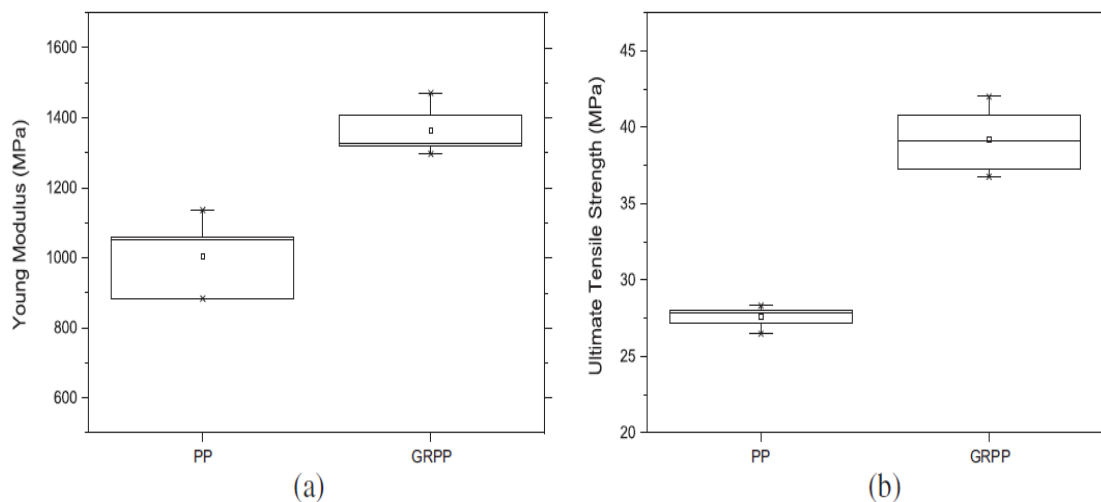


Figure 2.10 Tensile properties of polypropylene (PP) and glass reinforced polypropylene (GRPP) by FDM technique: (a) modulus; (b) strength [16]

Zhong et al. [25] developed ABS composites as a feedstock material for the FDM process by adding short glass fiber reinforcement. ABS polymer-commercial grade, short glass fiber reinforced ABS (GFABS-30), was used in this study. After being extruded and

cooled, the ABS composites could not be produced into filaments because of the brittleness of the material. Linear low density polyethylene (LLDPE) and PE wax were added into GFABS-30 to improve the processability. Due to the limited compatibility between the ABS composites and LLDPE, hydrogenated Buna-N was used to get rid of incompatibility problems. The results showed that the higher contents of short glass fibers from 0 to 18 wt% resulted in a higher tensile strength under longitudinal direction, as shown in Figure 2.11. However, adhesion strength between the layers of GFABS increased with the increase of short glass fiber content because it might enhance the chance of the layers getting adjacent to each other before the solidification. In conclusion, glass fibers significantly improved the tensile strength at the expense of reduced flexibility.

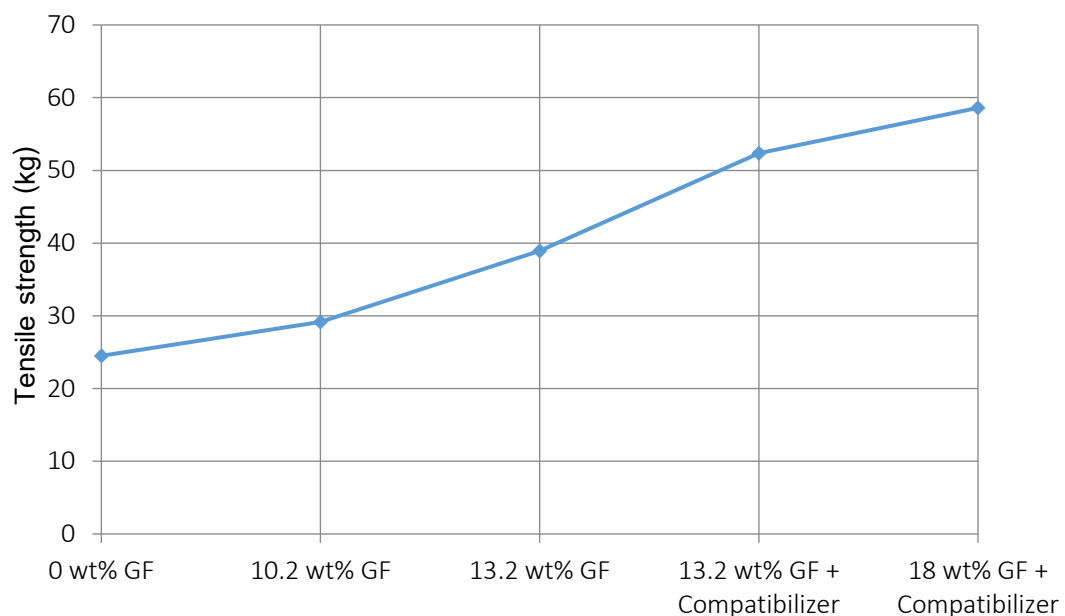


Figure 2.11 Tensile strength of short glass fiber reinforced ABS by FDM [25]

Tekinalp et al. [22] conducted experiments to study the effect of short carbon fiber on the mechanical properties of reinforced ABS composites. In this research, short carbon fiber-reinforced ABS composites at 10-40 wt% carbon fibers (CF) loading were produced

by compression molding (CM) and FDM process. The results of mechanical properties showed that tensile strength and modulus increased with increasing fiber loading in both techniques seen in Figure 2.12. In addition, the tensile properties of printed samples were still close to the CM samples owing to increasing the molecular orientation in the polymer chains and having good fiber dispersion. In summary, the carbon fiber reinforced composites had outstanding potential for the production of load-bearing parts.

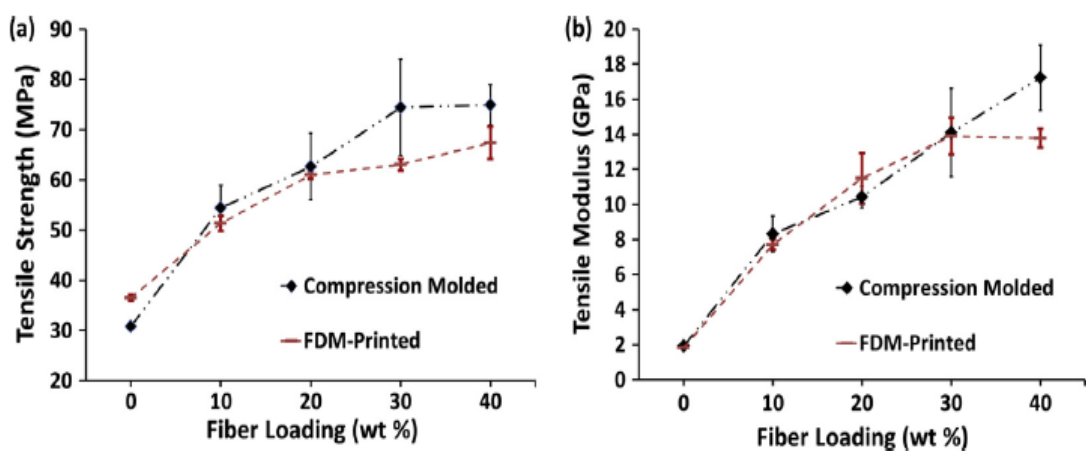


Figure 2.12 Effect of fiber loading and produced technique on (a) tensile strength, and (b) tensile modulus, of ABS/CF composites [22]

2.2.2 Effect of fillers on the shrinkage behavior of polypropylene

Jahani Y. [46] explained the effect of talc on the shrinkage behavior of PP. Neat PP resin had shrinkage in flow direction of about 1.67%. This study varied content of talc from 10 up to 50 wt% and the experiment found that higher content of talc in PP polymer gave lower shrinkage rate in flow direction as shown in Figure 2.13. It resulted from decreasing volume fraction of PP matrix.

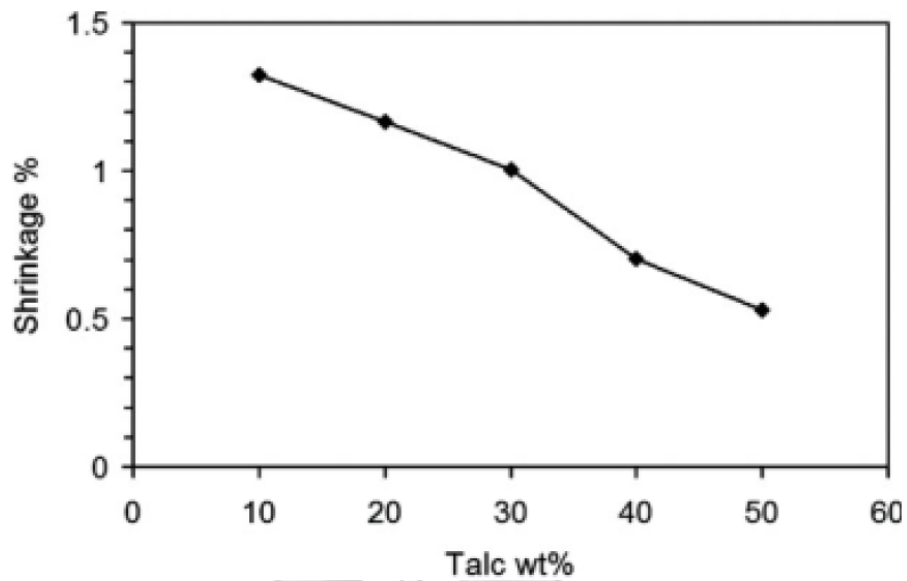


Figure 2.13 Shrinkage of various talc contents in flow direction [46]

Pontes et al. [47] indicated that content of glass fiber also effects on shrinkage of PP polymer. In this research, PP was mixed with various volume fractions of glass fiber (from 0 to 0.25). The results showed in Figure 2.14 that high volume fraction of glass fiber in PP matrix can extremely decrease shrinkage in the flow direction. The shrinkage fell from 1.3% of unfilled PP to 0.2% of 0.25 glass fiber fraction. On the other hand, the shrinkage in the across flow direction was not affected by adding glass fiber fraction.

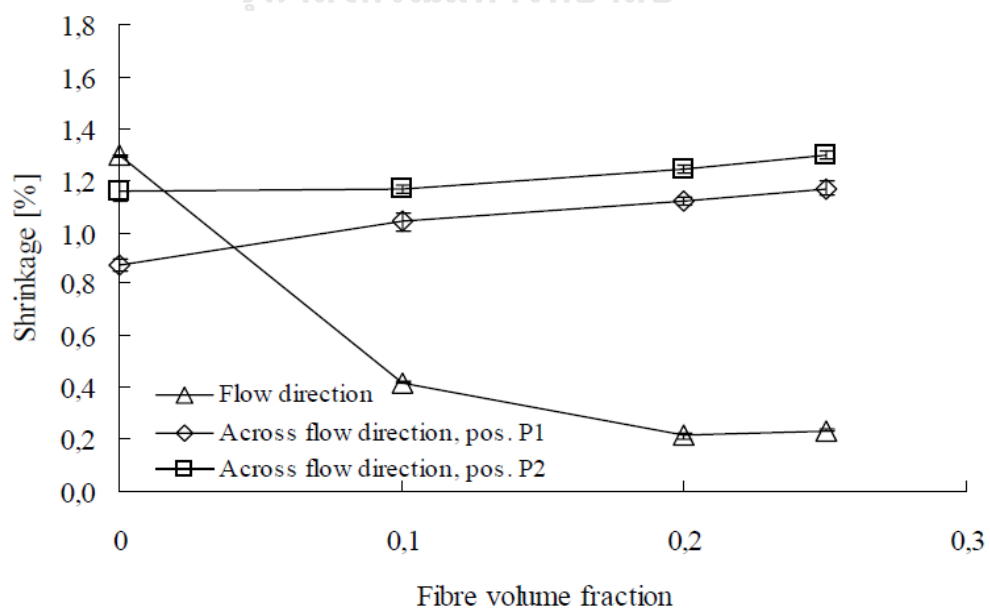


Figure 2.14 Shrinkage of PP at various amounts of glass fiber [47]

Karian H. G. [29] tested the shrinkage of mineral-filled PP composites with various loadings of 10-50 wt% CaCO_3 . From the results, increasing CaCO_3 content from 10 to 50 wt% showed that shrinkage value in the longitudinal flow direction decreased linearly from 1.3 to 0.8 % as seen in Figure 2.15. The reduction of shrinkage resulted from decreasing crystalline volume fraction of PP matrix resin.

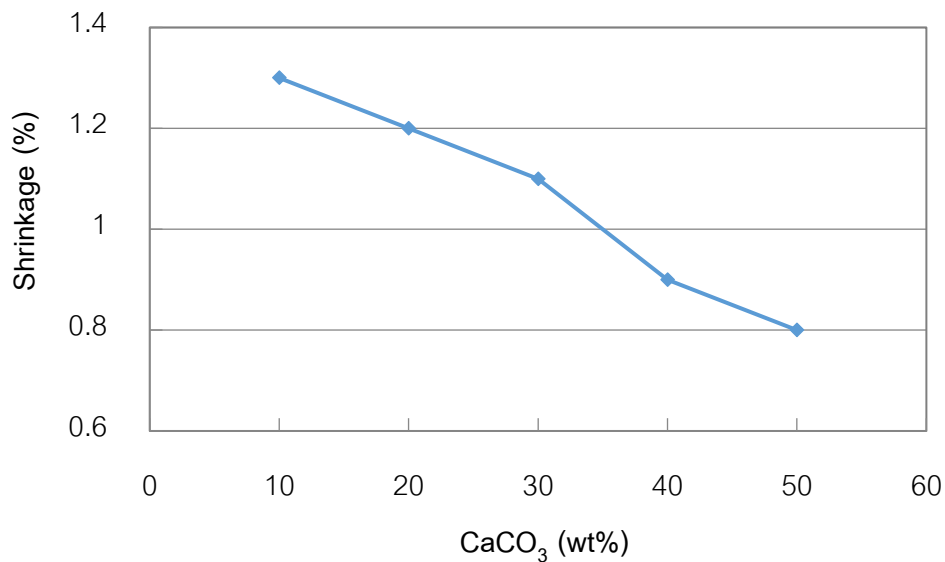


Figure 2.15 Shrinkage behavior of CaCO_3 filled-PP composites [29]

In addition, Karian H. G. [29] studied the effect of filler type on the shrinkage behavior in the parallel flow direction of polypropylene. Figure 2.16 exhibited a comparison of the shrinkage of PP composites filled with 40 wt% CaCO_3 , 40 wt% talc and 30 wt% glass fiber. This study found that 30 wt% glass fiber-filled PP had the lowest shrinkage behavior in the flow direction (0.3%). Afterward, 40 wt% talc-filled PP had a lower shrinkage than 40 wt% CaCO_3 -filled PP (1.2% versus 1.4%).

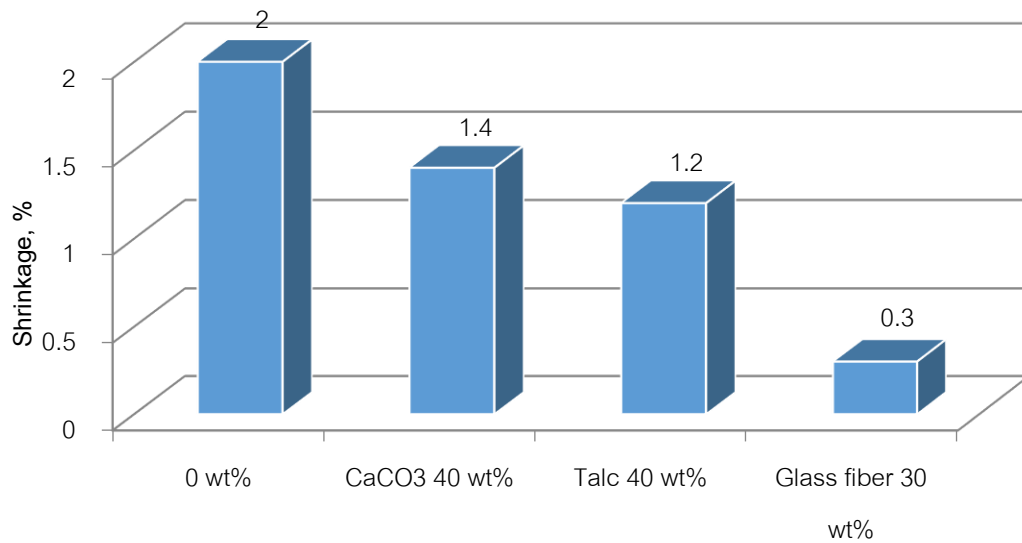


Figure 2.16 Effect of filler type on shrinkage behavior of polypropylene [29]

2.2.3 Effect of fillers on the filament bonding of the printed samples by FDM technique

Tekinalp et al. [22] studied the effect of short carbon fiber on the void formation of reinforced ABS composites. The short carbon fibers were added into ABS matrix at 10-40 wt% carbon fibers (CF) and produced by FDM process. However, at 40 wt% fiber content (high loading) it was difficult to process due to nozzle clogging. As presented in Figure 2.17e-h, the average size of the void among the filaments (inter-filament void) significantly decreased with the addition of carbon fibers compared to the FDM neat-ABS specimen. However, the augmentation of carbon fibers increased the inner-filament voids, which are gaps between fibers and polymer. These voids can generate stress concentration points inside leading to the samples failing at lower stress. Moreover, the presence of carbon fibers in the ABS matrix reduced die swelling and also increased thermal conductivity resulting in better adjacent filaments and smaller gaps.

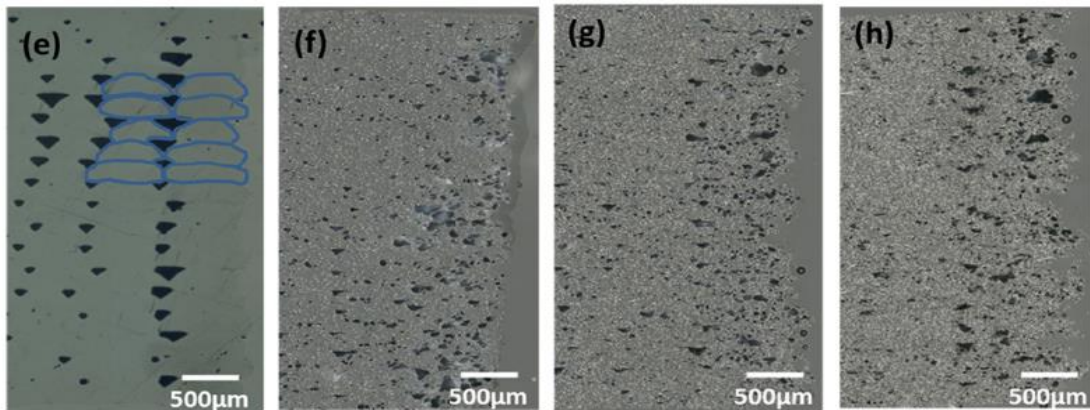


Figure 2.17 SEM micrographs of fracture surface of (e) Neat ABS, (f) 10%CF, (g) 20%CF, and (h) 30%CF [22]

2.2.4 Effect of printing conditions on the mechanical properties

Carneiro et al. [16] investigated the effect of the printing conditions including printing orientations, layer thickness and infill degree on the mechanical properties. For printing orientation study, 0° orientation sample showed the best result in tensile property when compared to other samples ($\pm 45^\circ$, 90° , 45° and $0-90^\circ$) with constant layer thickness and infill degree. This performance can be explained by printing orientation which aligned to applied stress direction. For effect of layer thickness, this parameter was studied by comparing between thickness of 0.20 and 0.35 mm. It can be seen that higher thickness layers perform a slightly higher tensile strength value. Moreover, infill degree effect was studied by varying percentage 20 to 100. This parameter significantly affected both of modulus and strength value. It showed a difference in result of more than 250%. Figure 2.18 concludes the overview effect of each parameter to mechanical property.

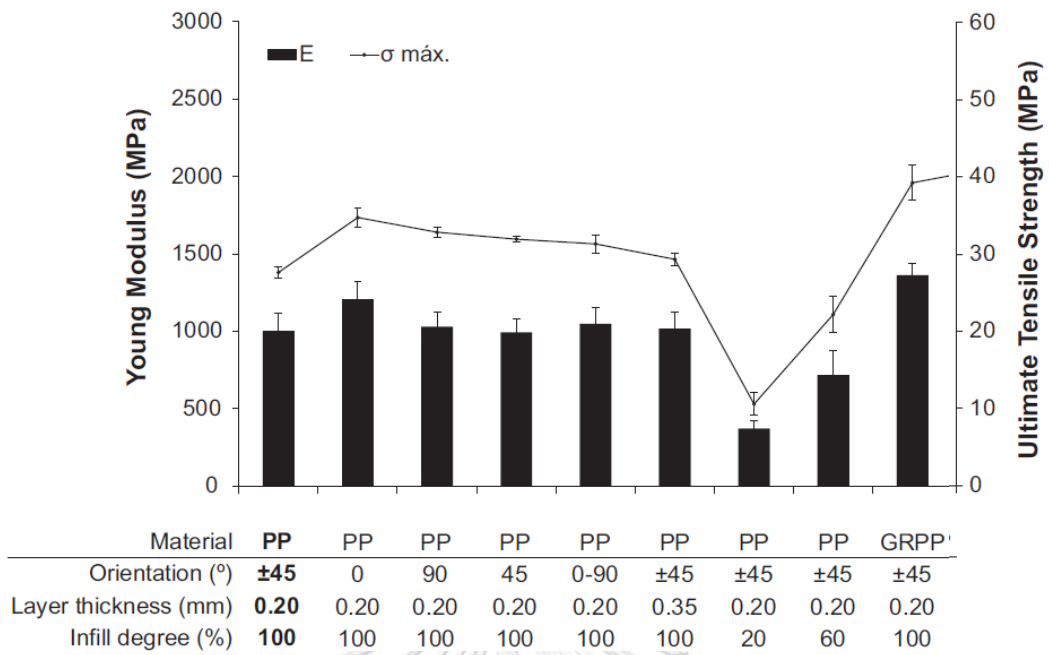


Figure 2.18 Tensile modulus and tensile strength of the printed parts by FDM [16]

CHAPTER III

EXPERIMENT

Procedure of the study is explained in this chapter which is divided into four sections. First, raw materials used in this study are shown in section 3.1. Next, material screening is described in section 3.2. Sample preparation is then explained in section 3.3. Finally, characterization methods in this research are proposed in section 3.4. Flowchart of experimental work is presented in Figure 3.1.

3.1 Materials

The raw materials used in this research were mainly polypropylene. Polypropylene homopolymers (6 grades) were obtained from HMC Polymers Co., Ltd., Thailand, as shown in Table 3.1. The filaments of PLA and ABS, the commercial 3D printing materials, were purchased from Siamregrap Company, Thailand. Talc (MICROTUFF[®] 1000 talc) with a median particle size of 1.2 μm was purchased from Minerals Technologies Inc. Milled glass fibers (EMG13-70 and EMG13-200) with a filament diameter of 13 μm , an average length of 70 μm and 200 μm , and silane-based sizing agent were bought from QUATEK Inc.

Table 3.1 Melt flow rate (MFR) of Polypropylene homopolymer

Polypropylene	MFR (g/10min)
PP1	2.0
PP2	2.1
PP3	2.8
PP4	3.5
PP5	4.0
PP6	6.0

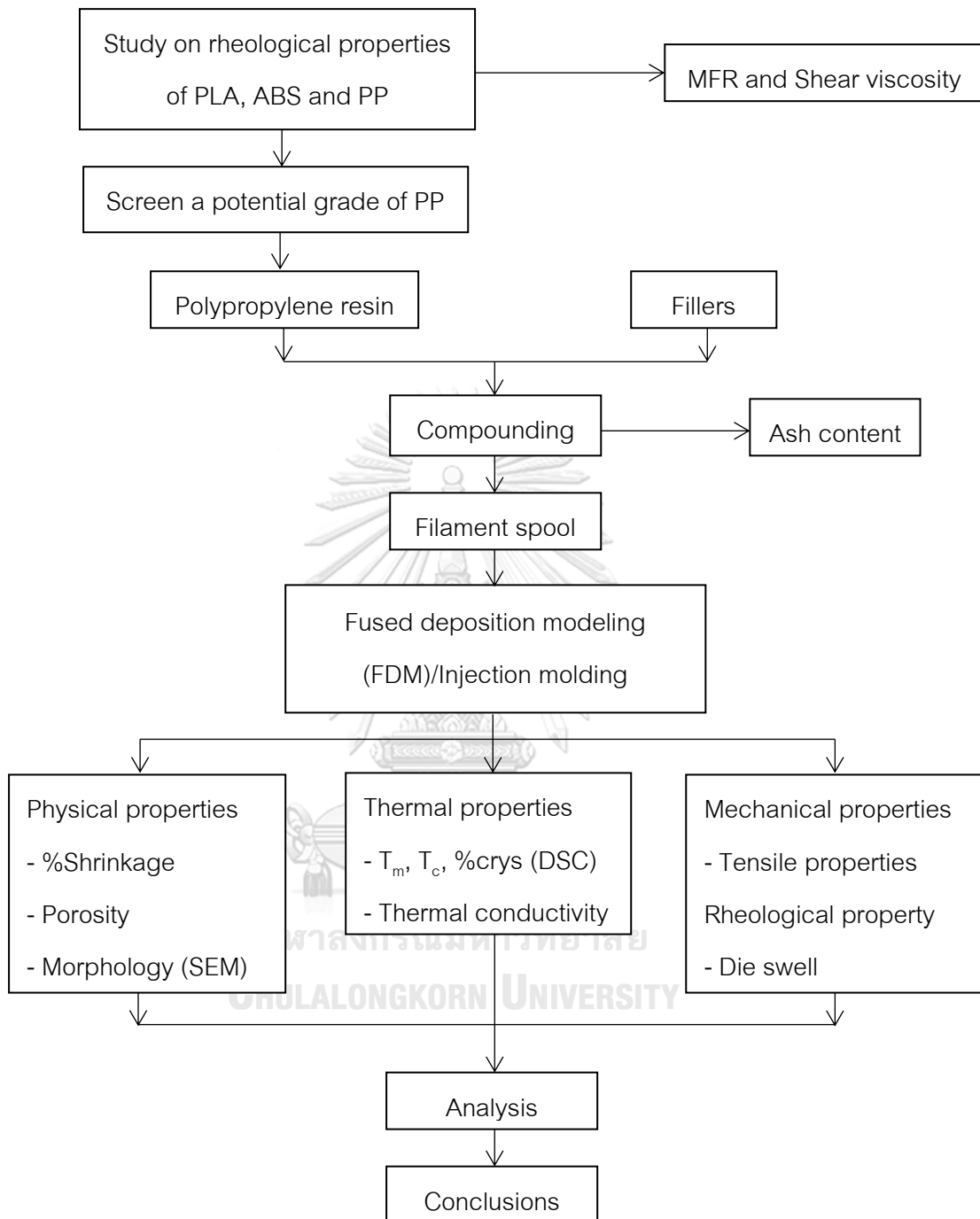


Figure 3.1 Flowchart of experimental work

3.2 Material Screening

The commercial printing materials, PLA and ABS, were measured in order to find a range of the melt flow rate (MFR) at its printing temperature. The shear viscosity of the six grades of PP was evaluated at various shear rate compared with PLA and ABS to select the potential PP grade.

3.2.1 Melt Flow Index Measurement

Melt flow indexer (Goettfert, Model MI-4) was used to study the melt flow rate of the existing materials (PLA and ABS) and neat PP. It measured the mass of polymer in grams per ten minutes (g/10min) with three repeats. The polymer flowed through a smooth straight die with a diameter of 2.0955 mm and 8.000 mm in die length according to ASTM D1238 standard. The materials were preheated for 7 minutes and extruded at 230°C/2.16kg load for PP, at 190°C/2.16kg load for PLA and at 230°C/2.16kg load for ABS. Figure 3.2 shows a melt flow indexer as used in this study.



Figure 3.2 Melt flow indexer (Goettfert, Model MI-4)

(Source: <http://www.asi-team.com/asi%20team/gottfert/Gottfert%20data/MI-english.pdf>)

3.2.2 Shear Viscosity Measurement

Capillary rheometer (Malvern, Model RH7), as shown in Figure 3.3, was used in order to determine the shear viscosity of the existing materials (PLA, ABS), neat PP and

compounded PP at various shear rates. The samples were tested at a shear rate ranging from 10 up to 1000 sec^{-1} . The length/diameter ratio (L/D) of the selected capillary die was 16 (L = 16 mm, D = 1 mm). The tests were performed at a constant temperature of 190 and 195°C for PLA, 230 and 235°C for ABS, and 230 °C for PP to simulate the actual processing temperature used in the fused deposition modeling (FDM) technique.



Figure 3.3 Capillary rheometer (Malvern, Model RH7)

(Source: <http://www.aimil.com/Resources/Products/Original/814.jpg>)

3.3 Sample Preparation

3.3.1 Polypropylene Compounding

The compounding process was carried out on a co-rotating twin screw extruder (LabTech, Model LTE26-40) with a screw diameter of 26 mm, length/diameter ratio (L/D) of 40 and downstream water bath connected to sidecut pelletizer (Figure 3.4). According to recipes in Table 3.2, the polypropylene pellets and fillers were fed into each main hopper by loss in weight gravimetric feeders. The screw speed was set at 400 rpm. The barrel temperature profile of 10 zones was 195 to 230°C from the feed section to die head. The compounded extrudates were cooled in room temperature water and then were chopped into granules by a pelletizer.



Figure 3.4 Twin screw extruder (LabTech, Model LTE26-40)

(Source: <http://www.milabtech.com/extruders.htm>)

Table 3.2 The recipes of composites used in this study

Sample	PP (wt%)	Talc (wt%)	Glass fiber- 70 μ m (wt%)	Glass fiber- 200 μ m (wt%)
PP	100	-	-	-
PP+10%talc	90	10	-	-
PP+20%talc	80	20	-	-
PP+30%talc	70	30	-	-
PP+10%MF (70 μ m)	90	-	10	-
PP+20%MF (70 μ m)	80	-	20	-
PP+30%MF (70 μ m)	70	-	30	-
PP+10%MF (200 μ m)	90	-	-	10
PP+20%MF (200 μ m)	80	-	-	20
PP+30%MF (200 μ m)	70	-	-	30

3.3.2 Ash content

Muffle Furnace (CABOLITE, model GPC12/131) as shown in Figure 3.5 was used in order to determine the content of filler in PP after compounding according to ASTM D5630. The samples of 10g were heated from room temperature to 350°C with a heat rate

of 10°C/min and then they were held for 1 hour at this temperature. The samples were heated again from 350°C to 650°C at 10°C/min and held for 1 hour. After the prescribed duration, the samples were cooled down to room temperature. Ash content was calculated by following equation:

$$\text{Ash content (\%)} = \frac{(W_3 - W_1)}{(W_2 - W_1)} \times 100 \quad (3)$$

where:

- W_1 = mass of crucible, g
- W_2 = mass of crucible plus mass of sample, g
- W_3 = mass of crucible plus mass of ash, g



Figure 3.5 Muffle Furnace (CABOLITE, model GPC12/131)

3.3.3 Filament Preparation

A single screw extruder (LabTech, LE25-30) equipped with a screw diameter of 25 mm, a length/diameter ratio (L/D) of 30 and a die diameter of 3 mm was used in order to fabricate the filament (Figure 3.6). The compounded samples were fed from the feed to die zones under the temperature profile of 230°C (5 zones). During the filament process, the extruder screw speed and pulling rolls speed were set at 80 rpm and 40 m/min to produce filaments diameter of about 1.75 mm (± 0.1 mm) for fused deposition modeling

(FDM) technique. All extrudates were cooled down to room temperature in water bath before spooling into the spool. The filament spool is shown in Figure 3.7.



Figure 3.6 Single screw extruder (LabTech, LE25-30)

(Source: <http://www.milabtech.com/extruders%20lab.htm>)



Figure 3.7 Filament spool of 1.75 mm diameter

(Source: <http://www.aliexpress.com/item/Impressora-3d-PRINTER-Flexible-PLA-filament-Soft-TPU-1-75mm-for-3D-printing-1kg-spool/32224593872.html>)

3.3.4 Test Specimen Preparation

3.3.4.1 3D Printing

In order to fabricate neat PP and compounded PP parts, the FDM 3D printer (Siamreap, Model Delta X pro) in Figure 3.8 was used. The nozzle diameter of

FDM 3D printer was 0.5 mm. The specimens of tensile (ASTM D638 type I, thickness of 2 mm) and shrinkage (square boxes of 25 mm length x 25 mm width x 10 mm height) were designed in CAD software, and STL file was converted to G-code before sending into 3D printer. During 3D printing process, the nozzle and bed temperatures were heated at 210°C and 80°C, respectively. The PP plate was used as bed for reason of adhesion improvement between the printed sample and the bed [16]. The velocity of printing was set at 20 mm/s for the first layer and 50 mm/s for other layers. The test specimens were printed with layers of 0.2 mm thickness each. The infill degree of 100% was chosen in this study. The print orientation of crossed 45° ($\pm 45^\circ$) for the tensile specimens and 0-90° for the square boxes were selected, as seen in Figure 3.9.



Figure 3.8 FDM 3D printer (Siamreap, Model Delta X pro)

(Source: <http://www.siamreap.com>)

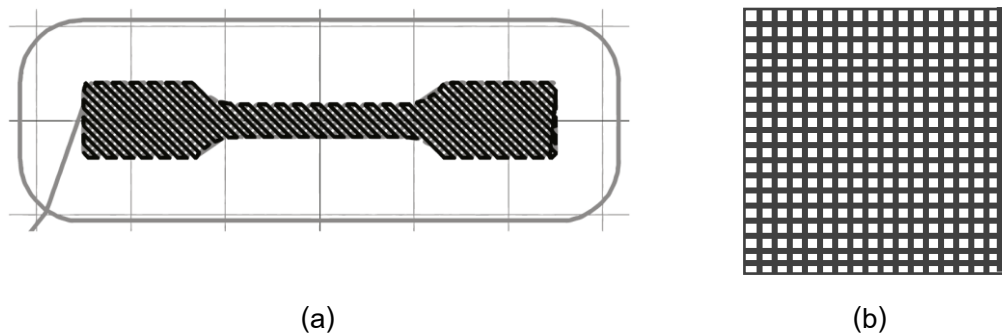


Figure 3.9 (a) Orientation of crossed 45° ($\pm 45^\circ$); (b) Orientation of 0-90°

(Source: Carneiro, O.S., Silva, A.F. and Gomes, R. Fused deposition modeling with polypropylene. *Materials & Design* 83 (October 2015) : 768–776.)

3.3.4.2 Injection

An electric injection machine (Toshiba, model EC100NII-2A) with a single screw extruder, seen in Figure 3.10, was used to produce the test specimens. Tensile type I and shrinkage specimens were injection molded at injection temperature range of 220 to 235°C from hopper to nozzle, mold temperature of 45°C, injection pressure of 85 MPa and injection speed of 25 mm/s.



Figure 3.10 Electric injection machine (Toshiba, model EC100NII-2A)

3.4 Characterization Methods

3.4.1 Differential Scanning Calorimetry (DSC)

The thermal analysis of the polymer and composites was characterized by a differential scanning calorimeter (DSC) model DSC 204 F1, manufactured by Netzsch (Figure 3.11). The sample of 5 mg was maintained at 30°C for 5 min and then heated from 30°C to 200°C (250°C for PLA and 300°C for ABS) with a heating rate of 10°C/min following ASTM D3418 standard. The sample was held for 5 min at this temperature to remove the previous thermal history. It was then cooled down to 30°C at 10°C/min (1st scan). Next the temperature was raised again at 10°C/min to 200°C (250°C for PLA and 300°C for ABS)

to obtain melting temperature (T_m). Finally, the sample was cooled down again to 30°C at 10°C/min to determine the crystallization temperature, T_c , (2nd scan). All samples were manipulated under a nitrogen atmosphere. The percentage of crystallinity (%crys) was calculated by following equation:

$$\%crys = \frac{\Delta H_m}{\Delta H_m^\circ} \times \frac{100}{X} \quad (4)$$

where: ΔH_m = specific heat of melting, J/g
 ΔH_m° = specific melting heat of 100% crystalline isotactic PP, 209 J/g
 X = weight fraction of PP in the composites



Figure 3.11 Differential Scanning Calorimeter (Netzsch, Model DSC 204 F1)

(Source: http://www.azonano.com/images/equipments/EquipmentImage_299.jpg)

3.4.2 Tensile Property Measurement

Tensile properties were determined by a universal testing machine (Zwick/Roell, Model Z050) according to ASTM D638 standard. Universal testing machine with a load cell of 2.5 kN is shown in Figure 3.12. Tensile Type-I were prepared by FDM technique and injection molding. At least five specimens were tested using a crosshead speed of 5 mm/min with the preload of 2 N for each composition to obtain ultimate tensile strength.



Figure 3.12 Universal testing machine (Zwick/Roell, Model Z050)

(Source: <http://www.zwickusa.com/en/products/static-materials-testing-machines/testing-machines-from-5-kg-to-250-kg/allround-line-materials-testing-machines.html>)

3.4.3 Scanning Electron Microscope (SEM)

The filament bonding and interfacial adhesion between matrix and glass fiber were obtained using scanning electron microscope (SEM) model JSM-6510LV, manufactured by JEOL, USA (seen in Figure 3.13). In order to study the dispersion of glass fiber in the matrix, the maps of distribution were carried out by using energy dispersive spectroscopy (EDS). The samples were soaked in liquid nitrogen for 15 minutes and then broken into pieces. The fracture surfaces were coated with gold using a sputter coater (JEOL, Model JFC-1600) to have an electrical conductivity. The SEM micrographs of the fracture interfaces were obtained at an acceleration voltage of 20 kV.



Figure 3.13 Scanning Electron Microscope (JEOL, Model JSM-6510LV)

(Source: http://www.jeol.co.jp/en/products/detail/product_file/file/p37_jsm6510_g01.jpg)

3.4.4 Die swell

The die swell ratio of the extrudate diameter to the die diameter was measured at various shear rates by capillary rheometer (Malvern, Model RH7) with the length/diameter ratio (L/D) of 16 (L = 16 mm, D = 1 mm). All compounded PP samples were measured under a shear rate range of 10 to 1000 sec⁻¹ and a constant temperature of 210°C.

3.4.5 Thermal conductivity

Thermal diffusivity (α) of the PP composites was evaluated by NETZSCH model LFA 447 according to ASTM E1461, flash method. The disc- shape samples of 12.7 mm in diameter and 2 mm in thickness were prepared. Thermal diffusivity was carried out in temperatures ranging from 25 to 100°C. Thermal diffusivity was calculated using Parker's equation as follows:

$$\alpha = 0.1388 \cdot \frac{l^2}{t_{1/2}} \quad (5)$$

where:

- α = thermal diffusivity, mm²/s
- l = thickness of the sample, mm
- $t_{1/2}$ = time to reach half of the maximum temperature increase, s

Specific heat capacity (C_p) was obtained by a differential scanning calorimeter (DSC), Netzsch model DSC 204 F1. A sapphire sample was used as a standard to calibrate in the same range of temperatures before testing. All samples were carried out at temperatures ranging from 0°C to 200°C with a heating rate of 20°C/min.

Density was measured by water displacement method using a top loading electronic balance (Mettler-Toledo, model XS204) with a density kit according to ASTM D792. The density was calculated by following equation:

$$\rho = \left(\frac{A}{A-B} \right) \cdot \rho_0 \quad (6)$$

where: ρ = density of the specimen, g/cm³
 A = weight of the specimen in air, g
 B = weight of the specimen in distilled water, g
 ρ_0 = density of the distilled water at testing temperature, g/cm³

Finally, the thermal conductivity was calculated as follows:

$$\lambda = \alpha \cdot C_p \cdot \rho \quad (7)$$

where: λ = thermal conductivity, W/(m·K)
 α = thermal diffusivity, mm²/s
 C_p = specific heat capacity, J/(g·K)
 ρ = density, g/cm³

3.4.6 Shrinkage Measurement

The shrinkage behavior of the 3D printed samples which were fabricated with FDM technique was studied using 3D scanner, INFINITE 2.0, CimCore as seen in Figure 3.14. A scan mode was used to scan the square boxes (a length of 25 mm, width of 25 mm, and height of 10 mm). The shrinkage rate was presented in 3D contour plot in X, Y and Z directions.



Figure 3.14 3D scanner (INFINITE 2.0, CimCore)

(Source: http://www.mahrkorea.co.kr/data/ect/07_New%20Cimcore%20INFINITE%202.0.pdf)

The injected specimens were used for the measurement of mold shrinkage in accordance with ASTM D955. At least five specimens were determined by a measuring microscope, StarLite Model 250, in Figure 3.15. The shrinkage was measured 48 hours after molding in the longitudinal flow and transverse flow directions.



Figure 3.15 Measuring microscope (StarLite, Model 250)

(Source: <http://www.mqs.co.uk/qvi-svg250.html>)

3.4.7 Fiber length measurement

The fiber degradation during single screw extrusion was investigated by average fiber length. According to DIN EN 60, the glass fibers were separated from the PP matrix using incineration. The composite materials were burnt off in a muffle furnace, CABOLITE,

model GPC12/131, at 650°C for 2 hours. At least 500 fibers were measured using microscope (Olympus model BX51 and DP72, in Figure 3.16) with 10X magnification and were analyzed with the aid of image analysis software, cellSens. The average fiber length was calculated as follows:

$$L_n = \frac{\sum n_i l_i}{\sum n_i} \quad (8)$$

where: L_n = average fiber length, μm
 n_i = number of fibers
 l_i = length of fiber, μm



Figure 3.16 Microscope (Olympus model BX51 and DP72)

(<https://reg.ntuh.gov.tw/WebAppointment/Intro/S705.aspx>)

3.4.8 Particle size analysis

The average particle size of talcum was determined using laser diffraction technique, Malvern Mastersizer 2000 equipped with Hydro 2000MU as shown in Figure 3.17. The range of particle analysis is between 0.02 to 2000 μm . The particle size is estimated from the diffraction pattern created by the scattering at different angles of a laser beam on the particles. A wet dispersion method was used and methanol (refractive index of 1.33) was selected as the dispersion medium. The talc samples that were burnt off in a muffle furnace (CABOLITE, model GPC12/131) at 650°C for 2 hours were added

into 500 ml of methanol and then sonicated for 1 min. For the test parameters, the pump speed was set at 2000 rpm and ultrasonic was turned off. The samples were measured in three repeats.



Figure 3.17 Particle Size Analyzer (Malvern model Mastersizer 2000)

3.4.9 Porosity calculation

The porosity of printed samples was calculated in order to explain the test results. The porosity or void content was generated during the FDM process by the voids between the filaments. The porosity was calculated as follows [48]:

$$P = 1 - \rho_t \left(\frac{PP,wt.}{\rho_{PP}} - \frac{Filler,wt.}{\rho_{Filler}} \right) \quad (9)$$

where:

P = Porosity, %

ρ_t = density of the specimen after the FDM process

ρ_{PP} = density of PP polymer (0.90 g/cm³)

ρ_{Filler} = density of filler (talc of 2.75, milled glass fiber of 2.58 g/cm³)

CHAPTER IV

RESULTS AND DISCUSSION

In this chapter, the experimental results are explained in five parts. The first part involves material screening by measuring flow behavior of materials. Second, ash content results of PP composites after compounding are presented. The third is the effect of filler content and filler type on void formation. The fourth and fifth parts explain the effects of filler content and filler type on tensile properties and shrinkage behavior, respectively.

4.1 Rheological properties of PLA, ABS and neat PP

Melt flow rate (MFR) of PLA and ABS was determined at its printing temperature in order to guide the selection of PP grades. PLA was performed at 190°C/2.16kg load and ABS was performed at 230°C/2.16kg load. The measurements are shown in Table 4.1. From the results, the range of MFR is approximately 2 to 4 g/10min so the six grades of PP were selected from HMC Polymers' technical data sheet (MFR at 230°C/2.16kg load), seen in Table 4.2.

Table 4.1 The measured melt flow rate (MFR) of PLA and ABS

Sample	MFR (g/10min)	
	Avg	SD
PLA (190°C/2.16kg)	3.89	0.07
ABS (230°C/2.16kg)	2.35	0.02

Table 4.2 PP in order of melt flow rate (MFR at 230°C/2.16kg load)

Polypropylene	MFR (g/10min)
PP1	2.0
PP2	2.1
PP3	2.8
PP4	3.5
PP5	4.0
PP6	6.0

Shear viscosity of the six grades of PP was measured at various shear rates ranging from 10 up to 1000 sec^{-1} . The tests were determined at 190 and 195°C for PLA, 230 and 235°C for ABS, and 230°C for PP. In order to select one potential grade of PP, the flow curve of PP was compared with PLA and ABS as shown in Figure 4.1. In this study, shear rate of the printing ranged from 300 to 350 s^{-1} . From the results, it can be seen that PP1 had a flow curve close to PLA and ABS at printing shear rate. It means that PP1 has the potential to be a raw material for FDM process. Therefore, PP1 was selected in this study.

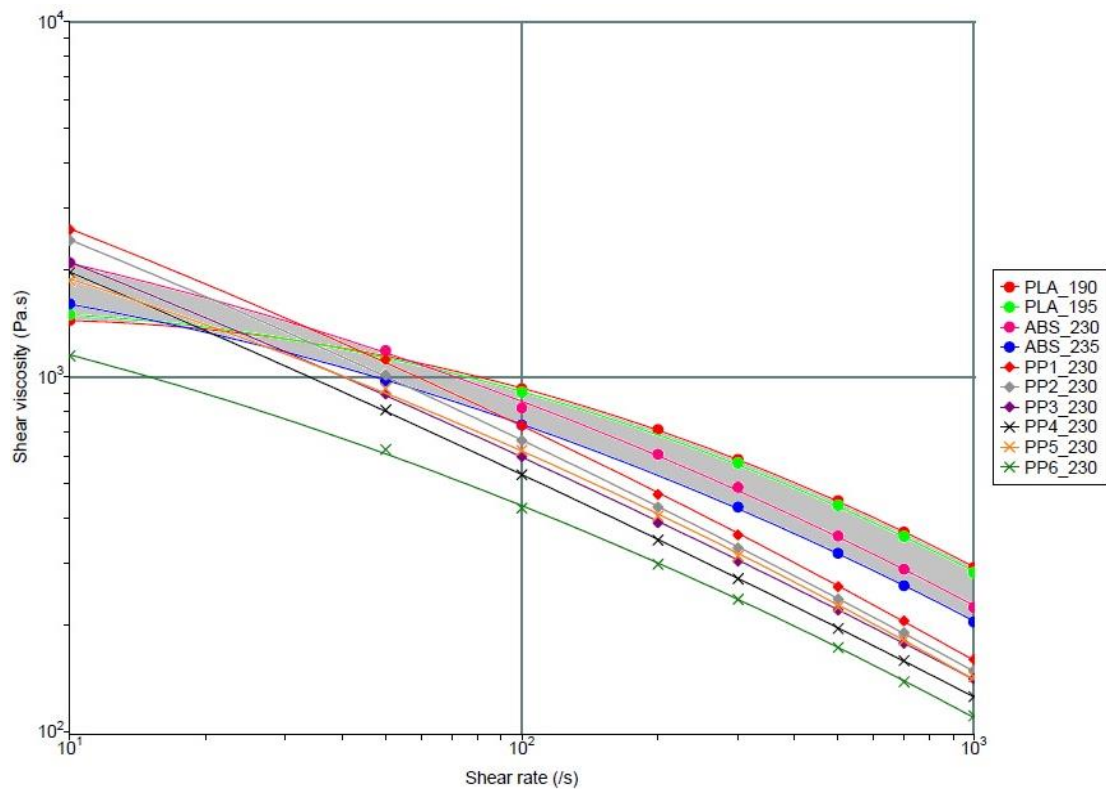


Figure 4.1 Shear viscosity vs shear rate flow curves of PLA, ABS and PP

4.2 Ash content measurement of PP composites

After the PP selection, PP was compounded with three fillers including talc, milled glass fiber with aspect ratio of 5.4 and milled glass fiber with aspect ratio of 15.4 ranging from 0 to 30 wt%. In order to ensure the compounding quality, ash content measurement of PP composites was observed to confirm the actual filler content in PP matrix after compounding. The ash content of PP with different filler contents is shown in Table 4.3. From the results, the ash content values are in an acceptable range with an error less than 5%. It can be seen that the compounding had a good quality control.

Table 4.3 Ash content of PP composites at various filler contents

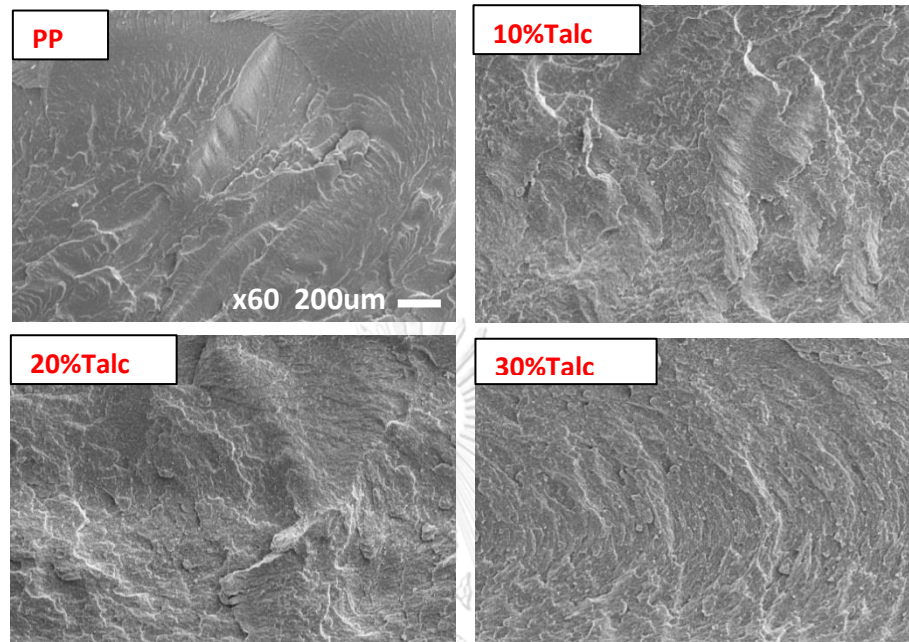
Sample	Ash content (%)	
	Avg	SD
PP+10%talca	10.04	0.0040
PP+20%talca	20.09	0.0042
PP+30%talca	30.10	0.0021
PP+10%MF (AR 5.4)	9.84	0.0028
PP+20%MF (AR 5.4)	20.02	0.0084
PP+30%MF (AR 5.4)	29.46	0.0059
PP+10%MF (AR 15.4)	10.54	0.0020
PP+20%MF (AR 15.4)	20.83	0.0324
PP+30%MF (AR 15.4)	29.52	0.0226

4.3 Effect of filler content and filler type on void formation

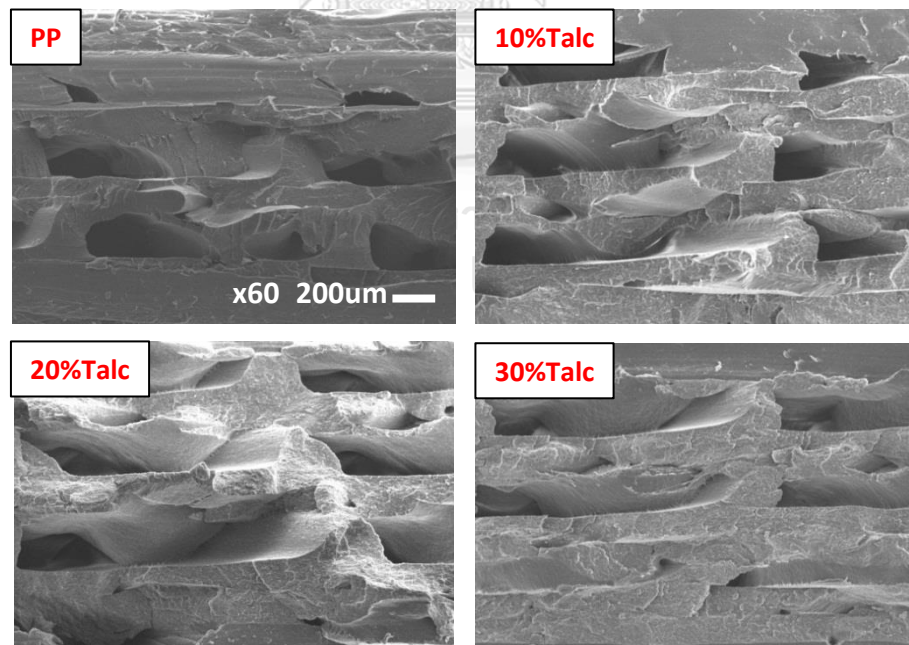
4.3.1 Filler content

The specimens were produced by two techniques, 3D printing and injection molding. The SEM micrographs of cross-sectional fractured surface of dog-bone samples are shown in Figure 4.2. The injected samples showed no visible void content but the FDM samples exhibited significant void formation. These voids are the pores between the adjacent filaments produced during the printing process. In addition, the increase of talc loading from 0 to 30 wt% decreased the void formation in the printed samples observed from Figure 4.2 (b), qualitative data. However, Figure 4.3 shows the quantitative data of void content related to the SEM micrographs. This phenomenon resulted from the increase of thermal conductivity (Figure 4.4) and the decrease of die swelling (Figure 4.5) with augmentation of talc content leading to improved filament bonding [22]. In fact, higher conductivity can transfer heat from a hot filament on top to the cooled bottom

filaments resulting to adhesion among them and smaller filaments aiding smaller inter-filament gaps.



(a) Injected samples



(b) FDM samples

Figure 4.2 SEM micrographs of cross-sectional fractured surface of talc-filled PP

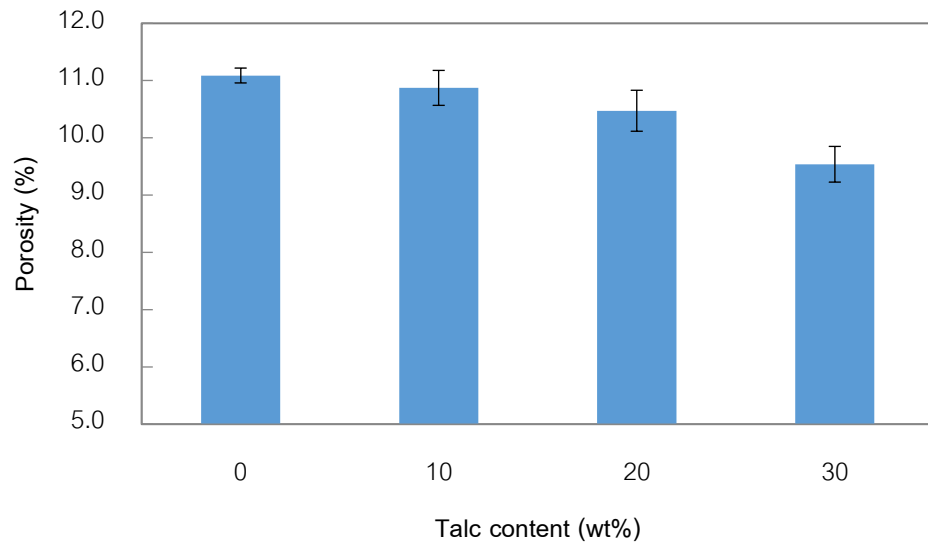


Figure 4.3 Porosity inside the printed samples of talc-filled PP

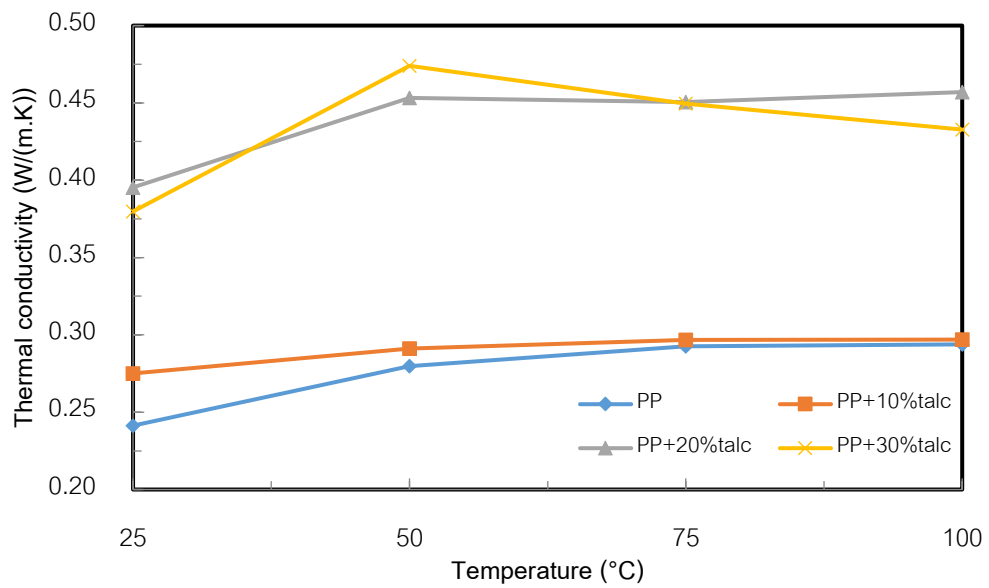


Figure 4.4 Thermal conductivity of talc-filled PP

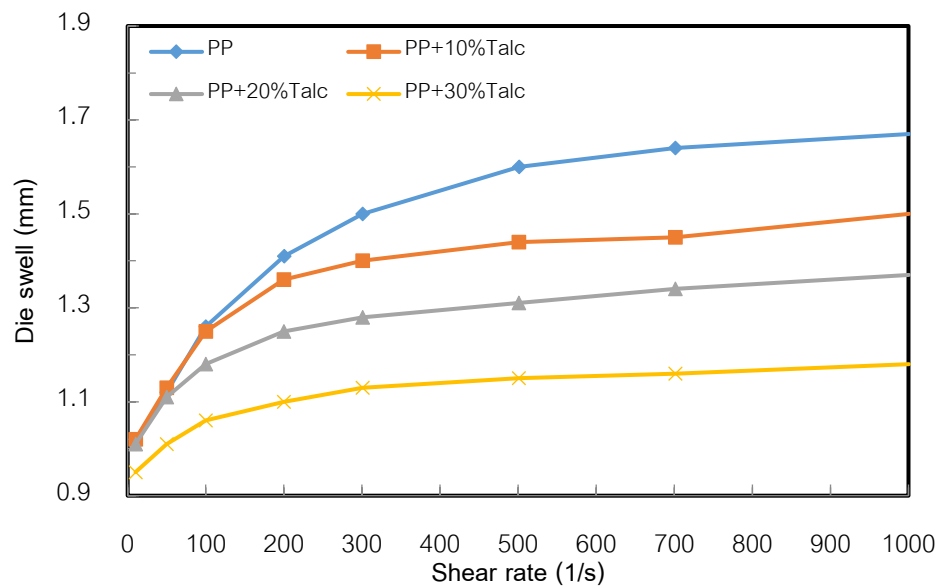


Figure 4.5 Die swell ratio of talc-filled PP

For the PP composites of milled glass fiber aspect ratio 5.4 and 15.4, it was found that the increasing of milled glass fiber from 0 to 30 wt% decreased the inter-filament void or porosity similarly to PP/talc composites caused by the increase of thermal conductivity and decrease of die swelling of filaments.

4.3.2 Filler type

The effect of filler type on void formation at the same content is discussed in this section. Figure 4.6 shows the SEM micrographs of fractured surface of FDM samples at 10wt% filler loading. From the results, it was found that all PP composites exhibited the same inter-filament void size and void content, in quantitative values observed from Figure 4.7, resulting from the similar thermal conductivity observed at high temperature (seen in Figure 4.8) and the same die-swell noted at a printing shear rate of about 300-350 s⁻¹ (seen in Figure 4.9). For this reason, the void formation at 10wt% filler loading was not different.

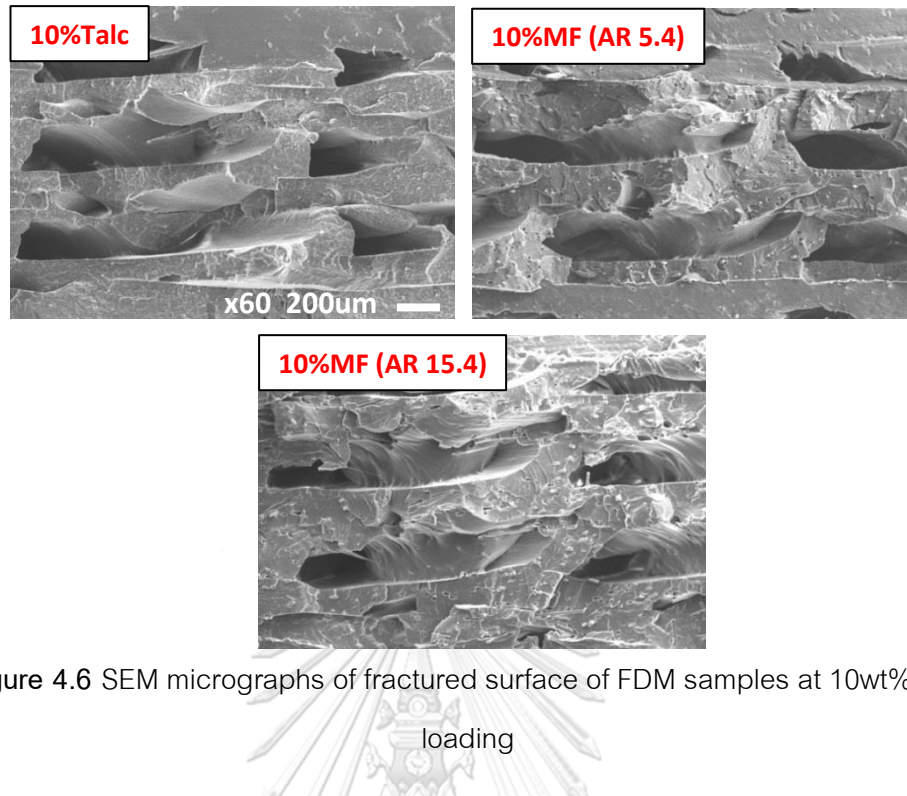


Figure 4.6 SEM micrographs of fractured surface of FDM samples at 10wt% filler loading

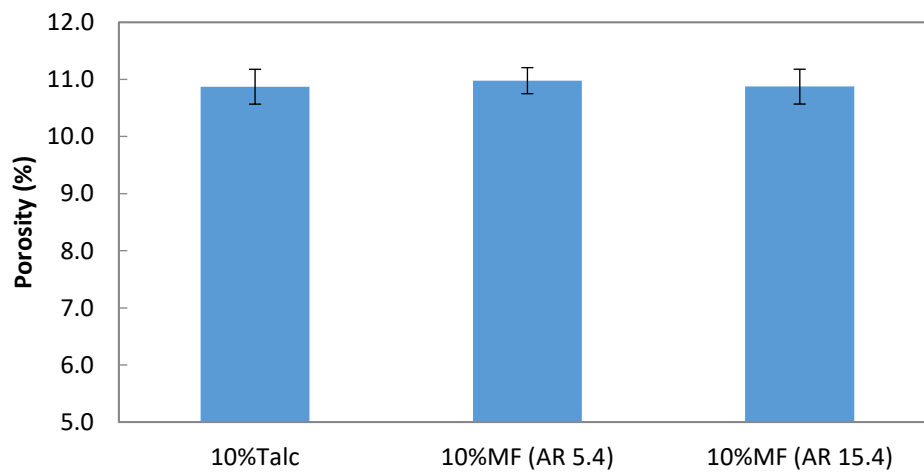


Figure 4.7 Porosity inside the printed samples at 10wt% filler loading

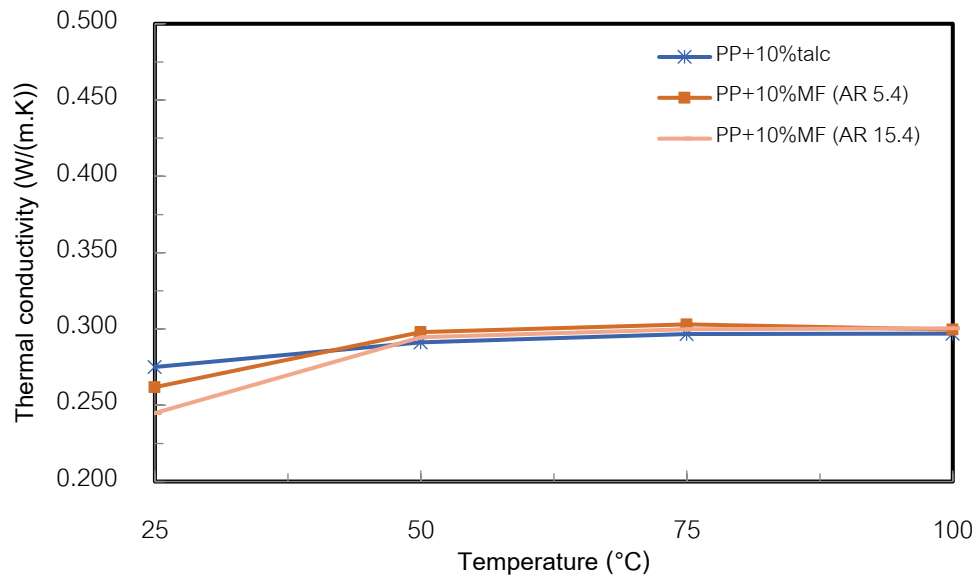


Figure 4.8 Thermal conductivity at 10 wt% filler loading

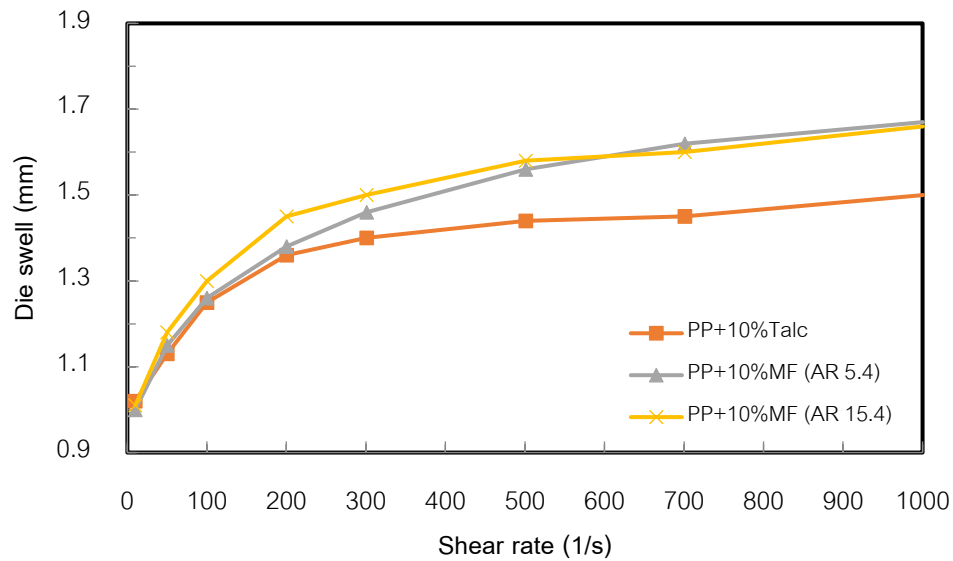


Figure 4.9 Die-swell at 10 wt% filler loading

Figure 4.10 and 4.11 present the SEM micrographs of fracture surface of printed samples and the porosity of the printed samples of different fillers at 20wt% filler loading, respectively. It seemed that the void formation, inside the samples that was generated during FDM process, was not significantly different although talc-filled PP had the higher thermal conductivity at high temperature and lower die-swell at printing shear rate (about 300-350 s^{-1}) than the other two fillers, shown in Figure 4.12 and 4.13. It may be due to talc-

filled PP exhibiting slightly faster cooling rate explained by the shift of crystallization temperature (T_c) to higher temperature, as shown in Figure 4.14.

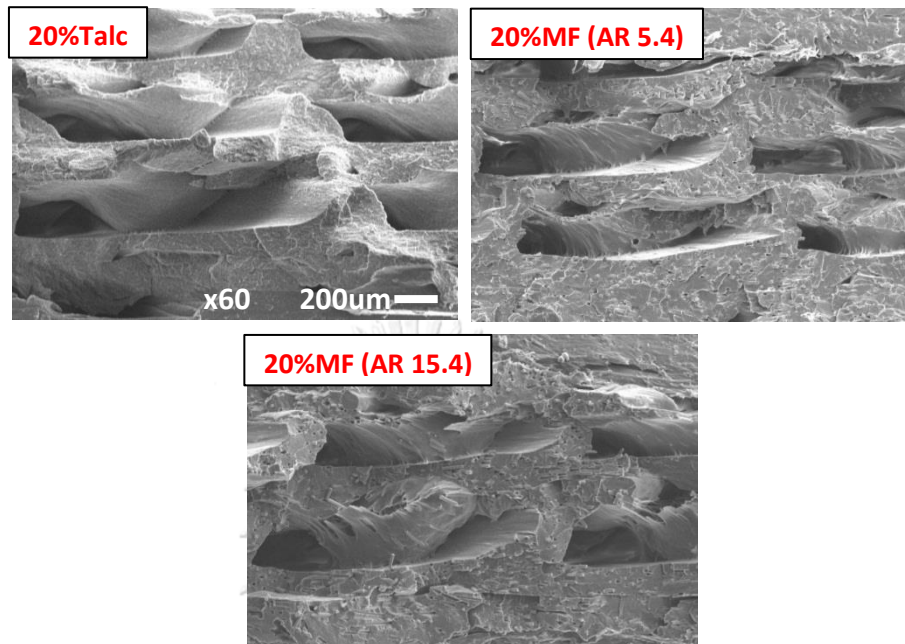


Figure 4.10 SEM micrographs of fractured surface of FDM samples at 20wt% filler loading

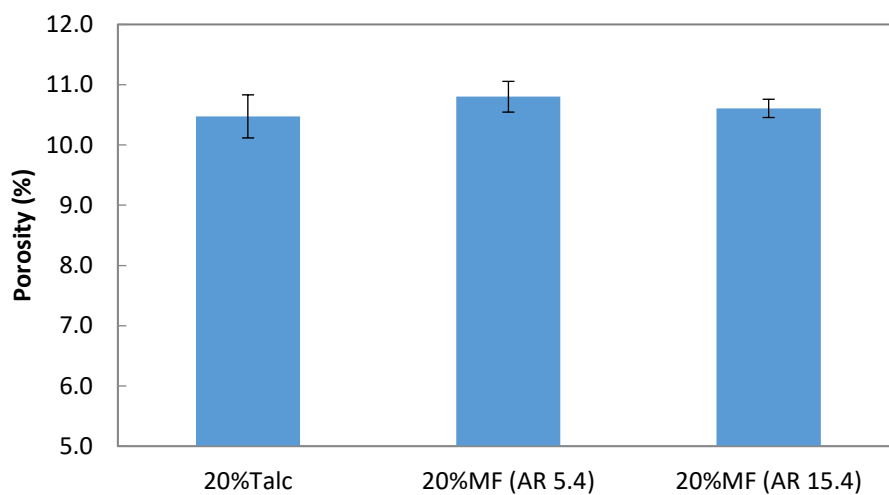


Figure 4.11 Porosity inside the printed samples at 20wt% filler loading

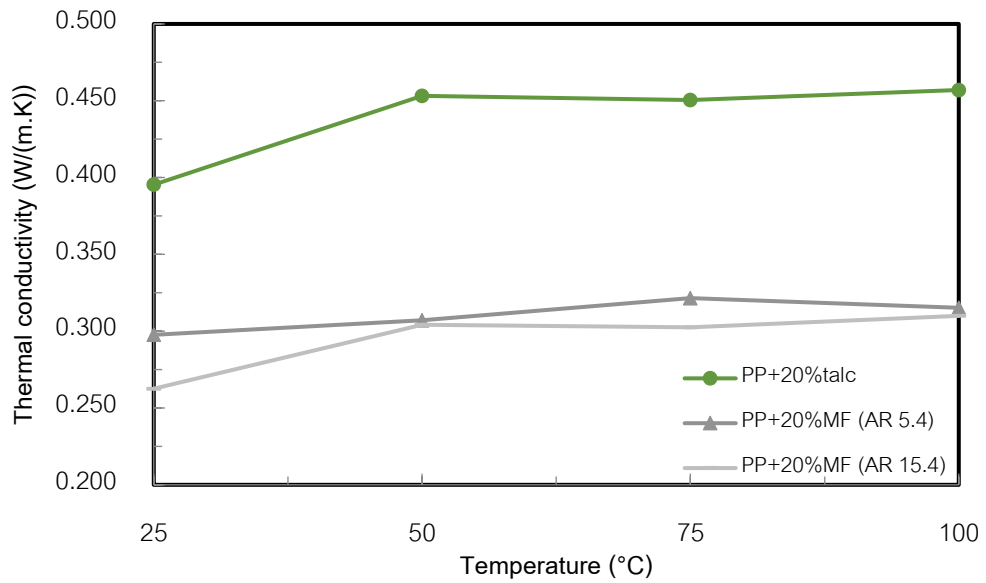


Figure 4.12 Thermal conductivity at 20wt% filler loading

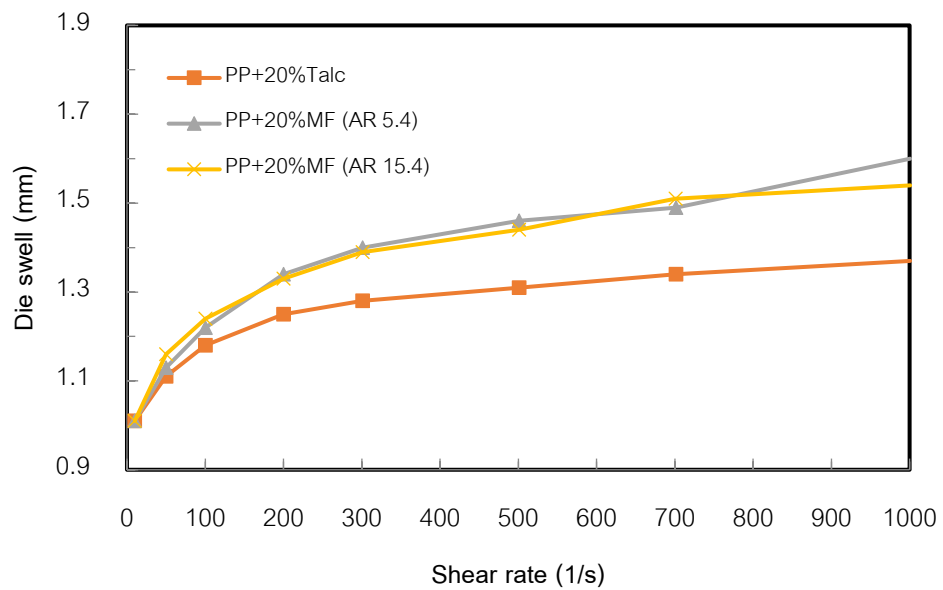


Figure 4.13 Die-swell at 20wt% filler loading

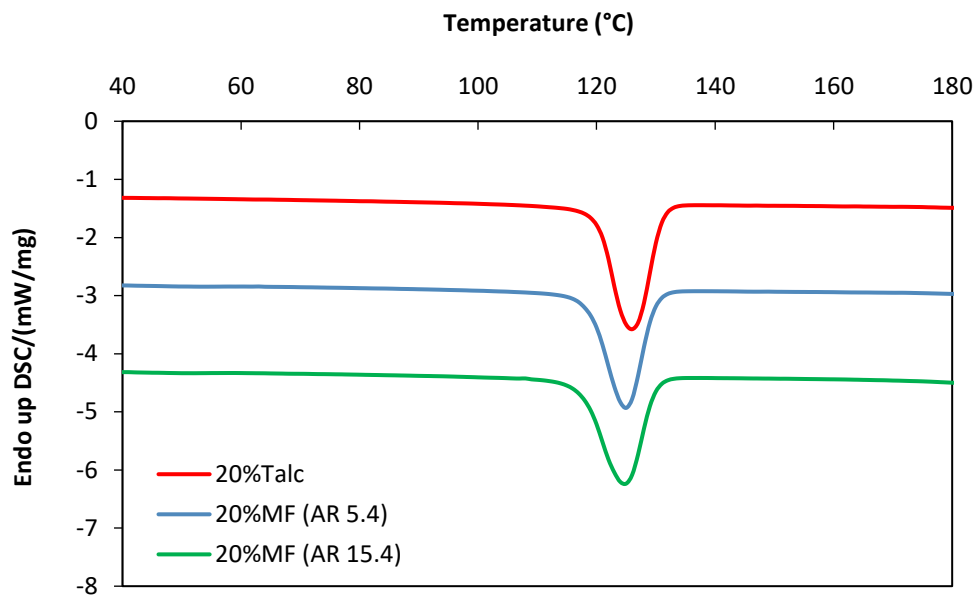


Figure 4.14 Dynamic DSC first cooling thermograms of 20wt% filler loading

In addition, it was found at 30wt% filler content that filler type did not affect the void formation inside the printed samples as similarly found with 20wt% filler content. Although talc-filled PP had the higher thermal conductivity at high temperature and lower die-swell at printing shear rate (about $300\text{-}350\text{ s}^{-1}$) than others, the void size and porosity were not significantly different as a result of faster cooling rate. The results were shown as follows (Figure 4.15 to 4.19).

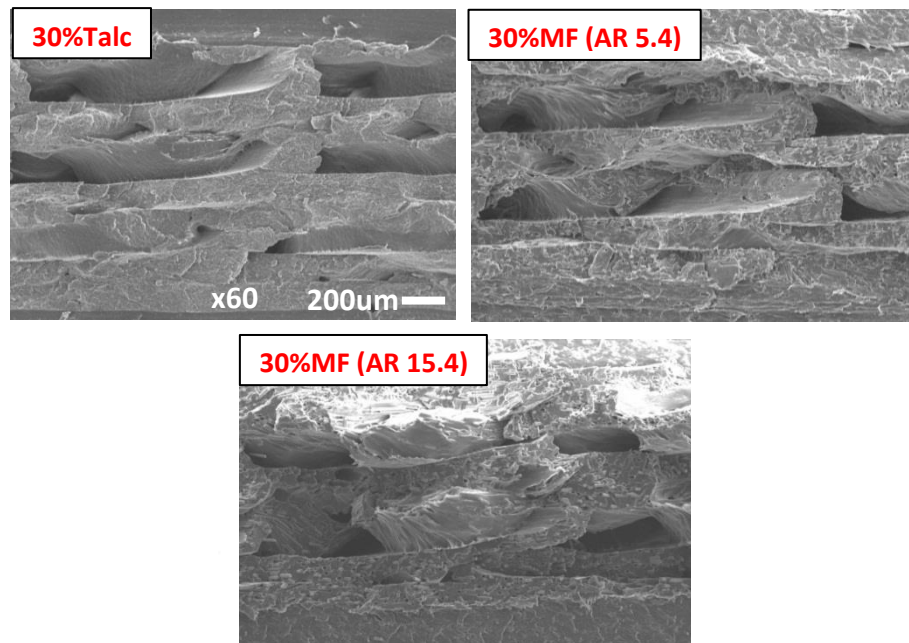


Figure 4.15 SEM micrographs of fractured surface of FDM samples at 30wt% filler loading

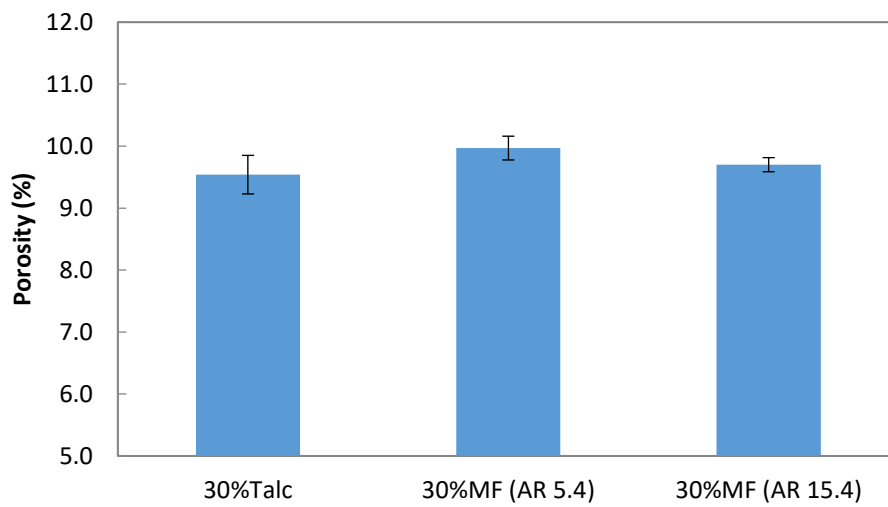


Figure 4.16 Porosity inside the printed samples at 30wt% filler loading

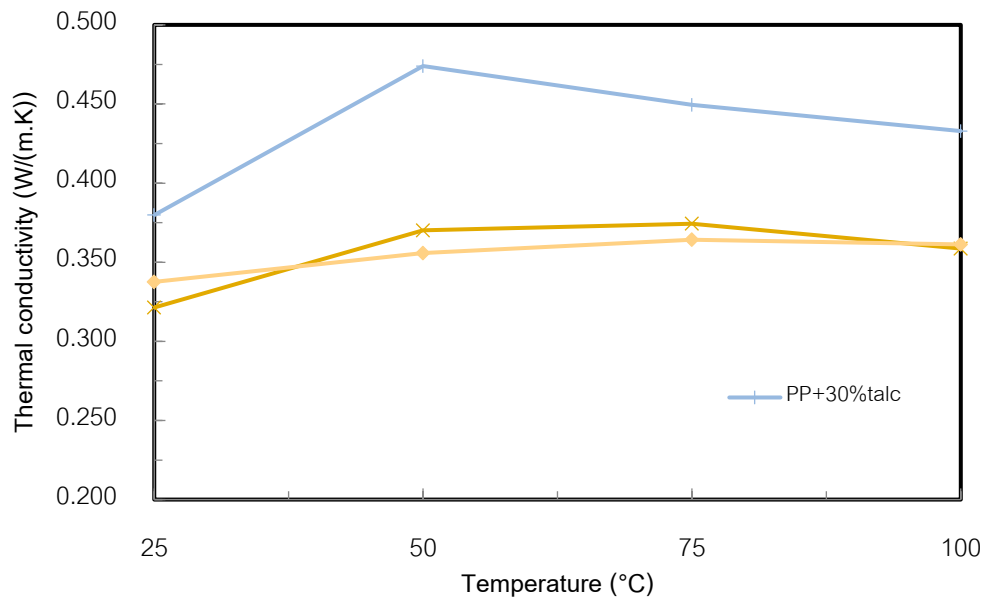


Figure 4.17 Thermal conductivity at 30wt% filler loading

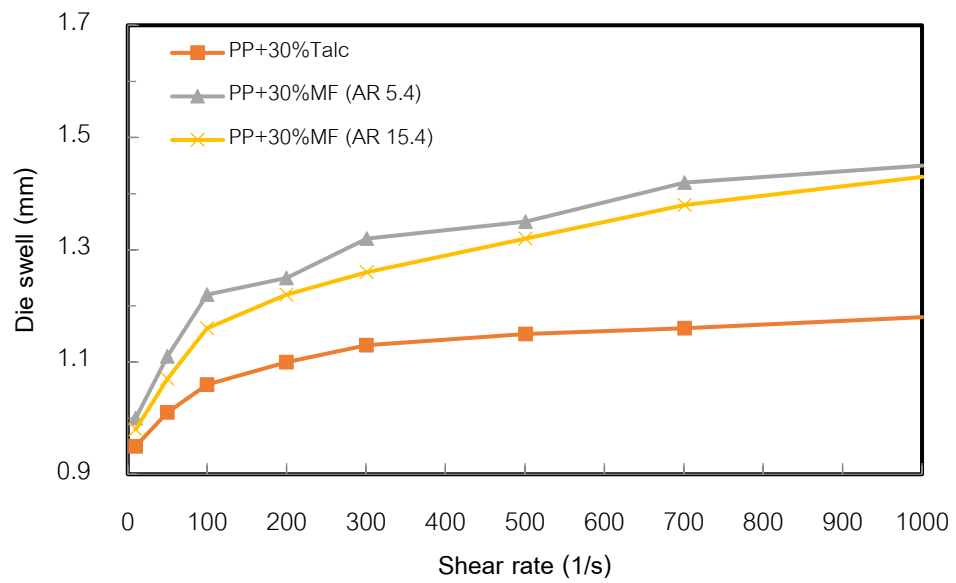


Figure 4.18 Die-swell at 30wt% filler loading

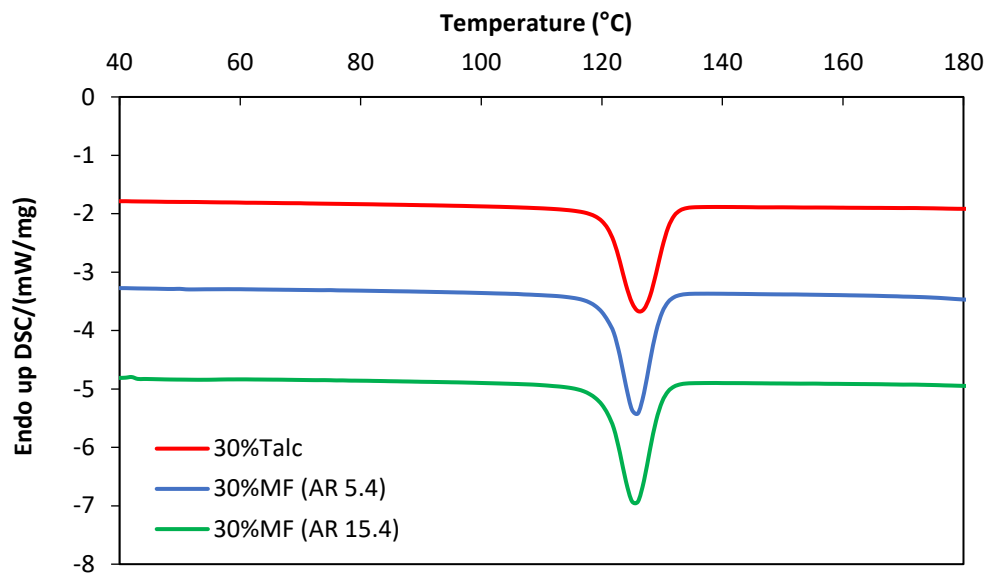


Figure 4.19 Dynamic DSC first cooling thermograms of 30wt% filler loading

4.4 Effect of filler content and filler type on tensile properties

4.4.1 Filler content

Figure 4.20 to 4.22 demonstrate the effect of filler content on tensile properties. Comparing the tensile modulus and tensile strength between two techniques, it was observed that the 3D printing samples had considerably lower tensile modulus and strength than the injected samples. It resulted from the void formation in the printed samples as evidenced in Figure 4.2. The presence of many voids in the samples adversely affected the stiffness and strength of the PP composites.

The effect of filler content on tensile modulus was observed. From the results, it was found that the increase of filler content from 0 to 30 wt% augmented the tensile modulus in both techniques (FDM and injection molding). It may be explained by the fact that fillers help to resist deformation when force was applied to specimens.

For the tensile strength, it can be seen that the addition of filler content from 0 to 30 wt% decreased the tensile strength in both techniques and three fillers except talc-filled PP molded by injection technique. The results of injected talc composites as shown

in Figure 4.20, may be explained by the fact that talc does not act as a reinforcing agent so the tensile strength remained unchanged despite the increasing of talc content. However, milled glass fibers are used as a reinforcing agent but it was found that the tensile strength of the injected samples decreased with the increasing of milled glass fiber content. As shown in Figure 4.23, it can be seen that most of the glass fibers were pulled out of PP matrix indicating poor interfacial adhesion between the fibers and PP matrix leading to a reduction of stress transfer from the PP matrix to fibers through the interface, resulting in a decrease in the tensile strength [22]. Moreover, the tensile strength of 3D printed samples had a similar trend with injection technique and tended to decrease due to the effect of inner-filament void generating stress concentration points causing the samples to fail at lower stress as mentioned earlier in literature review part [22].

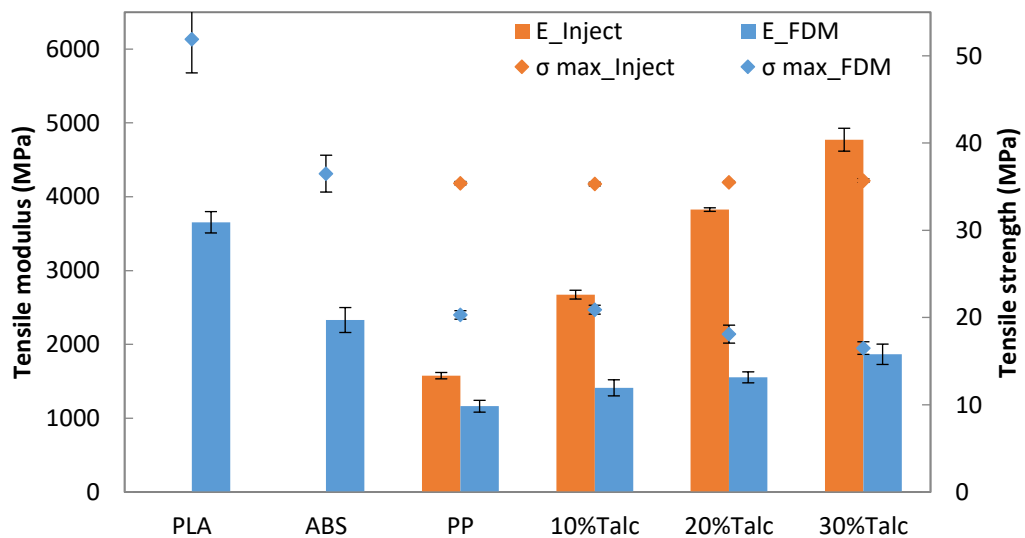


Figure 4.20 Tensile strength of talc-filled PP at various contents

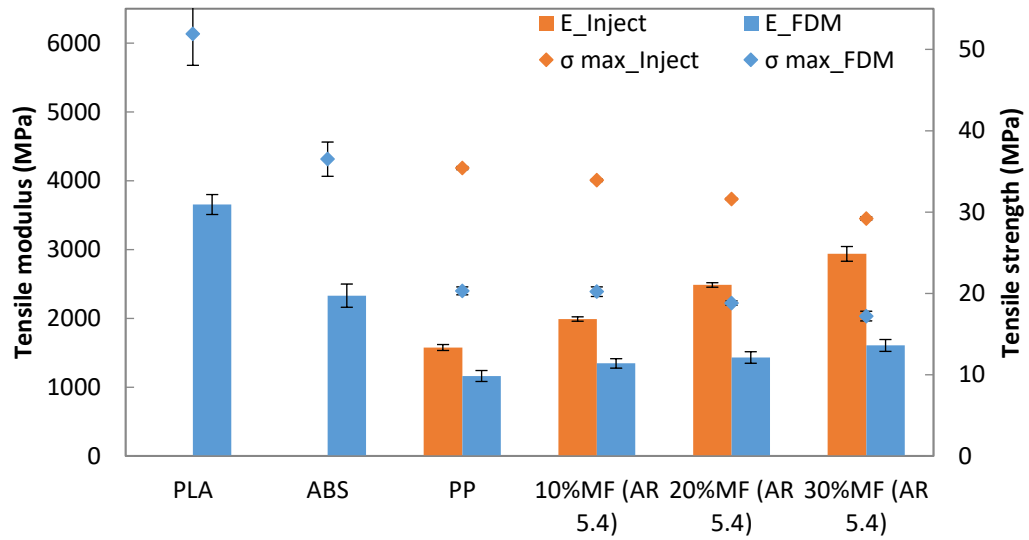


Figure 4.21 Tensile strength of milled glass fiber (AR 5.4)-filled PP at various contents

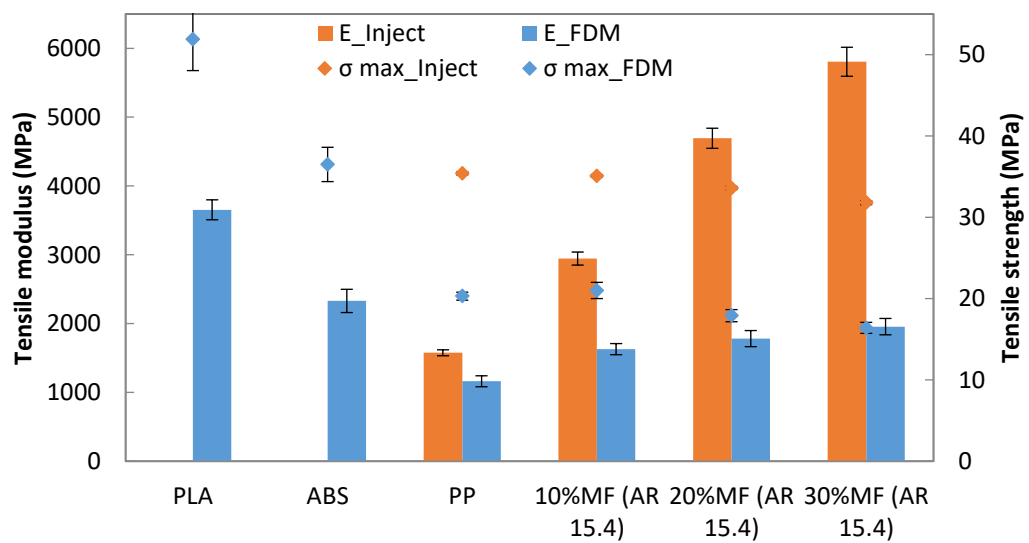


Figure 4.22 Tensile strength of milled glass fiber (AR 15.4)-filled PP at various contents

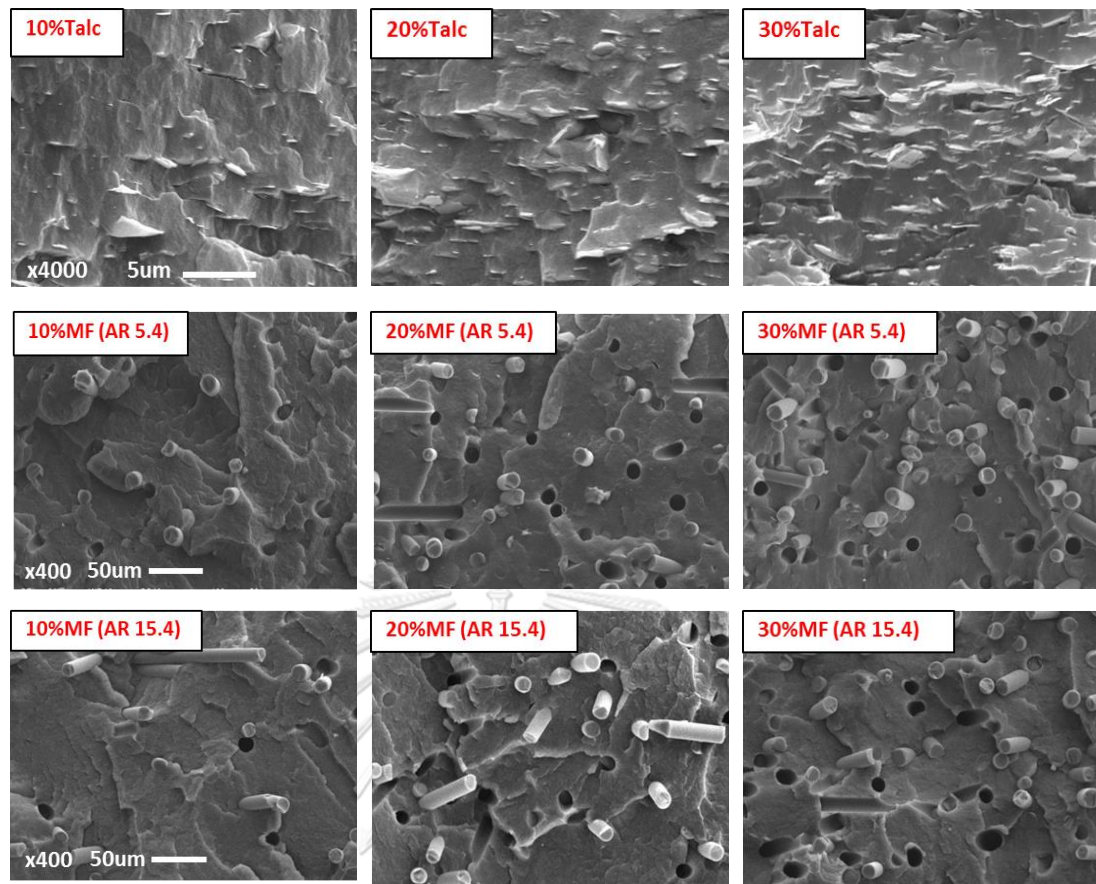


Figure 4.23 SEM micrographs of PP composites indicating interfacial adhesion between filler and PP matrix

4.4.2 Filler type

The effect of filler type on tensile modulus and strength at 10, 20 and 30 wt% filler loading was shown in Figure 4.24 to 4.26. One factor that influenced by degree of crystallinity is tensile modulus. Table 4.4 presents the degree of crystallinity of the PP composites. From the DSC results, it was found that the degree of crystallinity at the same filler loading exhibited roughly the same range in both first and second scans therefore in this case the tensile modulus is not influenced by degree of crystallinity. For injected samples, the milled glass fiber (AR 15.4) composites trended towards the highest tensile modulus while the second, talc-filled PP and the last, milled glass fiber (AR 5.4)-filled PP. This finding may indicate that higher aspect ratio of glass fiber has better continuous fiber-

reinforced and deformation resistance to applied force. However, talc-filled PP had higher tensile modulus than that with milled glass fiber (AR 5.4), it may be caused by the fact that talc has smaller particle size and also more surface contact area between matrix and particles leading to more deformation resistance to applied force. For tensile strength of injected samples, it was found that talc composites trended towards the higher tensile strength than that with milled glass fiber resulting from better interfacial adhesion, as seen in Figure 4.23, leading to better stress transfer from PP matrix to filler particles through the interfaces. While milled glass fiber with higher aspect ratio (AR 15.4) exhibited higher strength than lower aspect ratio (AR 5.4) owing to better reinforcement causing better stress transfer.

In FDM technique, it can be seen that both tensile modulus and tensile strength showed roughly the same range in different filler type. This finding may be explained by two reasons. Firstly the effect of inter-filament void suppresses the intrinsic properties and secondly, the amount of filler that was added into PP may be too much loading for filaments resulting in suppression of the intrinsic properties of composites.

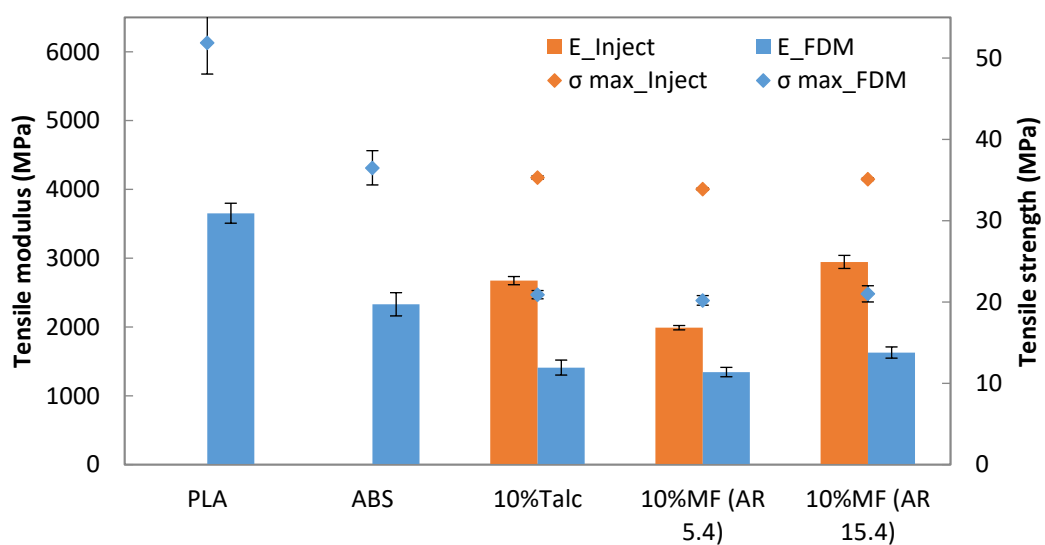


Figure 4.24 Effect of filler type on tensile strength at 10wt% filler loading

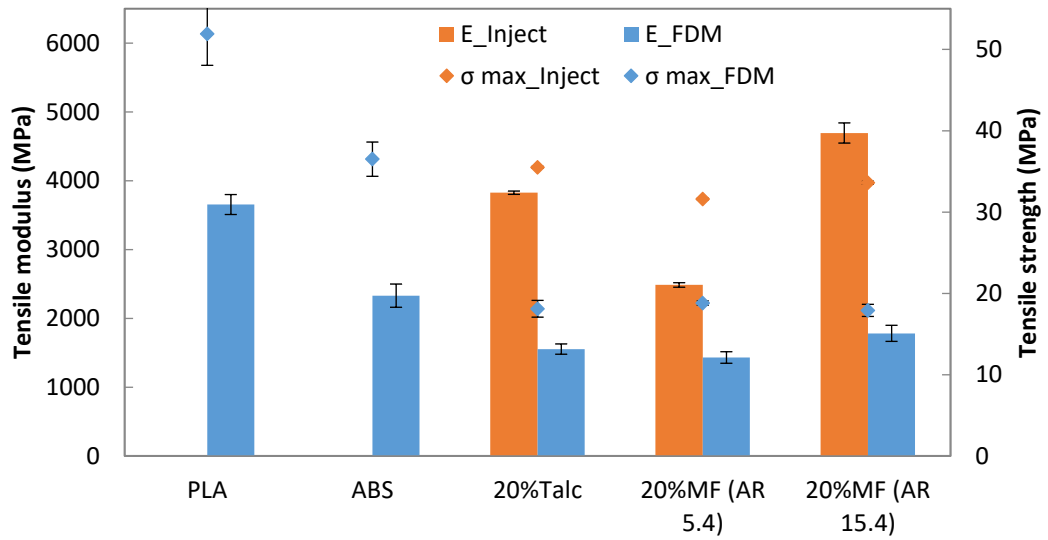


Figure 4.25 Effect of filler type on tensile strength at 20wt% filler loading

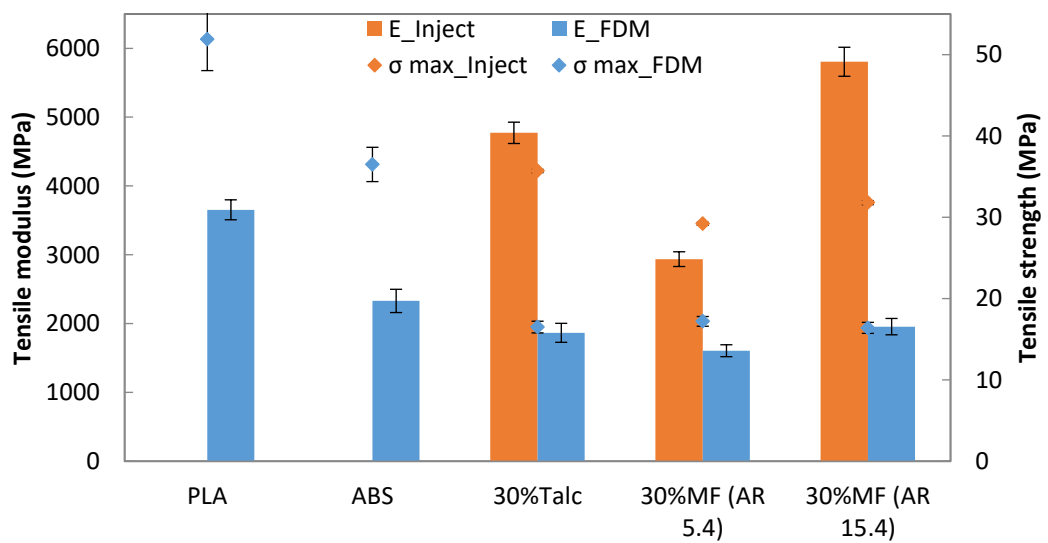


Figure 4.26 Effect of filler type on tensile strength at 30wt% filler loading

Table 4.4 Comparison of crystallinity of PP composites at the same loading

Sample	%Crys			
	1 st scan		2 nd scan	
	Avg	SD	Avg	SD
PP	61.2	1.34	65.4	1.34
PP+10%Talc	60.9	1.48	68.3	0.49
PP+10%MF (AR 5.4)	60.9	0.28	65.9	1.41
PP+10%MF (AR 15.4)	60.7	2.76	65.3	1.34
PP+20%Talc	61.1	1.48	67.4	0.85
PP+20%MF (AR 5.4)	60.2	3.39	66.8	1.91
PP+20%MF (AR 15.4)	58.4	0.00	65.2	0.57
PP+30%Talc	60.8	0.14	67.4	1.06
PP+30%MF (AR 5.4)	61.0	4.38	67.2	1.20
PP+30%MF (AR 15.4)	60.7	1.77	65.4	0.35

4.5 Effect of filler content and filler type on shrinkage behavior

4.5.1 Filler content

Figure 4.27 to 4.28 show the effect of filler content on shrinkage rate, the specimens prepared by injection molding technique according to ASTM D955. The results showed that the addition of filler content (talc and milled glass fiber) from 0 to 30 wt% into the PP matrix significantly decreased the shrinkage rate in both flow direction (MD direction) and cross direction (TD direction). For talc-filled PP, the shrinkage rate decreased about 40% and 38% in MD and TD directions, respectively. For milled glass fiber with aspect ratio 5.4-filled PP, the shrinkage rate decreased about 29% and 22% in MD and TD directions, respectively. Finally, milled glass fiber with aspect ratio 15.4

composites, the shrinkage rate decreased by about 33% in MD direction and 22% in TD direction.

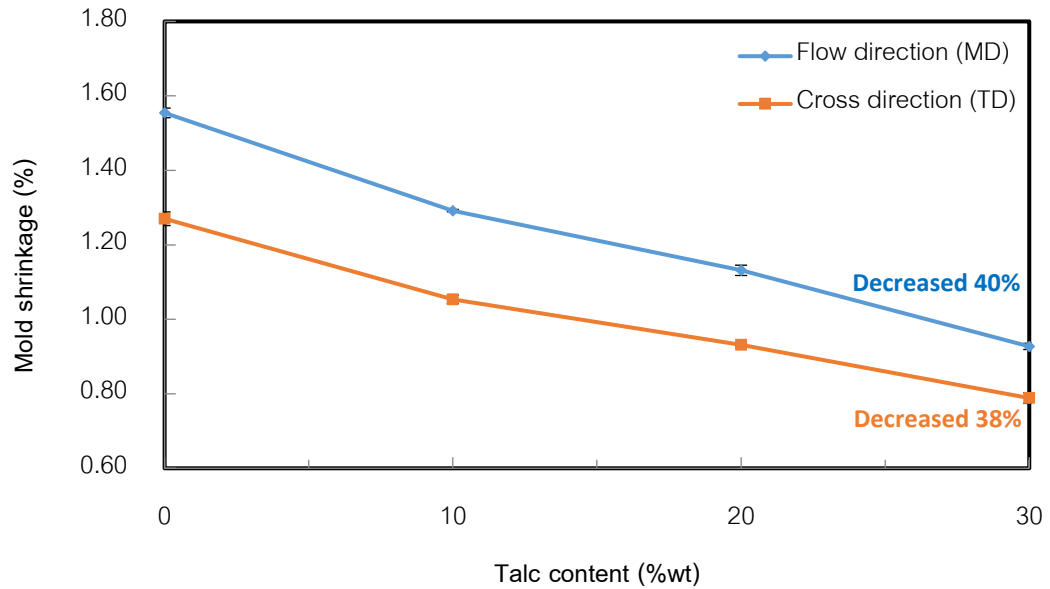


Figure 4.27 Mold shrinkage of talc-filled PP at various contents

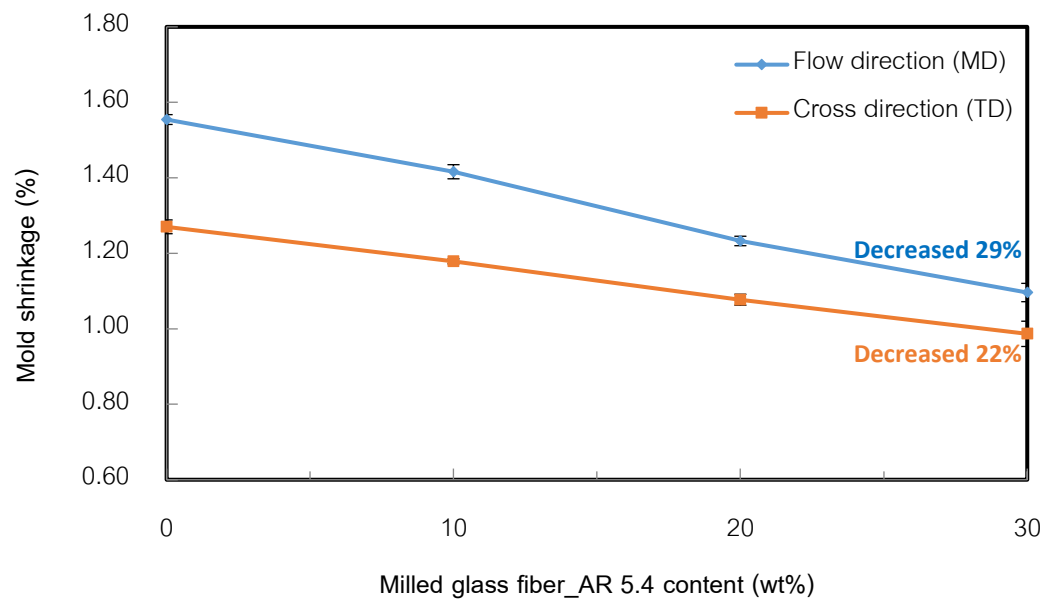


Figure 4.28 Mold shrinkage of milled glass fiber with aspect ratio 5.4-filled PP at various contents

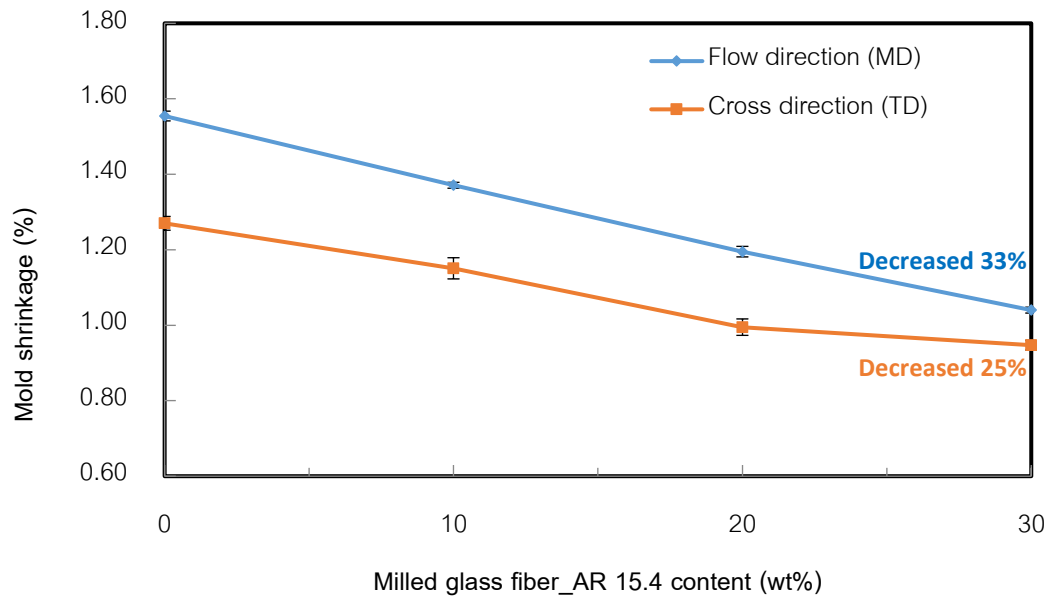


Figure 4.29 Mold shrinkage of milled glass fiber with aspect ratio 15.4-filled PP at various contents

Figure 4.30 exhibits the 3D shrinkage contour plot of PP composites at different contents in FDM process. The printed specimens were measured by 3D scanner and then scanned files were compared with CAD original file. The results were presented in color level (qualitative data) and quantitative data were shown by percentage of green color. Green color shows the acceptable range of shrinkage. From the 3D contour plot results, it was found that the increase of filler content from 0 to 30%wt (observed in Figure 4.30 from left to right) increased the percentage of green color; in other words, the results showed that the increase of filler content decreased the overall shrinkage rate similarly to the trend observed in mold shrinkage results.

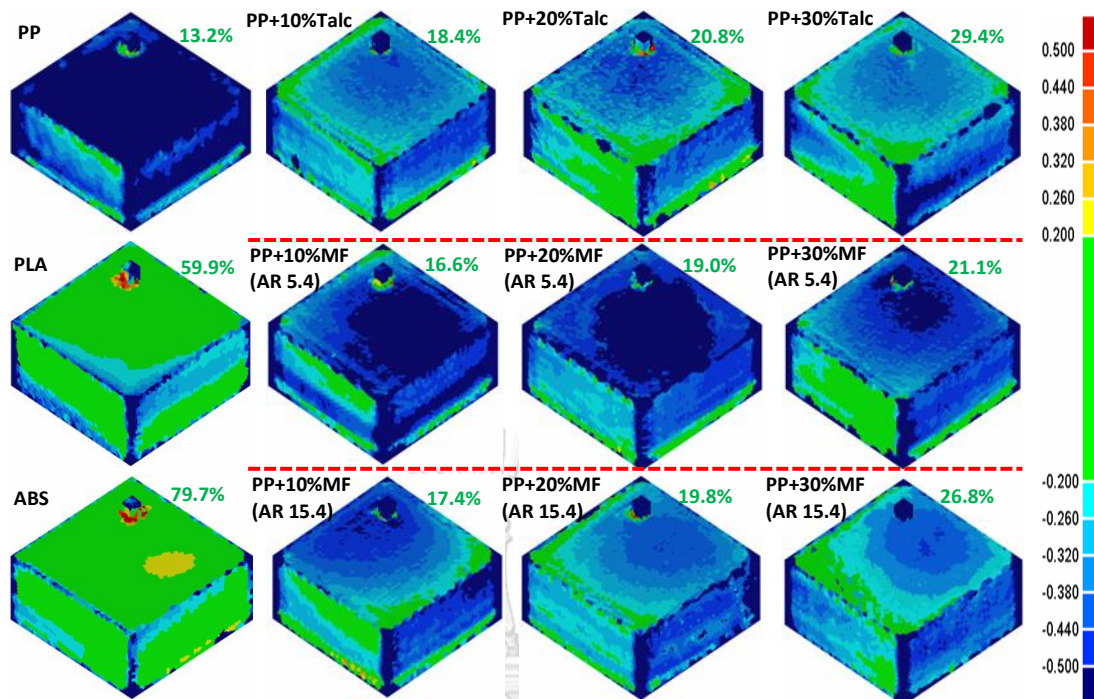


Figure 4.30 3D shrinkage contour plot at various contents in FDM process

Normally, key parameter for shrinkage behavior depends on degree of crystallinity of polymer. From Table 4.5, degree of crystallinity of PP composites, it can be seen that the crystallinity of all composites was in the same range in 1st and 2nd scan of DSC results. Therefore, it can be concluded that the reduction of shrinkage rate resulted from the reduction of volume fraction of PP resin in the parts [46, 49].

Table 4.5 Comparison of crystallinity of PP composites at various contents

Sample	%Crys			
	1 st scan		2 nd scan	
	Avg	SD	Avg	SD
PP	61.2	1.34	65.4	1.34
PP+10%Talc	60.9	1.48	68.3	0.49
PP+20%Talc	61.1	1.48	67.4	0.85
PP+30%Talc	60.8	0.14	67.4	1.06
PP+10%MF (AR 5.4)	60.9	0.28	65.9	1.41
PP+20%MF (AR 5.4)	60.2	3.39	66.8	1.91
PP+30%MF (AR 5.4)	61.0	4.38	67.2	1.20
PP+10%MF (AR 15.4)	60.7	2.76	65.3	1.34
PP+20%MF (AR 15.4)	58.4	0.00	65.2	0.57
PP+30%MF (AR 15.4)	60.7	1.77	65.4	0.35

4.5.2 Filler type

Figure 4.31 to 4.33 demonstrate the effect of filler type on the shrinkage rate in injection molding. It can be noticed that the shrinkage rate of talc-filled PP was lower than that of milled glass fiber-filled PP at both aspect ratio of 5.4 and 15.4. In addition, the higher aspect ratio of milled glass fiber (AR 15.4) exhibited a lower shrinkage rate than the lower aspect ratio (AR 5.4). For the 3D shrinkage contour plot of FDM technique as shown in Figure 4.34 (observed from top to bottom), the results demonstrated that the overall shrinkage rate had a similar trend with injection molding. The explanation for this finding would be 2 reasons; first, it resulted from the fact that the milled glass fiber used in this study was too short or shortened after compounding process therefore talc showed better performance than milled glass fiber in shrinkage reduction. Second, as mentioned earlier about faster crystallization rate of talc-filled PP composite, it may be due to the

better dimensional stability of filaments of talc-filled PP while being extruded from extruder resulting in lower shrinkage. Furthermore, the higher aspect ratio of milled glass fiber showed a lower shrinkage rate. This is probably because the longer glass fiber length has better continuous fiber-reinforced and aligned fiber composite than shorter glass fiber length. The synergistic phenomena led to the reduction of the degree of shrinkage of overall system.

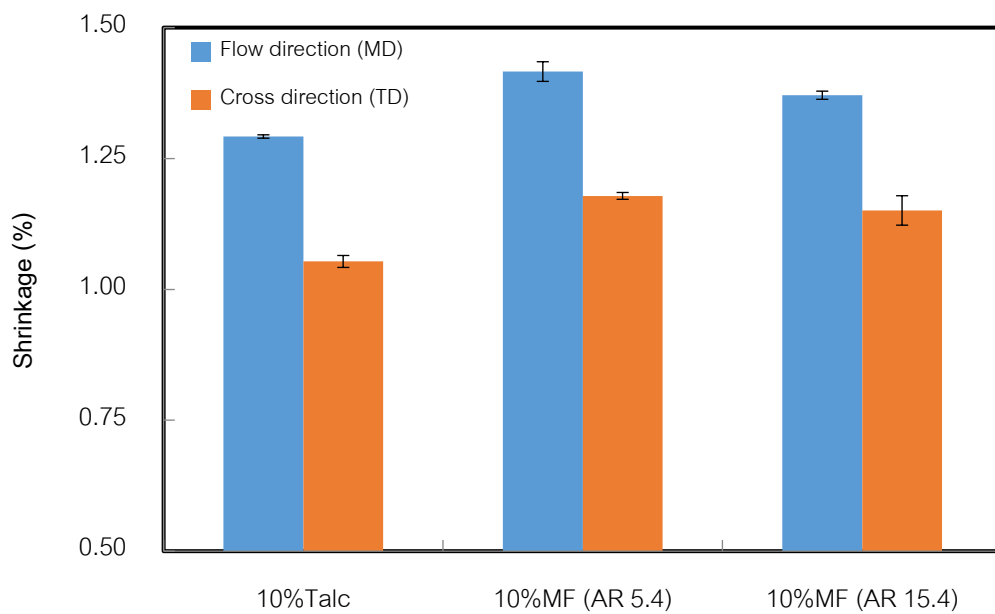


Figure 4.31 Effect of filler type on mold shrinkage at 10wt% filler loading

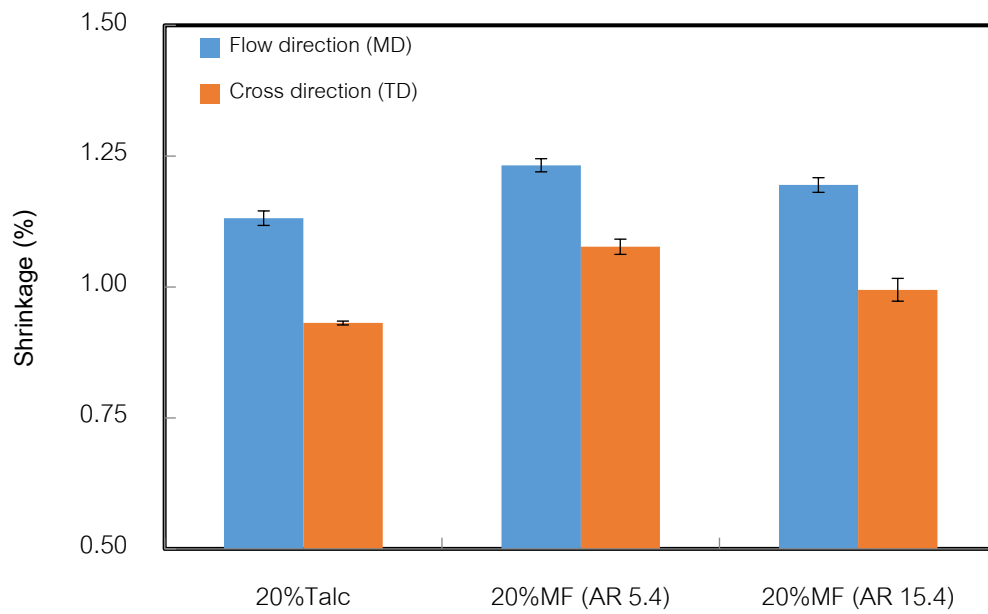


Figure 4.32 Effect of filler type on mold shrinkage at 20wt% filler loading

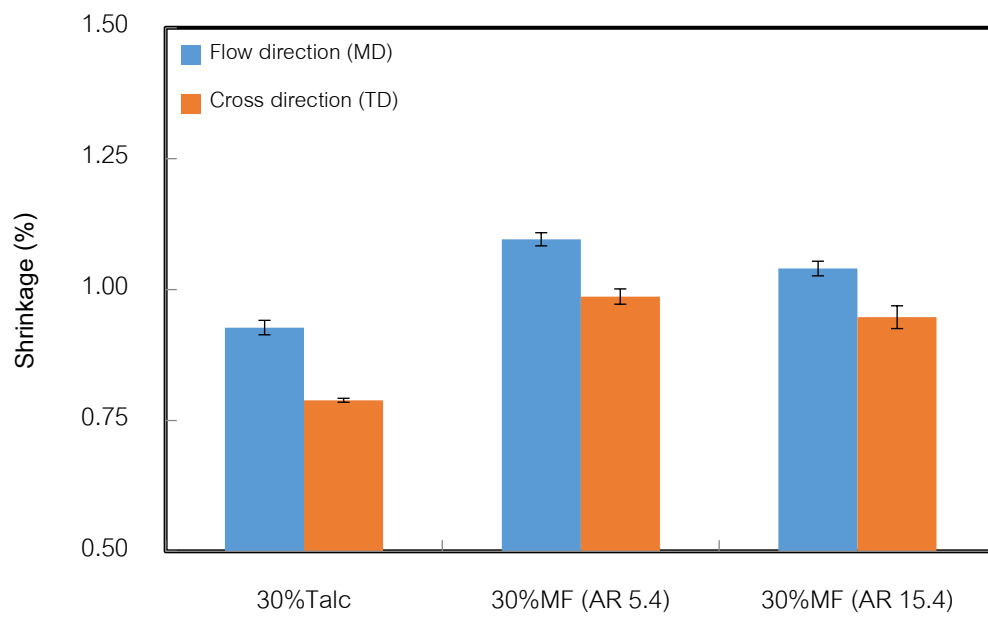


Figure 4.33 Effect of filler type on mold shrinkage at 30wt% filler loading

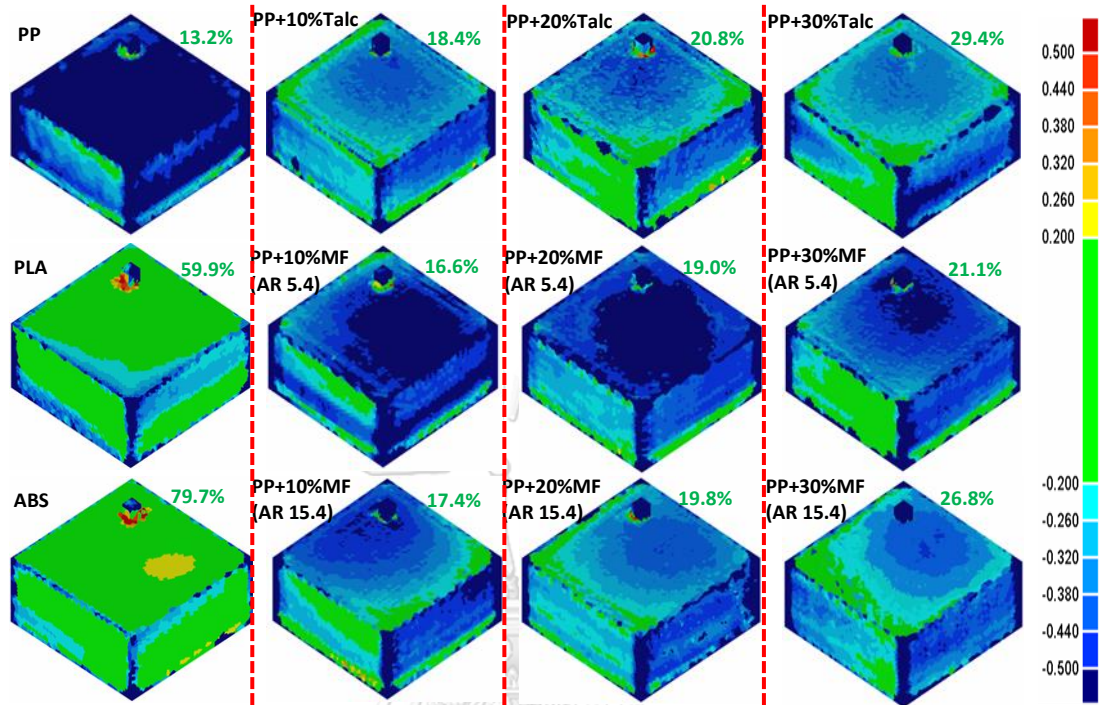


Figure 4.34 3D shrinkage contour plot in FDM process

CHAPTER V

CONCLUSIONS AND RECOMMENDATIONS

5.1 Conclusions

According to the aim of this research, the property improvement of PP to be a feedstock material for fused deposition modeling (FDM) technique was studied. Consequently, the effects of filler content and filler type on tensile properties and shrinkage behavior of PP composites were considered. The test samples were produced by FDM printer and injection molding technique to understand the intrinsic properties of the composites. The main conclusions of this study can be drawn as follows:

1. The effect of filler content on tensile properties was investigated. The increase of filler content increased the tensile modulus in both techniques. For tensile strength of FDM samples, it was found that the increase of talc did not affect the tensile strength as not acting as a reinforcing agent while the increase of milled glass fiber gradually decreased the tensile strength due to the poor interfacial adhesion between fibers and matrix. In addition, the results of FDM printed samples exhibited that the tensile strength trended to decrease with the increasing of filler content resulting from the effect of inner-filament void formation.

2. The effect of filler type on tensile properties was examined. From the results of injected samples, it was found that milled glass fiber (AR 15.4)-filled PP had the highest tensile modulus due to better reinforcement but talc-filled PP trended towards the highest tensile strength because of better interfacial adhesion between filler and polymer. Furthermore, higher aspect ratio of glass fiber had a higher tensile modulus and strength than lower aspect ratio owing to better reinforcement and stress transfer from matrix to filler particles. In FDM technique, the tensile modulus and strength exhibited roughly the same range at the similar filler loading. This finding can be explained by the fact that the

effect of inter-filament void suppresses the intrinsic properties and too much filler content for filaments resulting in the suppression of the intrinsic properties.

3. The effect of filler content on shrinkage behavior was studied. The results exhibited that the addition of filler content up to 30 wt% into the PP matrix obviously reduced the shrinkage behavior in both flow and cross directions for injection molding and overall for FDM technique. This can be clarified by the fact that the reduction of shrinkage resulted from the volumetric reduction of PP resin.

4. The effect of filler type on shrinkage behavior was studied. From the results, it can be found that there is a similar trend of shrinkage rate in both techniques (FDM and injection molding). The PP/talc composites trend towards the lower overall shrinkage rate than milled glass fiber composites due to too short or shorten length of milled glass fiber and faster crystallization rate of talc leading to better dimensional stability of filaments. The PP/milled glass fiber (AR 15.4) showed lower shrinkage than PP/milled glass fiber (AR 5.4) caused by the better continuous fiber-reinforced and higher possibly fiber alignment of the longer fiber length.

Finally, the requirements of material used for FDM technique as raw materials should have less shrinkage rate to achieve the part's dimensional stability and good mechanical properties to withstand the load when it is used. From the entire work, the 10 wt% talc-filled PP composites is the most suitable recipe to be a feedstock material for printing process because it exhibited lower shrinkage rate than milled glass fiber composites and maintained the tensile strength compared to neat PP. Moreover, all formulations in this research have lower tensile properties and higher shrinkage rate than PLA and ABS, commercial filaments. However, the PP composites can be a feedstock material for FDM technique to produce small parts or mockups.

5.2 Recommendations

1. Compatibilizer, such as maleic anhydride grafted PP (PP-a-MAH), should be added into the PP composites to improve the mechanical properties.

2. The effect of hybrid talc/milled glass fiber fillers or other fillers, such as calcium carbonate (CaCO_3) and carbon fiber on the mechanical properties and shrinkage behavior of PP should be studied.



REFERENCES

- [1] Kruth, J.P., M.C. Leu, and T. Nakagawa, Progress in Additive Manufacturing and Rapid Prototyping. CIRP Annals - Manufacturing Technology, 1998. 47(2): p. 525-540.
- [2] Wilkinson, S. and N. Cope, Chapter 10 - 3D Printing and Sustainable Product Development A2 - Dastbaz, Mohammad, in Green Information Technology, C. Pattinson and B. Akhgar, Editors. 2015, Morgan Kaufmann: Boston. p. 161-183.
- [3] Chang, K.-H., Chapter 14 - Rapid Prototyping, in e-Design. 2015, Academic Press: Boston. p. 743-786.
- [4] Wohlers, T.T., and Caffrey, T., Wohlers report 2015 : 3D printing and additive manufacturing state of the industry annual worldwide progress report. 2015.
- [5] Chua, C.K., Leong, K.F., and Lim, C.S., Rapid Prototyping: Principles and Applications. 2010.
- [6] Flowers, J., 3D Laser Scanning in Technology Education. Technology Teacher, 2000. 60(3): p. 27-30.
- [7] Ilardo, R. and C.B. Williams, Design and manufacture of a Formula SAE intake system using fused deposition modeling and fiber-reinforced composite materials. Rapid Prototyping Journal, 2010. 16(3): p. 174-179.
- [8] Kolarevic, B., Digital Fabrication Manufacturing Architecture in the Information Age. Association for Computer Aided Design in Architecture (ACADIA): Reinventing the Discourse, 2001: p. 268-277.
- [9] Petzold, R., H.F. Zeilhofer, and W.A. Kalender, Rapid prototyping technology in medicine—basics and applications. Computerized Medical Imaging and Graphics, 1999. 23(5): p. 277-284.
- [10] Vashishtha, V.K., R. Makade, and N. Mehla, Advancement of rapid prototyping in aerospace industry-a review. International Journal of Engineering Science and Technology, 2011. 3(3): p. 2486-2493.

- [11] Yan, X. and P. Gu, A review of rapid prototyping technologies and systems. Computer-Aided Design, 1996. 28(4): p. 307-318.
- [12] Alimardani, M., E. Toyserkani, and J.P. Huissoon, Three-dimensional numerical approach for geometrical prediction of multilayer laser solid freeform fabrication process. Journal of Laser Applications, 2007. 19(1): p. 14-25.
- [13] Bak, D., Rapid prototyping or rapid production? 3D printing processes move industry towards the latter. Assembly Automation, 2003. 23(4): p. 340-345.
- [14] Yakovlev, A., et al., Laser-assisted direct manufacturing of functionally graded 3D objects. Surface and Coatings Technology, 2005. 190(1): p. 15-24.
- [15] Zhai, Y., D.A. Lados, and J.L. LaGoy, Additive Manufacturing: Making Imagination the Major Limitation. JOM, 2014. 66(5): p. 808-816.
- [16] Carneiro, O.S., A.F. Silva, and R. Gomes, Fused deposition modeling with polypropylene. Materials & Design, 2015. 83: p. 768-776.
- [17] Stratasys, I., Technical application guide: FDM for Jigs and Fixtures, 3D Printers and Production Systems, in [Online]. 2013, Available from: http://usglobalimages.stratasys.com/Main/Secure/Technical_ApplicationGuidesTAG/SYS-TAG-JigsFixtures-11-13.pdf?v=635445826924414166 [2015, January 30].
- [18] Torrado, A.R., et al., Characterizing the effect of additives to ABS on the mechanical property anisotropy of specimens fabricated by material extrusion 3D printing. Additive Manufacturing, 2015. 6: p. 16-29.
- [19] Dudek, P., FDM 3D printing technology in manufacturing composite elements. Archives of Metallurgy and Materials, 2013. 58(4): p. 1415-1418.
- [20] Gibson, I., Rosen. D.W., and Stucker, B, Additive manufacturing technologies : rapid prototyping to direct digital manufacturing. 2010: p. 459.
- [21] Novakova-Marcincinova, L., et al. Special materials used in FDM rapid prototyping technology application. in 2012 IEEE 16th International Conference on Intelligent Engineering Systems (INES). 2012.

- [22] Tekinalp, H.L., et al., Highly oriented carbon fiber–polymer composites via additive manufacturing. Composites Science and Technology, 2014. 105: p. 144-150.
- [23] Gu, D., et al., Laser additive manufacturing of metallic components: materials, processes and mechanisms. International materials reviews, 2012. 57(3): p. 133-164.
- [24] Shofner, M., et al., Nanofiber-reinforced polymers prepared by fused deposition modeling. Journal of applied polymer science, 2003. 89(11): p. 3081-3090.
- [25] Zhong, W., et al., Short fiber reinforced composites for fused deposition modeling. Materials Science and Engineering: A, 2001. 301(2): p. 125-130.
- [26] Drummer, D., S. Cifuentes-Cuéllar, and D. Rietzel, Suitability of PLA/TCP for fused deposition modeling. Rapid Prototyping Journal, 2012. 18(6): p. 500-507.
- [27] Barna, J., Janak, M., and Fecova, V. , Technical and economical characteristics of 3D printing. In Progressive Technologies of Cutting, 2010: p. 67-74.
- [28] Tripathi, D., Practical Guide to Polypropylene. 2002, Shrewsbury, UK Rapra Technology Limited.
- [29] Karian, H., Handbook of polypropylene and polypropylene composites, revised and expanded. 2003: CRC press.
- [30] Kutz, M., Mechanical Engineers' Handbook: Materials and Engineering Mechanics. 3rd ed. 2006, New Jersey: John Wiley & Sons, Inc.
- [31] Maier, C. and T. Calafut, Polypropylene: the definitive user's guide and databook. 1998: William Andrew.
- [32] Spaleck, W., Polypropylene Handbook. Polymerization, Characterization, Properties, Processing, Applications. Herausgegeben von EP Moore, Jr. Hanser-Gardner, Cincinnati, 1996. 419 S., geb. 136.00\$.—ISBN 1-56990-208-9. Angewandte Chemie, 1997. 109(10): p. 1175-1175.
- [33] Hough. M.C., a.D., R. , The Plastic Compendium, Volume 1: Key Properties and Sources. 1995, Shrewsbury, UK Rapra Technology.

- [34] Kroschwitz, J.I., Concise Encyclopedia of Polymer Science and Engineering. 1st ed. 1990, New York: Wiley-Interscience
- [35] Karger-Kocsis., J., Polypropylene. An A-Z Reference. 1999, London, UK Kluwer Academic.
- [36] Velarde, D.A., and Yeagley, M.J. , Linear shrinkage differences in injection molded parts. Plastics Engineering 2000. 56: p. 60-64.
- [37] Shakoor, A. and N.L. Thomas, Talc as a nucleating agent and reinforcing filler in poly (lactic acid) composites. Polymer Engineering & Science, 2014. 54(1): p. 64-70.
- [38] Murphy, J., CHAPTER 4 - Modifying Specific Properties: Mechanical Properties – Fillers, in Additives for Plastics Handbook (Second Edition). 2001, Elsevier Science: Amsterdam. p. 19-35.
- [39] Tolinski, M., Chapter 7 - Overview of Fillers and Fibers, in Additives for Polyolefins. 2009, William Andrew Publishing: Oxford. p. 93-119.
- [40] Wypych, G., 2 - FILLERS – ORIGIN, CHEMICAL COMPOSITION, PROPERTIES, AND MORPHOLOGY, in Handbook of Fillers (Fourth Edition). 2016, ChemTec Publishing. p. 13-266.
- [41] Xanthos, M., Functional Fillers for Plastics. 2005, New York Wiley.
- [42] Matsuoka, T., Warpage and its prediction in injection-molded parts, in Polypropylene: An A-Z reference, J. Karger-Kocsis, Editor. 1999, Springer Netherlands: Dordrecht. p. 859-865.
- [43] Lati, Dimensional Modeling shrinkages of Thermoplastic Parts, in [Online]. 2008, Available from: http://www.lati.com/pdf/technical_data/dimensional-molding-shrinkages.pdf. [2015, January 31].
- [44] D955-08, A., Standard Test Method of Measuring Shrinkage from Mold Dimensions of Thermoplastics, in ASTM International. 2014, ASTM organization: West Conshohocken, USA.
- [45] SABIC, Understanding Shrinkage and Warpage of Reinforced and Filled Thermoplastics, in [Online]. Available from:

http://kbam.geampod.com/KBAM/Reflection/Assets/Thumbnail/7107_14.pdf
[2015, January 30].

- [46] Jahani, Y., Dynamic rheology, mechanical performance, shrinkage, and morphology of chemically coupled talc-filled polypropylene. Journal of Vinyl and Additive Technology, 2010. 16(1): p. 70-77.
- [47] A.J. Pontes, N.M.N., J.C. Velosa, A.R. Faria, António Sergio Pouzada, Glass Fibre Contents of PP Plates and their Properties: Part I: Shrinkage and Changes in Time. Key Engineering Materials, 2002. 230-232: p. 48-51.
- [48] Ning, F., et al., Additive manufacturing of carbon fiber reinforced thermoplastic composites using fused deposition modeling. Composites Part B: Engineering, 2015. 80: p. 369-378.
- [49] Shelesh-Nezhad, K. and A. Taghizadeh, Shrinkage behavior and mechanical performances of injection molded polypropylene/talc composites. Polymer Engineering & Science, 2007. 47(12): p. 2124-2128.
- [50] HMC, P., Product table in [Online]. 2014, Available from: <http://www.hmcpolymers.com/product-table> [2016, January 1].



APPENDIX

จุฬาลงกรณ์มหาวิทยาลัย
CHULALONGKORN UNIVERSITY

Appendix A

Data of raw material properties

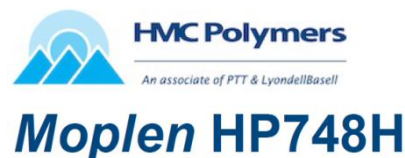
Polypropylene

1. Product identifier [50]

Company: HMC Polymers Co., LTD.

Trade name: Moplen HP748H

Substance name: Polypropylene Homopolymer



2. Composition of ingredients

Polypropylene Homopolymer >95 wt. %

Stabilizers (trade secret) <5 wt. %

3. Typical properties

Table A.1 Basic properties of Moplen HP748H

Properties	ASTM method	Value
Melt flow rate (230°C/2.16kg), g/10min	D1238	2.0
Density, g/cm ³	D792B	0.90
Tensile strength at yield, MPa	D638	38
Elongation at yield, %	D638	10
Flexural modulus, MPa	D790A	1800
Notched izod impact strength at 23°C, J/m	D256A	47
Deflection temperature, at 455kPa, °C	D648	115

4. Typical applications

- Thermoform packaging
- Microwavable food containers
- Extrusion sheet
- EBM bottles

Talcum

1. Product identifier

Company: Minerals Technologies Inc.

Trade name: MICROTUFF[®] 1000 talc

Substance name: Magnesium Silicate

2. Typical properties

Table A.2 Basic properties of MICROTUFF[®] 1000 talc

Properties	Unit	Value
Median Particle Size	µm	1.2
Hegman Fineness	minimum	6.0
Retention, 325 Mesh	%	-
Dry Brightness (Hunter Y, Rd Value)	-	89
Oil Absorption	-	52
Bulk Density	lb/ft ³	7.5
	g/cm ³	0.12
Tap Density	lb/ft ³	15.5
	g/cm ³	0.25
pH	-	8.9
Specific Gravity	-	2.8

3. Typical chemical composition

Table A.3 Chemical composition of MICROTUFF® 1000 talc

Properties		Value
Silicon Dioxide	SiO ₂	61%
Magnesium Oxide	MgO	31%
Calcium Oxide	CaO	<0.5%
Aluminum Oxide	Al ₂ O ₃	<2.0%
Iron As	Fe ₂ O ₃	<1.3%
Loss on Ignition	L.O.I.	7.0%
Moisture % (% weight loss @ 110°C)	H ₂ O	<0.5%

Milled glass fiber

1. Product identifier

Company: QUATEK Inc.

Trade name: EMG

Glass fiber type: E glass

2. Typical properties

Table A.4 Basic properties of milled glass fiber

Product	Sizing Agent	Filament Diameter (μm)	Loss on Ignition (%)	Moisture Content (%)	Average Residual Length (μm)
EMG13-70	Silane	13	≤1.05	≤0.1	70
EMG13-200	Silane	13	≤1.05	≤0.1	200

Appendix B
Data of mechanical properties

Table B.1 Tensile properties of PP (Injection molding)

No.	Tensile modulus (MPa)	Tensile strength (MPa)	Elongation at break (%)
1	1524	35.7	515
2	1547	35.2	454
3	1570	35.5	495
4	1616	35.4	558
5	1624	35.3	468
Avg	1576	35.4	498
SD	43.2	0.194	41.0

Table B.2 Tensile properties of PP+10wt%talca (Injection molding)

No.	Tensile modulus (MPa)	Tensile strength (MPa)	Elongation at break (%)
1	2696	35.0	350
2	2755	35.5	388
3	2622	35.3	310
4	2690	35.5	384
5	2610	35.4	339
Avg	2674	35.3	354
SD	59.5	0.213	32.6

Table B.3 Tensile properties of PP+20wt%talca (Injection molding)

No.	Tensile modulus (MPa)	Tensile strength (MPa)	Elongation at break (%)
1	3816	35.5	80.0
2	3789	35.4	73.0
3	3838	35.4	81.5
4	3852	35.7	62.0
5	3833	35.4	61.7
Avg	3826	35.5	71.6
SD	24.3	0.117	9.5

Table B.4 Tensile properties of PP+30wt%talca (Injection molding)

No.	Tensile modulus (MPa)	Tensile strength (MPa)	Elongation at break (%)
1	4614	35.4	27.0
2	4775	35.7	26.9
3	4798	35.6	28.0
4	5015	35.9	22.3
5	4663	35.8	29.2
Avg	4773	35.7	26.7
SD	155	0.200	2.63

Table B.5 Tensile properties of PP+10wt%MF (AR 5.4) (Injection molding)

No.	Tensile modulus (MPa)	Tensile strength (MPa)	Elongation at break (%)
1	1952	33.8	419
2	1979	34.1	420
3	1979	33.8	390
4	2001	33.9	411
5	2037	33.8	472
Avg	1990	33.9	422
SD	31.8	0.150	30.5

Table B.6 Tensile properties of PP+20wt%MF (AR 5.4) (Injection molding)

No.	Tensile modulus (MPa)	Tensile strength (MPa)	Elongation at break (%)
1	2483	31.7	366
2	2494	31.6	357
3	2523	31.4	361
4	2433	31.6	381
5	2491	31.5	357
Avg	2485	31.6	364
SD	32.6	0.0949	10.1

Table B.7 Tensile properties of PP+30wt%MF (AR 5.4) (Injection molding)

No.	Tensile modulus (MPa)	Tensile strength (MPa)	Elongation at break (%)
1	2990	29.5	199
2	2789	29.2	177
3	2884	29.0	196
4	3070	29.1	150
5	2953	29.2	180
Avg	2937	29.2	180
SD	107	0.187	19.6

Table B.8 Tensile properties of PP+10wt%MF (AR 15.4) (Injection molding)

No.	Tensile modulus (MPa)	Tensile strength (MPa)	Elongation at break (%)
1	3008	35.4	396
2	2993	35.1	432
3	2802	35.1	422
4	3030	35.0	419
5	2899	35.0	431
Avg	2946	35.1	420
SD	95.1	0.157	14.6

Table B.9 Tensile properties of PP+20wt%MF (AR 15.4) (Injection molding)

No.	Tensile modulus (MPa)	Tensile strength (MPa)	Elongation at break (%)
1	4465	33.6	320
2	4654	33.8	298
3	4778	33.6	360
4	4844	33.3	285
5	4731	33.7	297
Avg	4694	33.6	312
SD	146	0.194	29.6

Table B.10 Tensile properties of PP+30wt%MF (AR 15.4) (Injection molding)

No.	Tensile modulus (MPa)	Tensile strength (MPa)	Elongation at break (%)
1	5986	32.0	27.0
2	6031	31.4	25.1
3	5807	31.8	23.5
4	5523	31.8	28.0
5	5685	32.1	31.2
Avg	5806	31.8	26.9
SD	211	0.244	2.90

Table B.11 Tensile properties of PP+10wt%talca (FDM technique)

No.	Tensile modulus (MPa)	Tensile strength (MPa)	Elongation at break (%)
1	1264	19.9	6.86
2	1050	20.1	5.28
3	1199	20.9	4.61
4	1129	19.9	5.11
5	1168	20.8	4.67
Avg	1162	20.3	5.31
SD	79.7	0.486	0.92

Table B.12 Tensile properties of PP+10wt%talca (FDM technique)

No.	Tensile modulus (MPa)	Tensile strength (MPa)	Elongation at break (%)
1	1572	20.3	7.25
2	1434	21.1	7.38
3	1269	20.7	5.70
4	1381	20.7	7.20
5	1400	21.7	6.15
Avg	1411	20.9	6.74
SD	109	0.509	0.761

Table B.13 Tensile properties of PP+20wt%talca (FDM technique)

No.	Tensile modulus (MPa)	Tensile strength (MPa)	Elongation at break (%)
1	1524	16.9	9.00
2	1482	17.9	9.12
3	1564	17.4	8.10
4	1676	19.0	8.93
5	1521	19.3	9.39
Avg	1553	18.1	8.91
SD	74.4	1.03	0.485

Table B.14 Tensile properties of PP+30wt%talca (FDM technique)

No.	Tensile modulus (MPa)	Tensile strength (MPa)	Elongation at break (%)
1	1939	16.5	11.2
2	1716	16.8	10.1
3	1959	16.9	9.62
4	1998	17.0	9.82
5	1718	15.2	8.46
Avg	1866	16.5	9.84
SD	138	0.721	0.984

Table B.15 Tensile properties of PP+10wt%MF (AR 5.4) (FDM technique)

No.	Tensile modulus (MPa)	Tensile strength (MPa)	Elongation at break (%)
1	1385	19.3	7.56
2	1385	19.8	6.69
3	1287	20.4	7.32
4	1411	20.6	7.39
5	1257	20.7	7.30
Avg	1345	20.2	7.25
SD	68.3	0.589	0.331

Table B.16 Tensile properties of PP+20wt%MF (AR 5.4) (FDM technique)

No.	Tensile modulus (MPa)	Tensile strength (MPa)	Elongation at break (%)
1	1371	18.8	9.11
2	1425	19.2	9.39
3	1569	18.8	9.36
4	1433	18.5	9.98
5	1357	18.8	8.99
Avg	1431	18.8	9.37
SD	83.7	0.266	0.38

Table B.17 Tensile properties of PP+30wt%MF (AR 5.4) (FDM technique)

No.	Tensile modulus (MPa)	Tensile strength (MPa)	Elongation at break (%)
1	1551	18.0	10.2
2	1519	16.8	10.7
3	1707	16.7	11.7
4	1646	17.3	9.51
5	1610	17.2	12.2
Avg	1606	17.2	10.8
SD	74.7	0.518	1.08

Table B.18 Tensile properties of PP+10wt%MF (AR 15.4) (FDM technique)

No.	Tensile modulus (MPa)	Tensile strength (MPa)	Elongation at break (%)
1	1735	19.9	4.73
2	1536	20.5	5.14
3	1615	20.7	4.92
4	1573	21.2	4.08
5	1683	22.5	4.91
Avg	1629	21.0	4.76
SD	81.0	0.998	0.403

Table B.19 Tensile properties of PP+20wt%MF (AR 15.4) (FDM technique)

No.	Tensile modulus (MPa)	Tensile strength (MPa)	Elongation at break (%)
1	1661	18.7	6.34
2	1942	17.6	6.01
3	1829	18.8	5.80
4	1674	17.5	7.59
5	1805	17.1	5.63
Avg	1782	17.9	6.27
SD	117	0.745	0.78

Table B.20 Tensile properties of PP+30wt%MF (AR 15.4) (FDM technique)

No.	Tensile modulus (MPa)	Tensile strength (MPa)	Elongation at break (%)
1	1921	17.1	7.42
2	2100	16.7	7.62
3	1778	16.5	6.30
4	2006	15.3	6.82
5	1975	16.3	6.08
Avg	1956	16.4	6.85
SD	119	0.676	0.672

Appendix C
Data of shrinkage behavior

Table C.1 Shrinkage rate of PP (Injection molding)

No.	Flow direction (MD)	Cross direction (TD)
1	1.55	1.29
2	1.57	1.25
3	1.54	1.28
4	1.57	1.28
5	1.56	1.25
Avg	1.55	1.27
SD	0.0130	0.0182

Table C.2 Shrinkage rate of PP+10wt%talc (Injection molding)

No.	Flow direction (MD)	Cross direction (TD)
1	1.29	1.04
2	1.29	1.05
3	1.29	1.06
4	1.29	1.05
5	1.29	1.07
Avg	1.29	1.05
SD	0.00318	0.0114

Table C.3 Shrinkage rate of PP+20wt%talc (Injection molding)

No.	Flow direction (MD)	Cross direction (TD)
1	1.15	0.936
2	1.11	0.929
3	1.13	0.932
4	1.14	0.927
5	1.13	0.933
Avg	1.13	0.931
SD	0.0138	0.00374

Table C.4 Shrinkage rate of PP+30wt%talc (Injection molding)

No.	Flow direction (MD)	Cross direction (TD)
1	0.939	0.797
2	0.931	0.787
3	0.922	0.804
4	0.928	0.790
5	0.917	0.766
Avg	0.927	0.789
SD	0.00832	0.0144

Table C.5 Shrinkage rate of PP+10wt%MF (AR 5.4) (Injection molding)

No.	Flow direction (MD)	Cross direction (TD)
1	1.43	1.18
2	1.43	1.18
3	1.41	1.18
4	1.39	1.19
5	1.42	1.17
Avg	1.42	1.18
SD	0.0187	0.00655

Table C.6 Shrinkage rate of PP+20wt%MF (AR 5.4) (Injection molding)

No.	Flow direction (MD)	Cross direction (TD)
1	1.23	1.08
2	1.23	1.10
3	1.25	1.06
4	1.23	1.08
5	1.22	1.06
Avg	1.23	1.08
SD	0.0126	0.0146

Table C.7 Shrinkage rate of PP+30wt%MF (AR 5.4) (Injection molding)

No.	Flow direction (MD)	Cross direction (TD)
1	1.12	0.945
2	1.08	1.02
3	1.06	0.966
4	1.10	0.980
5	1.12	1.02
Avg	1.10	0.987
SD	0.0243	0.0335

Table C.8 Shrinkage rate of PP+10wt%MF (AR 15.4) (Injection molding)

No.	Flow direction (MD)	Cross direction (TD)
1	1.36	1.11
2	1.37	1.16
3	1.37	1.17
4	1.38	1.17
5	1.37	1.14
Avg	1.37	1.15
SD	0.00781	0.0281

Table C.9 Shrinkage rate of PP+20wt%MF (AR 15.4) (Injection molding)

No.	Flow direction (MD)	Cross direction (TD)
1	1.20	1.01
2	1.21	1.01
3	1.20	0.983
4	1.17	0.962
5	1.19	1.01
Avg	1.20	0.995
SD	0.0140	0.0217

Table C.10 Shrinkage rate of PP+30wt%MF (AR 15.4) (Injection molding)

No.	Flow direction (MD)	Cross direction (TD)
1	1.04	0.928
2	1.03	0.943
3	1.05	0.952
4	1.04	0.962
5	1.04	0.952
Avg	1.04	0.947
SD	0.00780	0.0128

Appendix D

Data of thermal properties

Table D.1 Thermal properties of PP

No.	At 1 st Scan		
	T _m (°C)	T _c (°C)	%Crys
1	165.0	123.5	60.2
2	166.9	124.0	62.1
Avg	166.0	123.8	61.2
SD	1.34	0.35	1.34

Table D.2 Thermal properties of PP+10wt%talca

No.	At 1 st Scan		
	T _m (°C)	T _c (°C)	%Crys
1	167.2	125.7	61.9
2	166.6	125.6	59.8
Avg	166.9	125.7	60.9
SD	0.42	0.07	1.48

Table D.3 Thermal properties of PP+20wt%talca

No.	At 1 st Scan		
	T _m (°C)	T _c (°C)	%Crys
1	167.8	126.7	60.0
2	165.3	126.0	62.1
Avg	166.6	126.4	61.1
SD	1.77	0.49	1.48

Table D.4 Thermal properties of PP+30wt%talc

No.	At 1 st Scan		
	Tm (°C)	Tc (°C)	%Crys
1	167.6	126.3	60.7
2	166.6	127.3	60.9
Avg	167.1	126.8	60.8
SD	0.71	0.71	0.14

Table D.5 Thermal properties of PP+10wt%MF (AR 5.4)

No.	At 1 st Scan		
	Tm (°C)	Tc (°C)	%Crys
1	169.5	125.3	60.7
2	169.4	124.8	61.1
Avg	169.5	125.1	60.9
SD	0.07	0.35	0.28

Table D.6 Thermal properties of PP+20wt%MF (AR 5.4)

No.	At 1 st Scan		
	Tm (°C)	Tc (°C)	%Crys
1	166.8	124.9	57.8
2	165.6	125.3	62.6
Avg	166.2	125.1	60.2
SD	0.85	0.28	3.39

Table D.7 Thermal properties of PP+30wt%MF (AR 5.4)

No.	At 1 st Scan		
	Tm (°C)	Tc (°C)	%Crys
1	167.9	125.6	57.9
2	167.4	125.4	64.1
Avg	167.7	125.5	61.0
SD	0.35	0.14	4.38

Table D.8 Thermal properties of PP+10wt%MF (AR 15.4)

No.	At 1 st Scan		
	Tm (°C)	Tc (°C)	%Crys
1	167.3	124.4	58.7
2	166.6	123.0	62.6
Avg	167.0	123.7	60.7
SD	0.49	0.99	2.76

Table D.9 Thermal properties of PP+20wt%MF (AR 15.4)

No.	At 1 st Scan		
	Tm (°C)	Tc (°C)	%Crys
1	167.3	124.7	58.4
2	167.9	125.0	58.4
Avg	167.6	124.9	58.4
SD	0.42	0.21	0.00

Table D.10 Thermal properties of PP+30wt%MF (AR 15.4)

No.	At 1 st Scan		
	Tm (°C)	Tc (°C)	%Crys
1	167.7	125.5	59.4
2	168.1	125.5	61.9
Avg	167.9	125.5	60.7
SD	0.28	0.00	1.77



Appendix E
Data of thermal conductivity

Table E.1 Thermal conductivity of PP

Temp, (°C)	Density at 23°C, (kg/m ³)	Thermal diffusivity, (m ² /s)	C _p , J/(kg.K)	Thermal conductivity, W/(m.K)
25	908	0.000000156	1704	0.241
50	908	0.000000147	2097	0.280
75	908	0.000000138	2336	0.293
100	908	0.000000130	2490	0.294

Table E.2 Thermal conductivity of PP+10wt%talca

Temp, (°C)	Density at 23°C, (kg/m ³)	Thermal diffusivity, (m ² /s)	C _p , J/(kg.K)	Thermal conductivity, W/(m.K)
25	972	0.000000170	1664	0.275
50	972	0.000000156	1920	0.291
75	972	0.000000145	2104	0.297
100	972	0.000000137	2229	0.297

Table E.3 Thermal conductivity of PP+20wt%talca

Temp, (°C)	Density at 23°C, (kg/m ³)	Thermal diffusivity, (m ² /s)	C _p , J/(kg.K)	Thermal conductivity, W/(m.K)
25	1043	0.000000257	1475	0.395
50	1043	0.000000236	1841	0.453
75	1043	0.000000216	2000	0.451
100	1043	0.000000195	2247	0.457

Table E.4 Thermal conductivity of PP+30wt%talc

Temp, (°C)	Density at 23°C, (kg/m ³)	Thermal diffusivity, (m ² /s)	Cp, J/(kg.K)	Thermal conductivity, W/(m.K)
25	1119	0.000000240	1414	0.380
50	1119	0.000000242	1750	0.474
75	1119	0.000000207	1940	0.449
100	1119	0.000000189	2046	0.433

Table E.5 Thermal conductivity of PP+10wt%MF (AR 5.4)

Temp, (°C)	Density at 23°C, (kg/m ³)	Thermal diffusivity, (m ² /s)	Cp, J/(kg.K)	Thermal conductivity, W/(m.K)
25	970	0.000000169	1597	0.262
50	970	0.000000151	2034	0.298
75	970	0.000000138	2263	0.303
100	970	0.000000126	2450	0.300

Table E.6 Thermal conductivity of PP+20wt%MF (AR 5.4)

Temp, (°C)	Density at 23°C, (kg/m ³)	Thermal diffusivity, (m ² /s)	Cp, J/(kg.K)	Thermal conductivity, W/(m.K)
25	1037	0.000000189	1519	0.298
50	1037	0.000000165	1795	0.307
75	1037	0.000000156	1988	0.322
100	1037	0.000000145	2097	0.315

Table E.7 Thermal conductivity of PP+30wt%MF (AR 5.4)

Temp, (°C)	Density at 23°C, (kg/m ³)	Thermal diffusivity, (m ² /s)	Cp, J/(kg.K)	Thermal conductivity, W/(m.K)
25	1115	0.000000186	1550	0.321
50	1115	0.000000173	1920	0.370
75	1115	0.000000159	2112	0.374
100	1115	0.000000145	2219	0.359

Table E.8 Thermal conductivity of PP+10wt%MF (AR 15.4)

Temp, (°C)	Density at 23°C, (kg/m ³)	Thermal diffusivity, (m ² /s)	Cp, J/(kg.K)	Thermal conductivity, W/(m.K)
25	976	0.000000164	1530	0.245
50	976	0.000000156	1935	0.295
75	976	0.000000143	2148	0.300
100	976	0.000000135	2280	0.300

Table E.9 Thermal conductivity of PP+20wt%MF (AR 15.4)

Temp, (°C)	Density at 23°C, (kg/m ³)	Thermal diffusivity, (m ² /s)	Cp, J/(kg.K)	Thermal conductivity, W/(m.K)
25	1043	0.000000178	1414	0.263
50	1043	0.000000162	1800	0.304
75	1043	0.000000148	1959	0.302
100	1043	0.000000136	2185	0.310

Table E.10 Thermal conductivity of PP+30wt%MF (AR 15.4)

Temp, (°C)	Density at 23°C, (kg/m ³)	Thermal diffusivity, (m ² /s)	Cp, J/(kg.K)	Thermal conductivity, W/(m.K)
25	1127	0.000000210	1427	0.338
50	1127	0.000000186	1698	0.356
75	1127	0.000000176	1837	0.364
100	1127	0.000000157	2043	0.361



Appendix F

Data of die swell

Table F.1 Die swell of PP

Shear rate (/s)	D1 (mm)
10.0	1.02
50.0	1.12
100	1.26
200	1.41
301	1.50
501	1.60
701	1.64
1001	1.67

Table F.2 Die swell of PP+10wt%talc

Shear rate (/s)	D1 (mm)
10.0	1.02
50.0	1.13
100	1.25
200	1.36
301	1.40
501	1.44
701	1.45
1001	1.50

Table F.3 Die swell of PP+20wt%talc

Shear rate (/s)	D1 (mm)
10.0	1.01
50.0	1.11
100	1.18
200	1.25
301	1.28
501	1.31
701	1.34
1001	1.37

Table F.4 Die swell of PP+30wt%talc

Shear rate (/s)	D1 (mm)
10.0	0.950
50.0	1.01
100	1.06
200	1.10
301	1.13
501	1.15
701	1.16
1001	1.18

Table F.5 Die swell of PP+10wt%MF (AR 5.4)

Shear rate (/s)	D1 (mm)
10.0	1.00
50.0	1.15
100	1.26
200	1.38
301	1.46
501	1.56
701	1.62
1001	1.67

Table F.6 Die swell of PP+20wt%MF (AR 5.4)

Shear rate (/s)	D1 (mm)
10.0	1.01
50.0	1.13
100	1.22
200	1.34
301	1.40
501	1.46
701	1.49
1001	1.60

Table F.7 Die swell of PP+30wt%MF (AR 5.4)

Shear rate (/s)	D1 (mm)
10.0	1.00
50.0	1.11
100	1.22
200	1.25
301	1.32
501	1.35
701	1.42
1001	1.45

Table F.8 Die swell of PP+10wt%MF (AR 15.4)

Shear rate (/s)	D1 (mm)
10.0	1.01
50.0	1.18
100	1.30
200	1.45
301	1.50
501	1.58
701	1.60
1001	1.66

Table F.9 Die swell of PP+20wt%MF (AR 15.4)

Shear rate (/s)	D1 (mm)
10.0	1.01
50.0	1.16
100	1.24
200	1.33
301	1.39
501	1.44
701	1.51
1001	1.54

Table F.10 Die swell of PP+30wt%MF (AR 15.4)

Shear rate (/s)	D1 (mm)
10.0	0.980
50.0	1.07
100	1.16
200	1.22
301	1.26
501	1.32
701	1.38
1001	1.43

Appendix G
Data of porosity

Table G.1 Porosity of PP

No.	ρ_t (g/cm ³)	PP (wt.)	Filler (wt.)	ρ_{PP} (g/cm ³)	ρ_{Filler} (g/cm ³)	P (%)	
1	0.800	1	0	0.90	2.75	11.1	
2	0.801	1	0	0.90	2.75	11.0	
3	0.799	1	0	0.90	2.75	11.2	
4	0.801	1	0	0.90	2.75	11.0	
5	0.798	1	0	0.90	2.75	11.3	
						Avg	11.1
						SD	0.130

Table G.2 Porosity of PP+10%talca

No.	ρ_t (g/cm ³)	PP (wt.)	Filler (wt.)	ρ_{PP} (g/cm ³)	ρ_{Filler} (g/cm ³)	P (%)	
1	0.860	0.9	0.1	0.90	2.75	10.9	
2	0.863	0.9	0.1	0.90	2.75	10.6	
3	0.858	0.9	0.1	0.90	2.75	11.1	
4	0.864	0.9	0.1	0.90	2.75	10.5	
5	0.857	0.9	0.1	0.90	2.75	11.2	
						Avg	10.9
						SD	0.305

Table G.3 Porosity of PP+20%talca

No.	ρ_t (g/cm ³)	PP (wt.)	Filler (wt.)	ρ_{PP} (g/cm ³)	ρ_{Filler} (g/cm ³)	P (%)	
1	0.935	0.8	0.2	0.90	2.75	10.1	
2	0.927	0.8	0.2	0.90	2.75	10.9	
3	0.931	0.8	0.2	0.90	2.75	10.5	
4	0.927	0.8	0.2	0.90	2.75	10.9	
5	0.933	0.8	0.2	0.90	2.75	10.3	
						Avg	10.5
						SD	0.358

Table G.4 Porosity of PP+30%talca

No.	ρ_t (g/cm ³)	PP (wt.)	Filler (wt.)	ρ_{PP} (g/cm ³)	ρ_{Filler} (g/cm ³)	P (%)	
1	1.017	0.7	0.3	0.90	2.75	9.8	
2	1.022	0.7	0.3	0.90	2.75	9.4	
3	1.023	0.7	0.3	0.90	2.75	9.3	
4	1.016	0.7	0.3	0.90	2.75	9.9	
5	1.024	0.7	0.3	0.90	2.75	9.2	
						Avg	9.5
						SD	0.311

Table G.5 Porosity of PP+10%MF (AR 5.4)

No.	ρ_t (g/cm ³)	PP (wt.)	Filler (wt.)	ρ_{PP} (g/cm ³)	ρ_{Filler} (g/cm ³)	P (%)	
1	0.854	0.9	0.1	0.90	2.58	11.3	
2	0.859	0.9	0.1	0.90	2.58	10.8	
3	0.857	0.9	0.1	0.90	2.58	11.0	
4	0.855	0.9	0.1	0.90	2.58	11.2	
5	0.859	0.9	0.1	0.90	2.58	10.8	
						Avg	11.0
						SD	0.228

Table G.6 Porosity of PP+20%MF (AR 5.4)

No.	ρ_t (g/cm ³)	PP (wt.)	Filler (wt.)	ρ_{PP} (g/cm ³)	ρ_{Filler} (g/cm ³)	P (%)	
1	0.923	0.8	0.2	0.90	2.58	10.8	
2	0.925	0.8	0.2	0.90	2.58	10.6	
3	0.921	0.8	0.2	0.90	2.58	11.0	
4	0.920	0.8	0.2	0.90	2.58	11.1	
5	0.926	0.8	0.2	0.90	2.58	10.5	
						Avg	10.8
						SD	0.255

Table G.7 Porosity of PP+30%MF (AR 5.4)

No.	ρ_t (g/cm ³)	PP (wt.)	Filler (wt.)	ρ_{PP} (g/cm ³)	ρ_{Filler} (g/cm ³)	P (%)	
1	1.003	0.7	0.3	0.90	2.58	10.3	
2	1.009	0.7	0.3	0.90	2.58	9.8	
3	1.007	0.7	0.3	0.90	2.58	10.0	
4	1.006	0.7	0.3	0.90	2.58	10.1	
5	1.008	0.7	0.3	0.90	2.58	9.9	
						Avg	10.0
						SD	0.192

Table G.8 Porosity of PP+10%MF (AR 15.4)

No.	ρ_t (g/cm ³)	PP (wt.)	Filler (wt.)	ρ_{PP} (g/cm ³)	ρ_{Filler} (g/cm ³)	P (%)	
1	0.857	0.9	0.1	0.90	2.58	11.0	
2	0.854	0.9	0.1	0.90	2.58	11.3	
3	0.862	0.9	0.1	0.90	2.58	10.5	
4	0.856	0.9	0.1	0.90	2.58	11.1	
5	0.859	0.9	0.1	0.90	2.58	10.8	
						Avg	10.9
						SD	0.305

Table G.9 Porosity of PP+20%MF (AR 15.4)

No.	ρ_t (g/cm ³)	PP (wt.)	Filler (wt.)	ρ_{PP} (g/cm ³)	ρ_{Filler} (g/cm ³)	P (%)	
1	0.926	0.8	0.2	0.90	2.58	10.5	
2	0.923	0.8	0.2	0.90	2.58	10.8	
3	0.927	0.8	0.2	0.90	2.58	10.4	
4	0.925	0.8	0.2	0.90	2.58	10.6	
5	0.926	0.8	0.2	0.90	2.58	10.5	
						Avg	10.6
						SD	0.152

Table G.10 Porosity of PP+30%MF (AR 15.4)

No.	ρ_t (g/cm ³)	PP (wt.)	Filler (wt.)	ρ_{PP} (g/cm ³)	ρ_{Filler} (g/cm ³)	P (%)	
1	1.010	0.7	0.3	0.90	2.58	9.7	
2	1.009	0.7	0.3	0.90	2.58	9.8	
3	1.011	0.7	0.3	0.90	2.58	9.6	
4	1.010	0.7	0.3	0.90	2.58	9.7	
5	1.008	0.7	0.3	0.90	2.58	9.9	
						Avg	9.7
						SD	0.114

VITA

Miss Chomphoonut Buaprommee was born on February 16, 1990 in Udon Thani province, Thailand. She graduated from Satri Rachinuthit High School, Udon Thani, Thailand in 2008. She received a Bachelor's degree with second-class honors in Chemical Engineering from Kasetsart University, Bangkok, Thailand in 2012. She has been studying for a Master's degree in Chemical Engineering at Chulalongkorn University, Bangkok, Thailand since 2014. At the same time, she is a research assistant at PTT Global Chemical Public Company Limited, Rayong, Thailand.

She joined oral presentation titled "Effect of milled glass fiber on the mechanical and physical properties of polypropylene for fused deposition modeling" at The 6th International Thai Institute of Chemical Engineering and Applied Science Conference (ITICHE2016) on October 27-28, 2016 in Bangkok, Thailand.